TOPICAL REPORT
FOR NRC USE

Copy Nº 03
WSTG-2-NP

MISSILE ENERGY ANALYSIS METHODS FOR NUCLEAR STEAM TURBINES

Submitted to:
NUCLEAR REGULATORY COMMISSION
May, 1981

Westinghouse Steam Turbine Generator Division

MISSILE ENERGY ANALYSIS METHODS
FOR NUCLEAR STEAM TURBINES

FOREWORD

This report compiles in one central source all of the current theory, assumptions, and procedures used to determine the dynamic properties of a hypothetical missile resutling from a posturlated bursting of a steam turbine rotor or disc. This report is divided into three parts:

A. Turbine Destructive Overspeed and Internal Missile Energies
B. Missile Energy Absorption in Nuclear Low Pressure Turbines
C. Missile Energy Absorption in Nuclear High Pressure Turbines

Data that is output from the report procedures includes:

- Disc internal energy properties at burst
- Disc and cylinder fragment energy properties exiting from the turbine
- Geometric parameters describing the missile fragments.

Parts A, B and C of this report and the data output are schematically connected as follows:

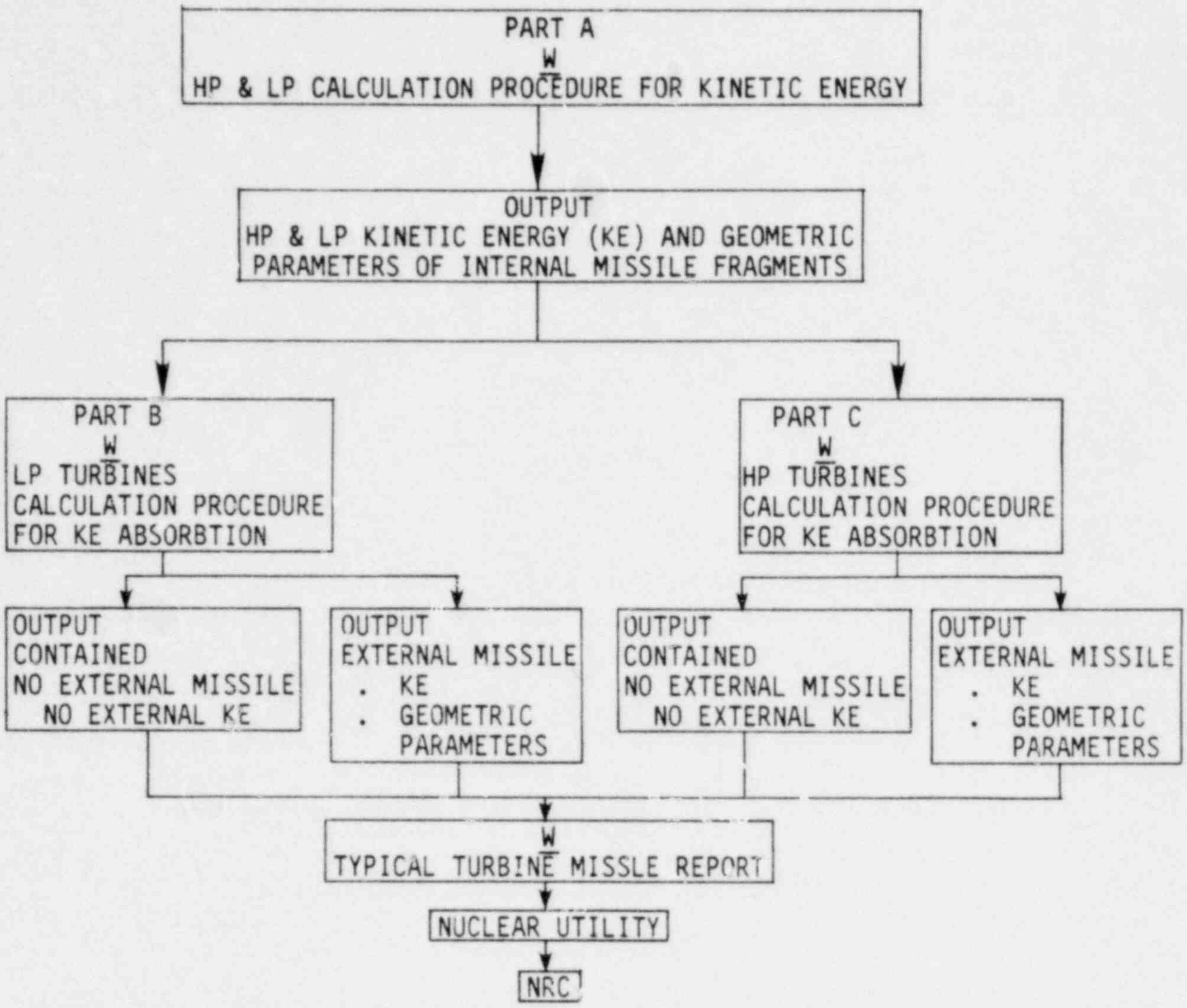

The above combined with the results from a probability analysis (the procedure, when investigating stress corrosion cracks in nuclear steam turbine is obtained in topical report "Procedures for estimating the probability of steam turbine disc rupture from stress corrosion cracking", May, 1981) comprises a complete package relative to turbine missile analysis and probability.

INTRODUCTORY NOTE

Each part (A, B, or C) of this report is written such that it can stand alone as a separate report. Each part has its own independent table of contents, nomenclature, references, appendices, and internal section and figure numbering systems. The user is therefore cautioned that when using a specific part of the report, any references to figures, section numbers, etc. apply only to the content of that part of the report unless specified otherwise.

PART A

Table of Contents

PART A

List of Figures

PART A

List of Tables

PART A

NOMENCLATURE AND UNITS

All nomenclature used in this part are defined as they appear in the text. Equations as written in this part are based on a system of units that are defined as follows:

TERM	UNITS
[ ]b	dimensionless
Energy and work	ft-lb
Weight density γ	lb/in^3
Material temperaure correction, Tc	dimensionless
Velocity	ft/sec
[ ]b	dimensionless
Strength or Stress	lb/in^2
Mass center ratio $\overline{R}$	in.
Kinetic Energy	ft-lb
Moment of Inertia I	in^4
Length, thickness, distance, radius,diameter	in
Angle	radians (as noted)
	degrees
Area	in^2
Gravitational constant, g	$386\ in/sec^2$

Introduction

In Part A the kinetic energy of external missiles that hypothetically could result if a turbine rotor were to rupture at normal speed, design overspeed or at destructive overspeed is calculated for units in nuclear power plant service. This part covers the theory and procedures for calculating the kinetic energy of the postulated rotor fragments before any interaction with the turbine stationary parts.

1.0 Initial Energy of Fragments of Turbine Discs and Rotors

1.1 Initial Energy of Fragments of Disc Type Elements

The kinetic energy of disc fragments depends on the weight of the fragment and the translational and angular velocity of the fragment. Since turbine discs are not designed to fail in certain sizes nor at certain speeds, some assumptions must be made as to the size of the fragment and the speeds of failure. The following discusses the assumptions and rationale behind the calculating of the factors involved in the kinetic energy. Once the factors are determined, the energies are calculated by the standard formulas of mechanics.

1.1.1 Fragment Size

Predetermined sizes of a failed turbine rotor disc cannot be predicted. There are no large cuts or planes that are substantially more highly stressed, on the average, than others. A flaw perhaps due to adverse operation or hostile environment, for example, develop at a location of metallurgical weakness, but such a site will be randomly located.

Depending upon the cause of failure and influenced by the disc design, there is a greater tendency for discs to fracture into approximately 180°, 120° or 90° segments than any other sizes.

Two modes of failure are possible - brittle fracture and ductile failure. A brittle failure will occur at gross section stress well below material yield strength if the stress intensity at the tip of a crack or flaw exceeds a critical value. A ductile failure will occur in the absence of any flaws when the gross section stress exceeds the material nominal ultimate strength.

[

]b

Westinghouse low pressure turbine discs for nuclear application contain
[
]a As a result of a hostile environment
[ ]b If left undetected these [ ]b could lead to
[ ]b type failure.

If there is only one crack of critical size and many cracks of subcritical size there is a good probability of [ ]b Once one plane is broken, the [ ]b away in the bore will be maximum and may be high enough to cause additional cracks to propagate. The subsequent [ ]b segment rotating about a new point will have a tendency to refracture into [ ]b segments, although the tendency is not as strong. Depending on the profile of the disc, once one plane is broken the bore stress for a large part of the periphery will exceed the material ultimate, so that even in the absence of a crack, ductile failure may occur.

Initial energy calculations show that [ ]b sectors always have greater energy than [ ]b sectors. The greater impact area of the [ ]b fragment also makes it a less critical missile. Therefore only the [ ]b are used for routine penetration calculations.

1.1.2 Fragment Weight

The major factors determining fragment weight are
[ ]b These factors are easily determined. A secondary but substantial factor, is the [ ]b

The typical blade has its greatest potential for failure from direct [ ]b, just above the [ ]b or in the [ ]b just below the [ ]b of the blade. Occasionally a [ ]b blade of a low pressure turbine will have its maximum [ ]b at a point considerably above the [ ]b

It is entirely possible that the blade may fail from direct stress at a [ ]b. A criterion to estimate failure from direct stress has been established. This criterion does not consider the effects of [-]b the assumption being that the speed increase is sufficiently rapid that a significant amount of [ ]b does not occur before the [ ]b

As turbine rotor speed rises toward destruction, the maximum direct stress reaches the tensile yield point and the blade begins to experience permanent growth. This permanent growth in turn causes an incremental increase of direct stress for the same speed.

The blade materials, whether machined or forged, exhibit a sufficiently high rate of [ ]b that this incremental stress does not cause a further increase of blade growth. Therefore, a further increase of speed is required to cause additional growth. Test cases calculated for a long blade indicate that a [ ]b is not likely until the maximum stress is very near the material nominal [ ]b While the plastic growth is sufficient to destroy the [ ]b, this may be neglected for simplicity since it is a very small fraction of the total blade mass. A small blade also will show no tendency to [ ]b until the base stress is very near the [ ]b Therefore, the [ ]b, corrected for operating [ ]b was chosen for the failure criterion.

Typically the only blade row which might suffer blade loss before disc failure is the [ ][b] of the LP and then only for some of the possible blade [ ][b] Under the system of reporting missile energies based on the lowest failure speed of all discs in a unit, the retention of the blades on a disc increases the fragment energy at failure speed while decreasing the failure speed of the particular disc. Loss of the blades in a row reduces fragment energy while increasing failure speed of the disc. In most cases to date, the [ ][b] does not control unit failure speed. In these cases, predicting blade retention is conservative from the point of view of reporting the highest energy missile. Since, once the value of destructive ovespeed is established for the unit, disc fragments with blades have higher mass and hence higher internal energies than those without blades. Accounting for blade loss is beneficial from the point of view of the protection designer, giving a lower energy missile. Fortunately the demarcation is very clear based upon the blade materials used.

1.1.3 Fragment Mass Center

The geometric factor affecting the determination of the translational velocity of the fragment is the location of the potential [ ][b] while the disc is still intact. The current practice is to calculate the [ ][b] with the blades [ ][b] This is chosen since this is the condition at the instant of initial fracture.

Almost instantly after fracture, and before a 180° sector could break into 90° sectors, the rotating blades will contact the cylinder rings. This impact is presumed to absorb substantial energy from the fragment, both translational and rotational, due to blade deformation and friction while also reducing the rotational inertia. Data presently available to Westinghouse does [ ][b] during deformation of the

blades. Indications are that friction primarily stops rotational motion while imparting minor damage to the containing cylinder. It might be assumed the blades are bent over with little strain energy involved, therefore the conservative assumption with free flight is that the major mass impacts the cylinder with the velocity of the mass center at the instant of fracture
[ ]b and the moment of secondary fracture
[ ]b

1.1.4 Velocity

As explained in (1)* a disc fracturing first into [ ]b a short time after the initial burst. The time interval is that required for a fast running ductile fracture crack to run from the inside to the outside of the disc. The resultant velocity of [ ]b is higher than the velocity of the segment before any fracture. This is due to rotation of the [ ]b about its mass-center during the refracturing phase. See (1) and Appendix B. The usual analysis is only true however if the disc fragment is in free flight. In the turbine, both rotation and translation are hindered almost instantly after the initial fracture, the internal clearances being very small compared to the distance traveled in free flight [ ]b Since the events in this interval are [ ]b the full value of the velocity augmentation is used as if the fragment were in free flight, yielding conservative values.

*Refers to reference numbers at the end of this part.

If the assumption is made that fracture is into [ ]^{b} no velocity augmentation occurs. Fracture may be assumed to be simultaneous or not, for if one sector comes out the remaining [ ]^{b} will continue to rotate about the rotor center until the second fracture is complete, at which time the two fragments will behave as the original.

The analysis applied to [ ]^{b} segments can be generalized to study the breaking of any initial size into smaller sizes. See Appendix B.

1.1.5 Disc Rupture Speed

For the purpose of calculating initial fragment energy a disc is presumed to have failed at two speeds where there would not normally be a failure. These are chosen because of the high probability of the turbine being at those speeds. One, of course, is running speed. The other is the design overspeed, i.e., that maximum speed which the turbine is expected to attain if the Overspeed Protection Controller fails, so that the unit is tripped by the emergency trip devices. This is normally [ ]^{b} of running speed. [ ]^{b}

The third speed for which energy is calculated is that at which [ ]^{a} and is therefore the limit of disc strength. The bursting speed of each disc is calculated. Upon failure of the disc with the lowest bursting speed, further acceleration of the unit is assumed to halt. For purposes of analysis, all discs in the same unit are calculated at the lowest speed of the unit.

1.2 Initial Energy of Fragments of Rotor Type Elements

As with disc type elements, the initial energy depends on the weight and translational and angular velocity of the fragment.

The following discusses the assumptions and rationale behind the calculation of the factors involved in the kinetic energy. For the most part, the reasoning parallels that for discs. Some differences exist because of the differences between discs and rotors.

1.2.1 Fragment Size

With a rotor type element specification must be made for the length of fragment and its sector size. [-

]^b Based on those fracture patterns, it is assumed that the HP rotors will [ ]^b extending from the centerline to the end of the main body.

The double flow HP rotors are similar to LP rotors except that the length of the center portion is considerably longer. There may be a tendency therefore for the rupture to leave the center section [ ]^b The judgement has been made to include a [ ]^a with the rest of the rotor for two reasons; a) [

]^b

1.2.2 Fragment Weight

The fragment weight is a function of the same factor as is the weight of a disc fragment. The rotors dealt with in this work were for HP turbines. Since the HP blade direct stresses are low compared to the ultimate, prior failure of blades was not considered. Should the occasion arise, however, the adjustment can be made as in the disc type elements.

1.2.3 Fragment Mass Center

The radial position of the mass center is determined, as with the disc elements, with blades upright.

1.2.4 Velocity

The velocity of the mass center is calculated as for a disc element. [

]b

1.2.5 Rotor Rupture Speed

For the purpose of calculating initial fragment energy, a rotor is presumed to have failed at running speed and design overspeed. [

]b

1.2.6 Fragment Energy

Fragment energies are calculated at running speed and design overspeed. The energy is not calculated at rotor burst speed because this is above the theoretical speed the turbine can reach with all throttle, governor, interceptor, and reheat stop valves failed in the wide open position on a full load trip. The energy is calculated at LP burst speed but not used for penetration calculations because the combined probability of reaching that speed and having a brittle burst at that speed is sufficiently low.

2.0 Calculation Procedures

2.1 HIGH PRESSURE (HP) Turbine Destructive Overspeed and Missile Energy

The rotor of an HP turbine for nuclear application must be analyzed to determine the size and energy of missiles that would result in the unlikely event a rotor would burst at running speed or design overspeed. The speed at which the rotor would burst must also be determined.

The rotor, containing all its blades is assumed to burst such that the body of the rotor
[
]^a through the diameter. Each [ ]^a also breaks in half at the plane of symmetry. The fracture process is assumed to occur in [ ]^a similar to that of a disc (see Sect. 2.2) so that there is gain of velocity on two of the [ ]^a on each end. See Figs. 1, 2 and 3 for various typical geometries of HP rotors. The heavy lines indicate the
[ ]^a

The criterion by which the failure speed is determined is the speed at which the
[
]^a For this purpose the material maximum ultimate strength is estimated for the grade of material from data covering the rotors manufactured of that material.

2.1.1 Rotor Average Tangential Stress

In order to determine the average stress the total outward centrifugal force from the blading and rotor body forces must be calculated. In the same operation the radial location of the quadrant mass center may be calculated.

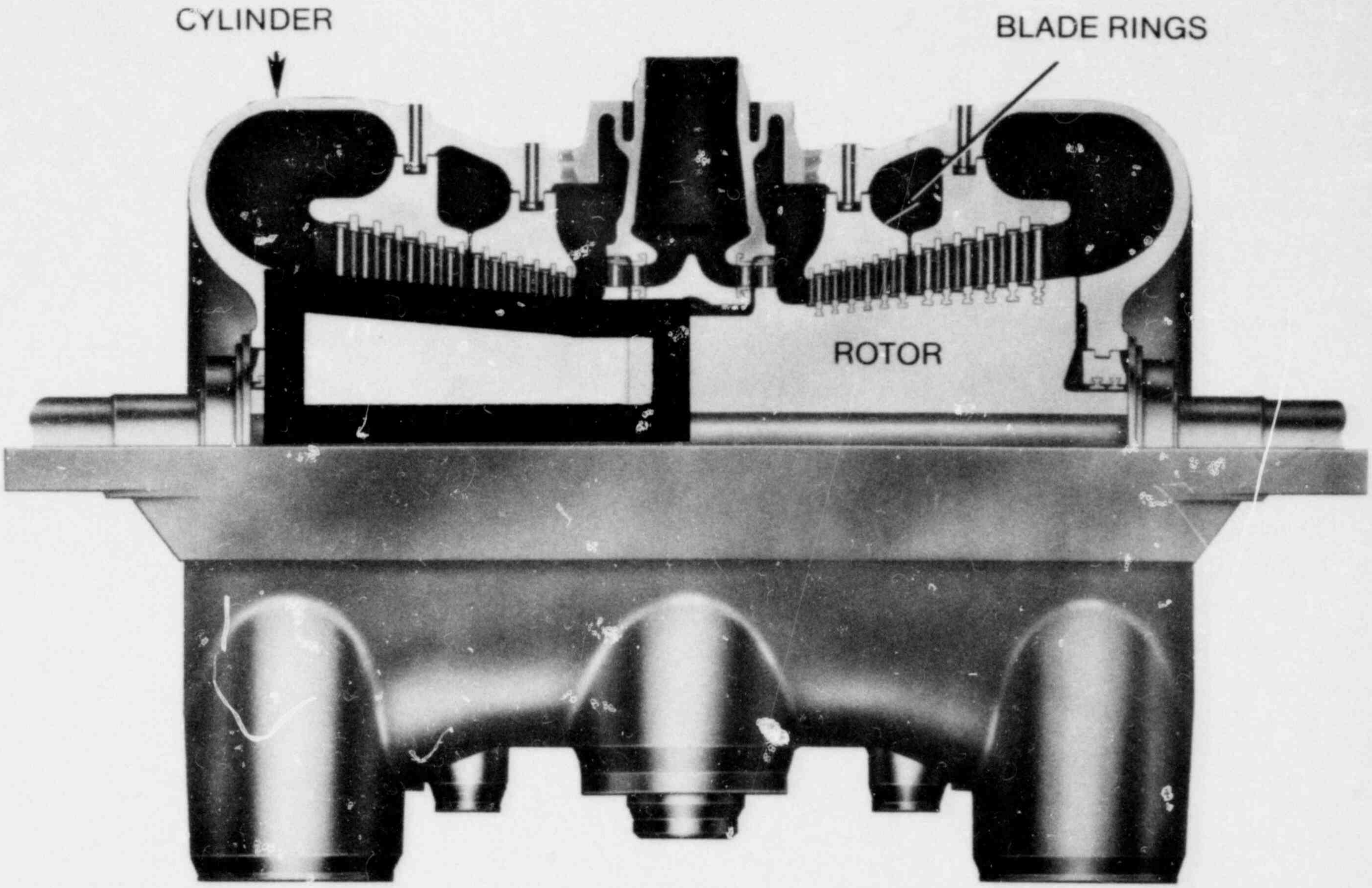

Figure 1
PARTIAL SECTION OF HP TURBINE TYPE I
A14

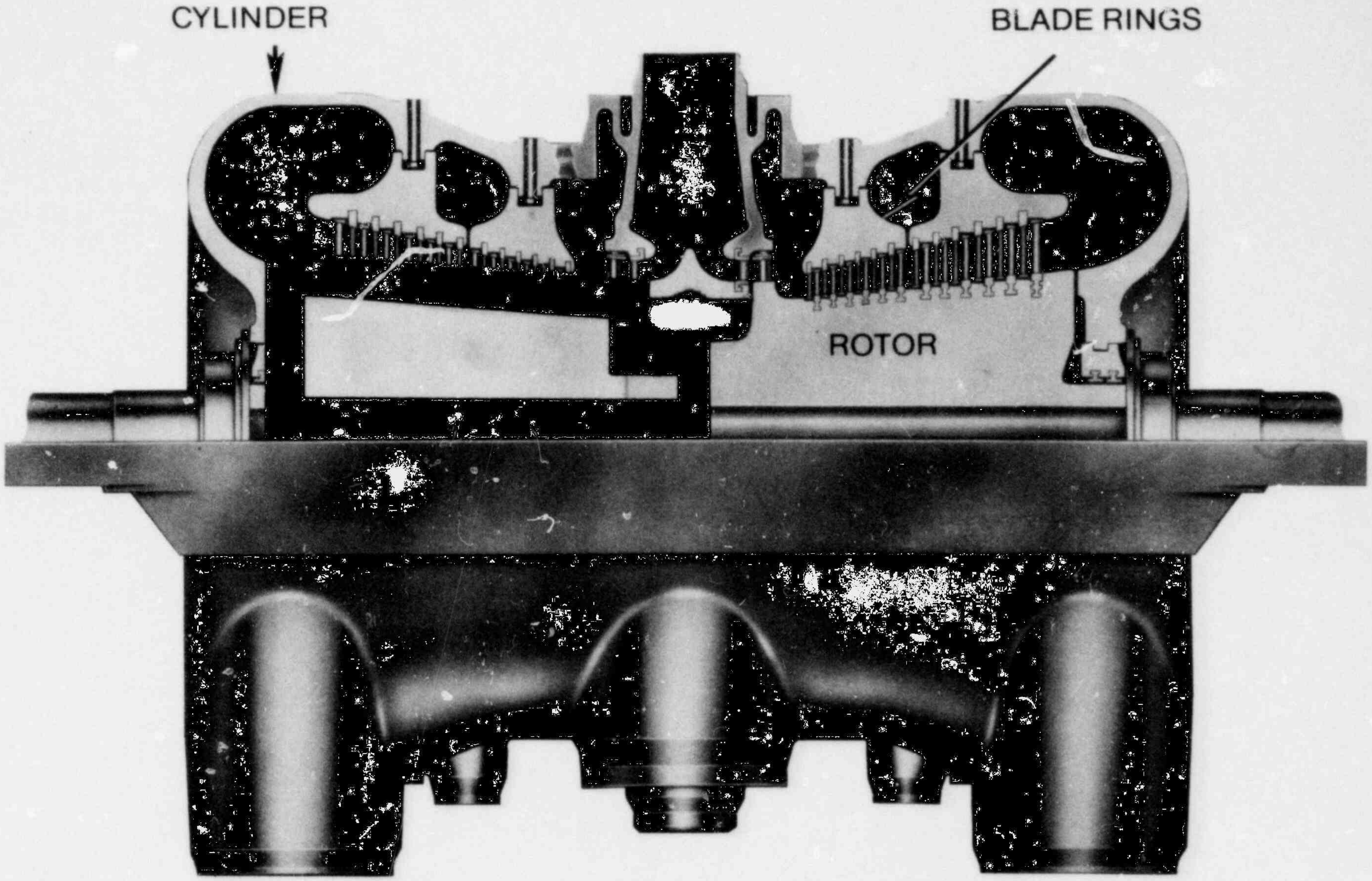

Figure 2
PARTIAL SECTION OF HP TURBINE TYPE II

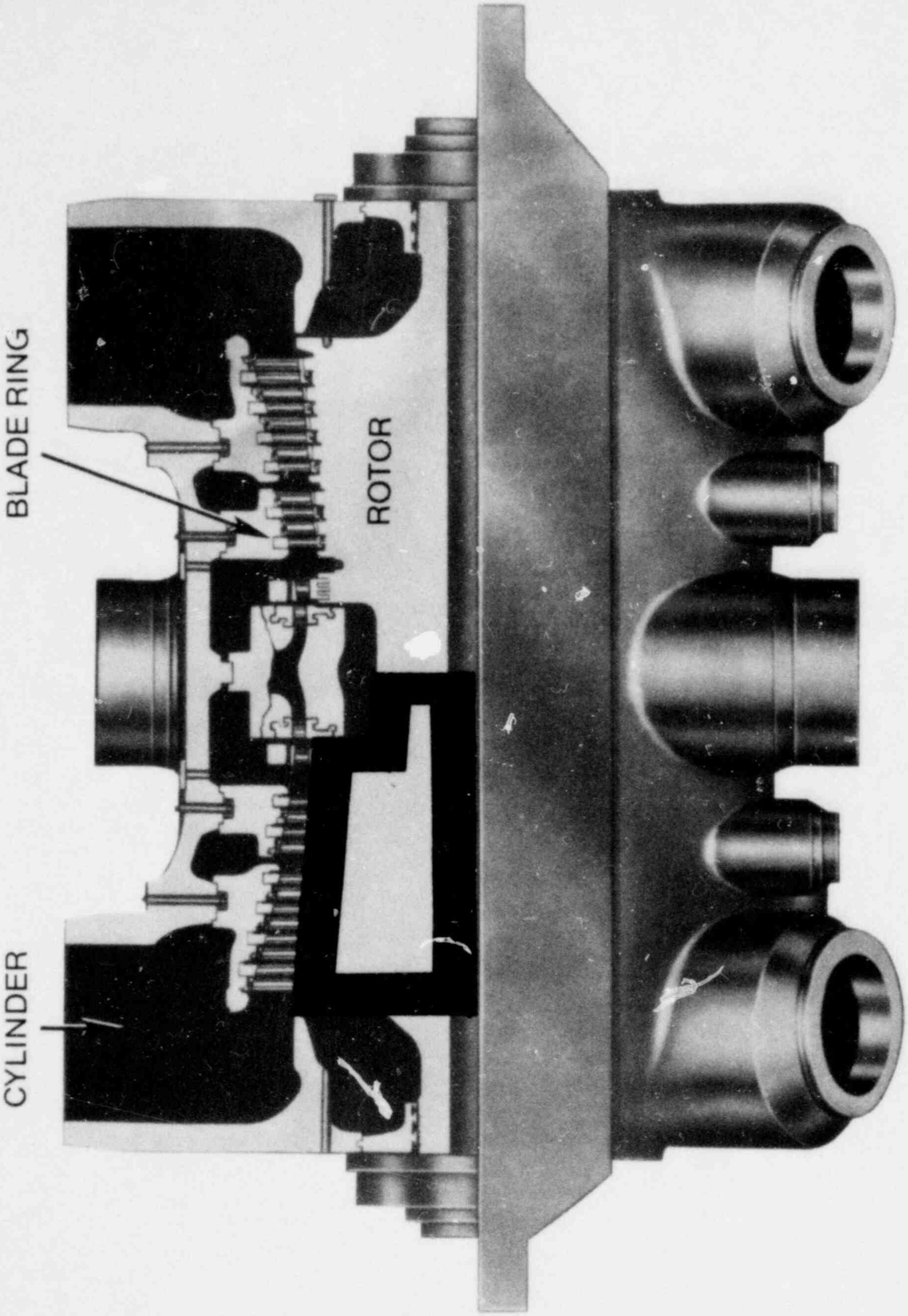

Figure 3

PARTIAL SECTION OF HP TURBINE TYPE III

2.1.2 Reaction Blade Properties

From HP rotor information tabulate on the worksheets, Fig. 4, the blade style, number of blades/row, height at exit edge, mean diameter at exit edge, shroud angle and platform angle. If the blade has a [ ]^a, use for D_R the rotor diameter at the inlet side of the blade. There is no D_O. If the blade has a [ ]^a, use for D_R the "Nom Rotor Dia" under the blade and for D_O, the rotor diameter at the inlet side of the blade, neglecting the undercut fillets. See Figures 5A, 5B for examples of geometry.

From the tabulated data the remainder of the data may be calculated.

Calculate the following data and enter on the worksheet.

Blade mean height

$$H_m = H_e + 1/2\ W_n\ (\tan\theta_p - \tan\theta_s)$$

Where Θ_p and Θ_s are positive as shown.

Blade mean radius

$$\bar{R}_b = 1/2\ \bar{D}_e - 1/4\ W_n\ (\tan\theta_p + \tan\theta_s)$$

Shroud mean radius

$$\bar{R}_s = 1/2\ (\bar{D}_e + H_e - W_n \tan\theta_s) + \bar{y}_s$$

Shroud weight/row

$$W_s = [\qquad\qquad\qquad]^a$$

ROW NO						
BLD STYLE						
BLD NOM WIDTH (IN.) W_n						
NO BLDS/ROW N_b						
BLD HT @ EXIT EDGE (IN.) H_e						
BLD MEAN DIA @ EXIT EDGE $\bar{D}_e$ (IN.)						
SHRD ANGLE (DEGREES) θ_S						
PLTFRM ANGLE (DEGREE) θ_P						
ROTOR DIA (IN.) D_R						
ROTOR DIA (IN.) D_O						
BLD MEAN HT (IN.) H_m						
BLD MEAN RAD (IN.) $\bar{R}_b$						
BLD WT/ROW (LBS.) W_b						
BLD $W\bar{R}$/ROW (IN. - LBS.) $W\bar{R}_b$						
SHRD AREA (IN.^{2}) A_S						
SHRD $\bar{Y}$ (IN.) $\bar{Y}_S$						
SHRD MEAN RAD (IN.) $\bar{R}_S$						
SHRD WT/ROW (LBS.) W_S						
SHRD $W\bar{R}$/ROW (IN. - LBS.) $W\bar{R}_S$						
PLTFRM AREA (IN.^{2}) A_P						
PLTFRM MEAN RAD (IN.) $\bar{R}_P$						
PLTFRM WT ROW (LBS.) W_P						
PLTFRM $W\bar{R}$/ROW (IN - LBS.) $W\bar{R}_P$						
ROOT STEEPLE WT/ROW (LBS.) W_r						
ROOT STEEPLE $W\bar{R}$/ROW (IN. - LBS.) $W\bar{R}_r$						
Σ WT/ROW (LBS.) W_{bi}						
$\Sigma W\bar{R}$/ROW (IN. - LBS.) $W\bar{R}_{bi}$						

Σ WT (ROWS____ THRU____) W_b = __________

$\Sigma W\bar{R}$ (ROWS____ THRU____) $W\bar{R}_b$ = __________

BLADING CF (ROWS____ THRU____) CF_b = __________

Figure 4

HP TURBINE BLD DATA WORKSHEET

[

][a]

Figure 5A
TYPICAL "T" - ROOT GEOMETRY

[

][a]

Figure 5B
TYPICAL SIDE ENTRY ROOT GEOMETRY

Shroud $\overline{WR}$/row

$$\overline{WR}_s = W_s \bar{R}_s$$

Blade weight/row

$$W_b = [\qquad\qquad]^a$$

Blade $\overline{WR}$/row

$$\overline{WR}_b = W_b \bar{R}_b$$

Platform properties

$$\bar{y}_p = \frac{h_1^2 + h_1 h_2 + h_2^2/3}{2h_1 + h_2} \qquad \text{where } h_2 = B_p \tan\theta_p$$

$$h_1 = 1/2\ (\bar{D}_e - H_e - D_R) - h_2$$

$$\bar{R}_p = 1/2\ D_R + \bar{y}_p$$

$$A_p = (1/2\ h_2 + h_1)\ B_p$$

Platform weight/row

$$W_p = [\qquad\qquad]^a$$

Platform $\overline{WR}$/row

$$\overline{WR}_p = W_p \bar{R}_p$$

If the blade has a [ ]^a the additional properties for the blade root and rotor steeple combined material must be calculated.

Root-Steeple weight/row

$$W_r = [\qquad\qquad\qquad]^a$$

Root-Steeple WR/row

$$\bar{WR}_r = 1/4\ (D_R + D_0)\ W_r$$

Sum for each row the components of weight and $\bar{WR}$. Sum also the weights and $\bar{WR}$ of all rows.

Blading CF = $K_1 \sum \bar{WR}$ where $K_1 = 1/g\ N^2\ (\pi/30)^2 = [\qquad]^a$ at N = 1800 RPM (see Sect. 2.1.3 for inclusion of loading from control stage). Use N in RPM and gravitation constant g in in/sec^2.

2.1.3 Control Stage Blade Properties

The information for the [ ]^a may be found from HP information. The exact calculation is carried out the same as for the [ ]^a. A modification is made for the [ ]^a type assembly, where the entire portion of rotor above the bottom of the groove is treated as if it were cut, the same as for a side-entry root. No credit is given to the rotor fingers for carrying tangential stress because of the pin holes. See Figures 6A, 6B for examples of geometry.

A satisfactory approximation can be made by considering the row to be composed of two or three rings of material. Calculate the weight and $\bar{WR}$ for each ring by adapting the equation for the root-steeple and summing the quantities for the row. Include the data as one of the blade rows on Fig. 4. This approximation assumes that the blade is solid up to the mean diameter and missing above that.

[

][a]

Figure 6A

CONTROL STAGE WITH SIDE ENTRY ROOT

[

][a]

Figure 6B

CONTROL STAGE WITH TRIPLE PIN ROOT

2.1.4 Rotor Properties

On the rotor drawing, mark off section of the rotor of uniform diameter, disregarding small reliefs and appurtenances. Include all of the rotor from the centerline to the end of the main body. Where the rotor has [ ][a], the sections may usually extend from the exit side of one row to the exit side of the next, except where there are changes in rotor diameter between rows or extraction zones which interrupt the blade path. In that case additional sections are added as required. See Fig. 7.

For rotors with [ ][a], the sections may extend from the exit side of the relief on the exit side of the blade to the same point on the next row, disregarding the small reliefs. Additional sections are added as necessary. Material not included as part of the blading is included as rotor. For convenience, the outer diameter (OD) of a section with a blade may be the rotor diameter ahead of the blade. For sections with tapered OD, the average diameter may be used.

Tabulate the width and outer and inner diameter of each rotor section on the worksheet, Fig. 8. For sections with blading, add to the table, the ro weight of the blading.

For each section calculate the required properties.

W_{ri} = [ ][a]

$$I_i = 1/24\ B_i\ (D_i^3 - D_B^3)$$

$$A_i = 1/2\ B_i\ (D_i - D_B)$$

For each section determine X_i, the distance from the axial centerline fracture plane to the center of the section. Multiply each section weight or sums of weight by its X and sum the whole.

[

][a]

Figure 7A

DIVISION OF ROTOR WITH "T" GROOVES

[

]a

Figure 7B

DIVISION OF ROTOR WITH SIDE ENTRY GROOVES

RTR.SECT.	B_i	D_i	D_B	$\bar{X}_i$	W_{ri}	W_{bi}	$\bar{X}_i(W_{ri}+W_{bi})$	I_i	A_i
1									
2									
3									
4									
5									
6									
7									
8									
9									
10									
11									
12									
13									
14									
15									
16									
17									
18									
SUMS	$L_T=$				$W_T=$	$W_b=$	$W\bar{X}=$	$I_R=$	$A_G=$

[ ][ab]

Figure 8
HP TURBINE ROTOR DATA WORKSHEET

On a rotor with [ ]^a the area calculated above is not all capable of carrying tangential load. It is necessary to deduct the area for the [ ]^a provided to permit blade roots to be inserted into the [ ]^a.

[

]^a See Fig. 9 for the dimension of the root and slot. The net area is found by deducting from the gross area A_G the required quantities. Obtain A_G from Fig. 8.

$$A_{N1} = A_G - 2 \sum_{i=1,3,5\ldots} (T_i e_i) - 1/2 \sum_{i=1,3,5\ldots} (T_i - a_i)(D_{i+1} - D_i)$$

$$- \sum_{i=2,4,6\ldots} A_{ri}$$

$$A_{N2} = A_G - 2 \sum_{i=2,4,6\ldots} (T_i e_i) - 1/2 \sum_{i=2,4,6\ldots} (T_i - a_i)(D_{i+1} - D_i)$$

$$- \sum_{i=1,3,5\ldots} A_{ri}$$

Net effective area A_N is the lessor of A_{N1} and A_{N2}.

Blade root areas, and entering slot side widths T (See Figure 9A) may be entered in the table, Fig. 9B for ease of use.

2.1.5 Rotor Average Tangential Stress

Calculate the average stress in the rotor due to blade forces and rotor body forces.

[ ]^a

[

][a]

Figure 9A
TYPICAL "T" ROOT ROTOR GROOVE

BLADE ROW	ENTERING SLOTS IN EVEN ROWS A_{ri}	e_i	T_i	a_i	D_{i+1}	D_i	ENTERING SLOTS IN ODD ROWS A_{ri}	e_i	T_i	a_i	D_{i+1}	D_i		
1	—							—	—	—	—	—		
2		—	—	—	—	—	—							
3	—							—	—	—	—	—		
4		—	—	—	—	—	—							
5	—							—	—	—	—	—		
6		—	—	—	—	—	—							
7	—							—	—	—	—	—		
8		—	—	—	—	—	—							
9	—							—	—	—	—	—		
10		—	—	—	—	—	—							
11	—							—	—	—	—	—		
12		—	—	—	—	—	—							
[													]a	
	=							=						

Figure 9B

HP TURBINE ROTOR DATA - "T" ROOT WORKSHEET

2.1.6 Rotor Bursting Speed Ratio

The ratio of bursting speed to running speed is

[ ][a]

where σ_{ULT} = rotor material specification minimum ultimate strength, psi

σ_{ULT} = [ ][a]

σ_{ULT} = [ ][a]

T_c = material temperature correction, Fig. 10. Estimate the temperature as the [ ][a] and exhaust temperature.

2.1.7 Rotor Fragment Weight, Velocity and Kinetic Energy

The weight, velocity of the mass center and kinetic energy of a 90° sector fragment are calculated at various ratios of speed to normal running speed.

Fragment weight W_{90} = 1/4 (Total Rotor Weight) lb. from Table, Fig. 8.

[ ][a]

[ ][a]

* [ ][a] Some units have a higher value, the correct value should be determined.

**Current practice is to calculate the HP rotor at the lowest failure speed of all the discs on the associated LP.

ω_o = 188.5 Rad/sec for 1800 RPM

K_V = [ ][a]

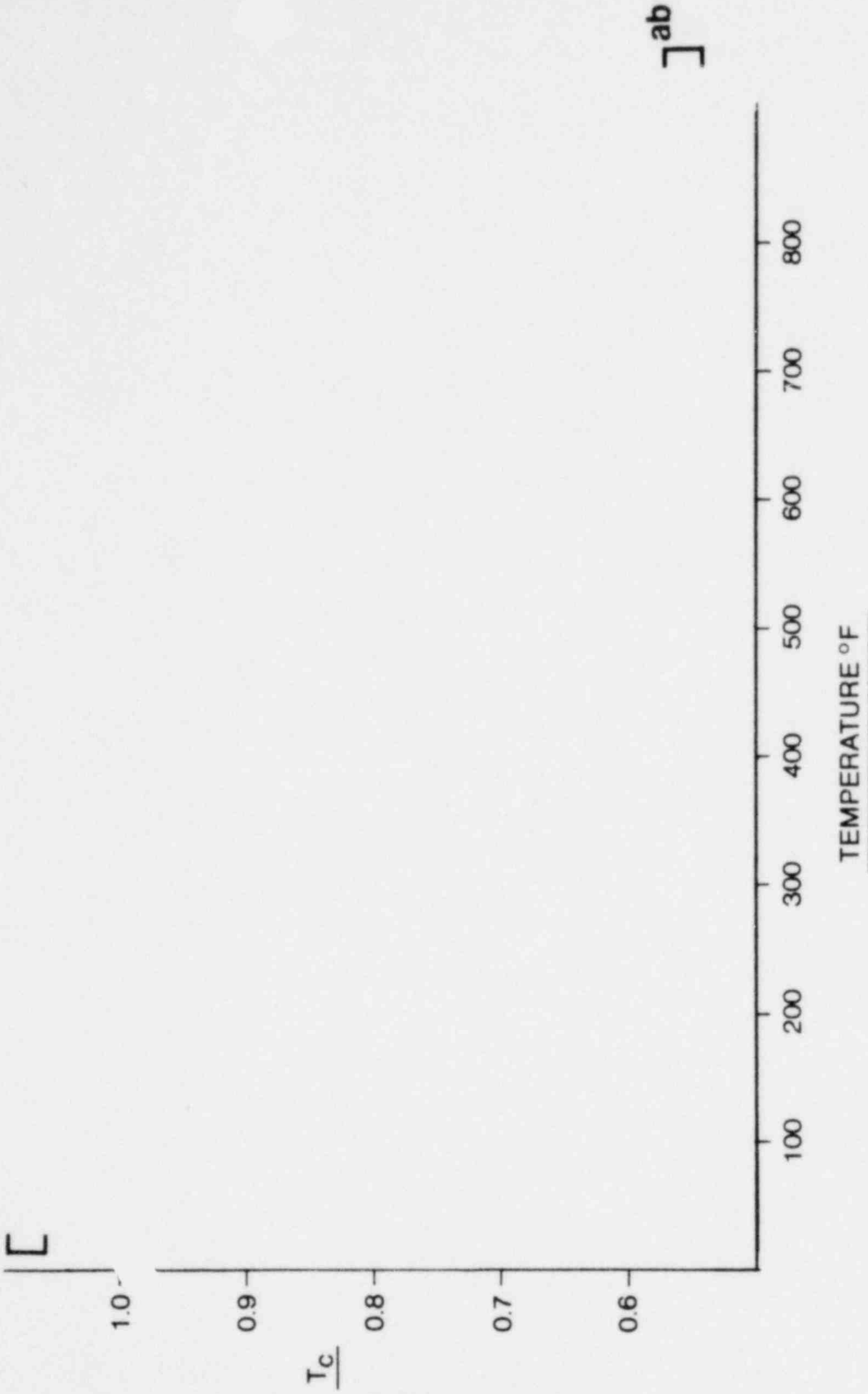

Figure 10

STRENGTH TEMPERATURE CORRECTION FACTOR

$$\theta = \frac{l\omega}{65000}$$

l = average radial thickness of main body of rotor (see Fig. 7a).

[

]a

Kinetic Energy KE = [ ]a

Report these values on the report sheet, Fig. 11.

2.1.8 HP Rotor Missile Geometry

The areas and lengths of certain views of the hypothetical HP rotor fragment are reported to the customer. Other dimensions are used to determine the affect of the rotor fragment on the turbine cylinder.

The geometric properties of the rotor fragment that are to be reported are shown in Fig. 12. The definition of additional dimensions needed to calculate the reported properties are shown in Fig. 13. Figure 14 may be used as a work sheet.

The nature of the ultimate use of the data permits a substantial simplification in the description of rotor geometry. The areas required are defined by drawing an envelope around the major rotor features. A slightly different approximation is used for areas A_1 and A_5.

[ ]a.

[

]a The area calculated is the plan view area. [

]a The length of this

(1.) $\frac{N_f}{No.}$ = ________ HP rotor

(2.) $\frac{N_f}{No.}$ = ________ (Lowest $\frac{N_f}{No}$ of LP Discs) (Disc No. ______, S.O. ______)

(3.) $\frac{N_f}{No.}$ = ________ (Highest $\frac{N_f}{No}$ of LP Discs) (Disc No. ______, S. O. ______)

90° SEGMENT MISSILE

WEIGHT = ________________ 1 = ________________ $\bar{y}$ = ________________

$\frac{N}{No}$ = 1.0 V = ____________Ft/Sec KE = ____________$\times 10^6$ Ft.Lb.

$\frac{N}{No}$ = 1.2 V = ____________Ft/Sec KE = ____________$\times 10^6$ Ft.Lb.

$\frac{N_f{}^*}{No}$ = _____ V = ____________Ft/Sec KE = ____________$\times 10^6$ Ft.Lb.

*Calc. for Item (2) Above

Figure 11

HP ROTOR INTERNAL MISSILE ENERGY - REPORT SHEET

Figure 12

HP ROTOR MISSILE GEOMETRY - REPORT SHEET

area is usually defined by the relief between the control stage and the reaction blading. On rotors where there is no relief, the length would include the seal turn under 1C out to the step-up. The area calculated is the developed area of the cone segment and represents the impact area on the blade rings. The side areas A_2 and A_4 are a mix of the outlines used for A_1 and A_5. The tapered area is the same as defined by A_5. The relief between control and reaction stages is accounted for since no material packed into this space would support an impact.

Figure 13 defines the rotor in simplest terms; the calculator may need to increase the complexity to suitably describe the rotor.

Definition of HP Rotor Fragment Dimensions (see Fig. 13). After calculating the following they are entered on Figure 14.

L_1 - Overall length, inches

L_2 - Axial length of reaction blade portion of rotor, inches

L_3 - Slant length of reaction blade portion of rotor, inches

L_4 - Overall length less central portion, inches

L_5, L_6, L_7 - Component lengths, inches

R_1 - Rotor radius at exhaust end of main body, inches

R_2 - Rotor radius at base diameter of control stage, inches

R_3 - Rotor radius at inlet end of main body or reaction blading, inches

R_4 - Rotor radius of relief, inches

R_5 - Rotor radius of central portion, inches

R_B - Rotor bore radius, inches

Figure 13

HP ROTOR MISSILE GEOMETRY - SYMBOL DEFINITION SHEET

L_1 = __________

L_2 = __________

L_4 = __________

L_5 = __________

L_6 = __________

L_7 = __________

R_1 = __________

R_2 = __________

R_3 = __________

R_4 = __________

R_5 = __________

R_B = __________

[

]a

Figure 14

HP TURBINE MISSILE GEOMETRY - WORKSHEET

Calculated Properties

$W_1 = 2 R_1 \sin 45°$

$W_2 = 2 R_2 \sin 45°$

$L_3 = [(R_1 - R_3)^2 + L_2{}^2]^{1/2}$

$A_1 = 1/2\ L_4 (W_1 + W_2)$

$A_2 = A_4 + L_1 R_B (1 - \cos 45°)$

$A_3 = 2 R_B L_1$

$A_4 = 0.5 (R_1 + R_3) L_2 + R_4 L_5 + R_2 L_6 + R_5 L_7 - R_B L_1$

$A_5 = 1/4\ \pi L_3 (R_1 + R_3)$

$A_6 = 1/4\ \pi (R_5{}^2 - R_B{}^2)$

$\bar{X}$ is calculated from mass distribution data, see Sect. 2.1.4.

2.2 Low Pressure (LP) Turbine Destructive Overspeed and Missile Energy

The rotor of an LP turbine for nuclear application must be analyzed to determine the size and energy of missiles that would result in the unlikely event a disc would burst at running speed or design overspeed. The speed at which the discs would burst must also be determined.

The rotor discs are [ ]b along radial planes containing the centerline. In the case of [ ]b, the disc is assumed to first [ ]b and then [ ]b in rapid succession. This is based on observations of the failure process of small test discs. As a result of the two step process and the finite crack growth time, two quadrants, diametrically opposite have velocity higher than the other two quadrants.

The criterion by which the failure speed is determined is the speed at which the disc [ ]b equals the [ ]b For this purpose the material maximum ultimate strength is estimated for the grade of material from data covering discs manufactured of that type of material. In the case of [ ]b, the material throughout is assumed to have the strength of the hub area.

2.2.1 Disc Average Tangential Stress

In order to determine the average tangential stress (σ_{AT}) the total outward centrifugal force from the blading and disc body forces must be calculated. In the same operation may be calculated the factors from which the radial distance of the sector mass center from the center of rotation is determined.

Calculation of the failure speed of a disc is a several step process. The σ_{AT} of a disc is dependent upon speed and the presence or absence of the blades or part of blades. Current practice is to calculate the [ ]b and then reduce the centrifical (CF) loading and system mass accordingly for all speeds above that. In the case of discs with several rows of blades, [ ]b, thereby raising further the final failure speed. On the other hand, the disc may fail before [ ]b

The criterion by which a [ ]b is when the maximum direct stress in [ ]b at point of fixity equals the material mean ultimate strength.

2.2.2 Blade Properties

For each row of blades, seven pieces of information is normally needed.

1. Maximum direct stress (psi).

2. CF of row of blades at radius of maximum stress (lbs).

3. Weight of row of blades above radius of maximum stress (lbs).

4. CF of row of blades at bottom of platform. Usually for this the CF at point of fixity may be used (lbs).

5. Weight of row of blades above bottom of platform (lbs).

6. Blade material designation.

7. Blade operating temperature (^{o}F)

Enter this information on rotor blade data sheet, Figure 15.

2.2.2.1 Parallel Section Blades

Parallel section blades used in LP turbines normally have a [ ]b from blade center to blade exit. Typical characteristics of turbine blades, for example, blade style, number of blades/row, height at exit edge, mean diameter at exit edge, shroud angle, and nominal rotor diameter and tabulated on Figure 4.

Row No.	1	2	3	4	5	6	7	8	9	10	11
Bld Style											
Blds/Row											
Bld MD @ Exit											
Pld Ht @ Exit											
Shrd & Foil Wt/Row											
Shrd & Foil & Pltfrm Wt/Row											
Shrd & Foil CF/Row											
Shrd & Foil & Pltfrm CF/Row											
Bld Base Stress											
Bld Root Stress											
Bld Max Stress											
Rad of Max Stress (R^*)											
Foil & Pltf Wt Below R^*/Row											
Foil & Pltf CF Below R^*/Row											
Stage Inlet Temp. (Given)											
Stage Avg Temp											
Bld Mtl											
Mtl Strength											
Failure Speed Ratio											

Figure 15

LP TURBINE BLADE DATA

From the tabulated data most of the remainder of the data may be calculated.

Calculate the following data and enter on the worksheet.

Blade mean height

H_m = [ ]^a

Blade mean radius

$\bar{R}_b$ = [ ]^a

Shroud mean radius

$$\bar{R}_s = 1/2\ (\bar{D}_e + H_e - W_n \tan \theta_s) + \bar{y}_s$$

Shroud weight/row

W_s = [ ]^a

Shroud $\bar{WR}$/row

$$\bar{WR}_s = W_s\ \bar{R}_s$$

Blade weight/row

W_b = [ ]^a

Blade $\bar{WR}$/row

$$\bar{WR}_b = W_b\ \bar{R}_b$$

Platform properties

h = [ ]^a

$\bar{R}_p = 1/2\ (D_R + h)$

$A_p = h\ B_p$

Platform weight/row

$W_p = [\qquad\qquad\qquad]^a$

Platform $\bar{WR}$/row

$\bar{WR}_p = W_p\ \bar{R}_p$

Root - Steeple weight/row

$W_r = [\qquad\qquad\qquad\qquad]^a$

Root - Steeple $\bar{WR}$/row

$\bar{WR}_r = 1/4\ (D_R + D_O)\ W_r$

where D_O is taken as the effective outside diameter of the disc area able to carry tangential stress. See Sect. 2.2.3.

Sum for each row the components of weight and $\bar{WR}$. Calculate row CF. Enter the data on the blade data sheet, Figure 15 and disc work sheet, Figure 16.

Calculate the direct stress due to CF at [ ]a

[ ]a

Calculate direct stress due to CF in root below [ ]a

[ ]a

DISC PROPERTIES

DISC σAT ______________________ DISC MLT'L ______________________

TANG STRESS AREA ______________________ MISSILE OUT'R RAD ______________________

DISC WEIGHT ______________________ STRESS AREA OUTER RAD ______________________

DISC WR ______________________ BORE DIA ______________________

MIN SPEC σUT ____________ AVG TEMP ____________ STRENGTH CORR. ____________

BLADE		SHRD, BLD, PLTFRM		STEEPLES		DISC σ_{AT} ADDER		DATA
ROW NO	NF/NO	WEIGHT	W$\bar{R}$	WEIGHT	W$\bar{R}$	SH, BL, PL	STEEPLES	LINE
								1
								2
								3
								4
								5

BLADE SPEED RANGE	DATA LINE COMB.	DISC TOTAL σ_{AT}	DISC NF/NO	TOTAL WEIGHT	TOTAL W$\bar{R}$	MASS RAD $\bar{R}$
1.000 < N/NO <						
< N/NO <						
< N/NO <						
< N/NO <						

MISSILE PROPERTIES

N/NO	Kv	WEIGHT, LBS	$\bar{y}$, INCHES	V FT/SEC	KE X10^{-6} FT-LB
[ ]a					
1.0					
[ ]a					
1.0	1.0				
	1.0				
	1.0				
	1.0				
	1.0				
	1.0				
[ ]a					
1.0	1.0				
	1.0				
	1.0				
	1.0				
	1.0				

Figure 16

LP DISC INTERNAL MISSILE ENERGY - WORKSHEET - REPORT SHEET

where A_r is the area of the root at the point of fixity.

The failure speed ratio is determined by:

[ ]^a

where σ_{ULT} is the blade mean ultimate strength at operating temperature and σ_D is the larger of σ_{BL} or σ_R. Enter this value on Figure 15 and Figure 16.

2.2.2.2 Tapered Section Blades

Calculate $\bar{WR}_B$/row for [ )]^a

[ ]^a

where $K_1 = 1/g\ (N\pi/30)^2 = 92.048$ at N = 1800 RPM.

Calculate the weight and WR for Root-Steeple as in Section 2.2.2.1. Enter the weight and WR data on Figure 15 and Figure 16.

Calculate the failure speed ratio

[ ]^a

as in Section 2.2.2.1 except examine the data for the possibility of a direct stress being greater in the [ ]^a at some other radius than the base.

If the maximum stress is in [ ]^a, then on the disc worksheet enter a second line for $N/N_0 > N_f/N_0$ for which weight and $\bar{WR}_B$ is zero. If the maximum stress is at the [ ]^a or higher, enter a second line for that row for which:

$W_B = W_B$/row - (Weight per row of lost portion)

[ ][a]

where CF* is the CF force of one blade at radius of failure. Since it is assumed that failure does not occur in the steeple, the weight per row and WR per row of the Root-Steeple is added in full to the disc and remaining blade values.

2.2.3 Disc Properties

The disc properties needed are:

1. Cross section stress area, A_T
2. Disc weight W_D
3. Second moment of cross section area about axis of rotation - usually termed I
4. Disc free bore average tangential stress, σ_{AT}
5. Disc product of weight x radius to center of mass, $W\bar{R}_D$

Some of these properties are related.

$W\bar{R}_D = \gamma(2\pi)I$ where γ is the material density, [ ][a]
[ ][a]

Much of the data may be available for previously designed discs. For the purpose of the missile calculation it will be assumed the stress is [ ][a], therefore the full dimensions must be used. This also assures that the full weight will be used. For simplicity small lips at the rim and hub and small undercuts may be disregarded. For the seal lip this is offset by some energy being absorbed in shearing it off that is not accounted for. Larger seal lips should be included for weight and stress area, etc.

The outside diameter of the disc stress area is taken at the bottom of the [ ][a] except in the case of multiple blade row discs where the outer diameter of the disc between the steeples may be used if the difference is small.

Enter the disc free bore σ_{AT}, tangential area A_T, disc weight and $W\bar{R}$ at the top of Figure 16.

2.2.4 Disc Average Tangential Stress and Bursting Speed Ratio

The component of disc stress due to blade and steeple loading is:

[ ][a]

using corresponding values of $W\bar{R}$. Enter the data on the worksheet.

In the third zone of the worksheet, show the disc total σ_{AT}, weight and $W\bar{R}$ that would exist for the various speed intervals defined by the successive failure of blades on the assumption that the disc has not failed.

Calculate mass center radius:

$\bar{R}$ = Total $W\bar{R}$/Total W

For the same line, calculate the speed at which the disc would fail if no change of blade loading occurs.

[ ][a]

where σ_{ULT} = disc material specification minimum ultimate strength, psi, see Table 1.

T_c = material temperature correction, Figure 10.

Disc average temperature is estimated as the average of [ ]^a for all discs except the last. For the last disc, the exhaust side temperature should be the [ ]^a. This is [ ]^a for nuclear units.

TABLE 1

DISC MATERIAL SPECIFICATIONS

Material	Min. σ_{ULT}, psi	Material	Min. σ_{ULT}, psi
A	[ ]^a	F	[ ]^a
B	[ ]^a	P	[ ]^a
C	[ ]^a	Q	[ ]^a
D	[ ]^a	S	[ ]^a
E	[ ]^a	T	[ ]^a

If the failure ratio for this disc is lower than that for any of the blades, the disc is assumed to fail with all blades intact. If the failure ratio for the disc is higher than that for one or more rows of blades, the blades are assumed to fail before the disc when loaded as calculated. It is then necessary to remove blade loading assumed lost and determine disc failure again, repeating the process until the true disc failure speed is determined.

2.2.5 Disc Fragment Weight, Velocity and Kinetic Energy

The weight, velocity of mass center and kinetic energy of sectors of 90°, 120° and 180° included angle are calculated at various ratios of speed to normal running speed.

For the three sizes, enter the weight of the disc fragment at running speed ($N/N_0 = 1.0$), design overspeed [

]^a and, disc failure speed from Section 2.2.4, accounting for the possible loss of blades before the speed concerned. After all of the discs of a given unit have been finished, the lowest failure ratio from all the discs is used as a common value for all discs and the corresponding energy determined.

For 90° disc fragment

$W_{90} = W_{TOTAL}/4$ (lbs.)

[ ]^a

$V_{90} = \omega K_v \bar{y}/12$ ft/sec

$\omega = 1.0\ \omega_0,\ 1.2\ \omega_0$ etc. as defined above

$\omega_0 = 188.5$ Rad/sec for 1800 RPM

[ ]^a

$\theta = l\omega/65000$ rad

l = radial thickness of disc stress area

[ ]^a

[ ]^a

For 120° disc fragment

$W_{120} = W_{TOTAL}/3$ lb

[ ]^a

$$V_{120} = \omega \bar{y}_{120}/12 \text{ ft/sec}$$

$$KE_{120} = 1/2\ (1/32.2)\ W_{120}\ V_{120}^2 \text{ ft-lb}$$

For 180° disc fragment

$$W_{180} = W_{TOTAL}/2 \text{ lb}$$

$$\bar{y}_{180} = [\qquad\qquad]^a$$

$$V_{180} = \omega \bar{y}_{180}/12 \text{ ft/sec.}$$

$$KE_{180} = 1/2\ (1/32.2)\ W_{180}\ V_{180}^2 \text{ ft-lb}$$

Summarize the missile information on the LP Turbine Internal Energy Summary, Figure 17.

2.2.6 LP Disc Missile Geometry

The areas and lengths of certain views of the hypothetical LP disc fragments are reported to the customer. The geometric properties of the disc fragment to be reported are shown in Figure 18.

The dimensions of the missile are based on the following assumptions:

1. The outside radius of the missile is equal to the [ ]^a radius on single row discs and the average of [ ]^a on multi-row discs. Also enter Missile Outer Radius on Figure 16.

2. The disc, even if asymmetric about the center plane of the disc web, is symmetric (by using [ ]^a and adjusting positions).

Lowest Frame Burst Speed

$\frac{N_f}{No.}$ = ____________________ Disc No. ________________ End ____________ LP No. ____

Greatest Internal Energy at Frame Burst Speed

Disc No.	LP No.	End	Weight LB	Velocity Ft/Sec	Energy Ft-Lb x 10^{-6}	Disc. Temp. ^{o}F
1						
2						
3						
4						
5						
6						

Greatest Burst Speeds and Energy

Disc No.	$\frac{N_f}{No.}$	LP No.	End	At Burst			Disc Temp. ^{o}F
				Weight Lb	Velocity Ft/Sec	Energy Ft-Lb x10^{-6}	
1							
2							
3							
4							
5							
6							

Note: The discs listed under "Greatest Internal Energy at Frame Burst Speed" do not necessarily generate the greatest external missile due to differences in cylinder structure.

Figure 17

LP TURBINE INTERNAL MISSILE ENERGY - SUMMARY - REPORT SHEET

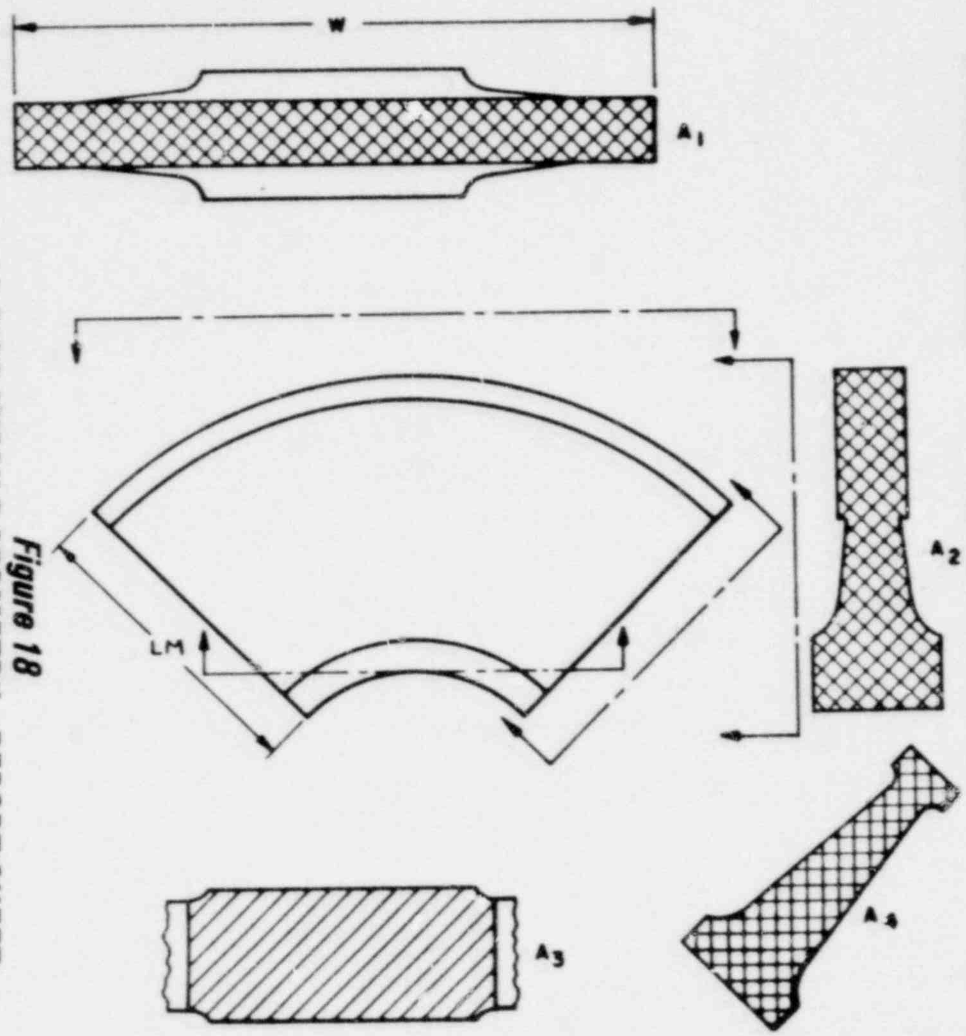

TABLE 3.

DISC DIMENSIONS AND IMPACT AREAS FOR 90° MISSILES

DISC NO.	1	2	3	4	5	6
A1 (SQ. FT.)						
A2 (SQ. FT.)						
A3 (SQ. FT.)						
A4 (SQ. FT.)						
W (FT)						
LM(FT)						

TABLE 4.

DISC DIMENSIONS AND IMPACT AREAS FOR 120° MISSILES

DISC NO.	1	2	3	4	5	6
A1 (SQ. FT.)						
A2 (SQ. FT.)						
A3 (SQ. FT.)						
A4 (SQ. FT.)						
W (FT)						
LM(FT)						

TABLE 5.

DISC DIMENSIONS AND IMPACT AREAS FOR 180° MISSILES

DISC NO.	1	2	3	4	5	6
A1 (SQ. FT.)						
A2 (SQ. FT.)						
A3 (SQ. FT.)						
A4 (SQ. FT.)						
W (FT)						
LM(FT)						

Figure 18
LP DISC MISSILE GEOMETRY - REPORT SHEET

The dimensions to be reported are:

W = chord length of sector at outside radius. (in.)

LM = radial length from IR to OR, i.e. from disc bore to blade base radius. (in.)

A_1 = area of view of rim = W x rim width. in^2.
The rim width is determined as follows.

Case 1: For discs with lightweight sealing areas that are less than [ ][a] in radial thickness next to the steeples, the rim width is taken to be the steeple width or the total width across the steeples on multi-row discs.

Case 2. For discs with heavy sealing areas that are greater than [ ][a] in radial thickness next to the steeples, the rim width is taken out to that width where the radial thickness equals [ ][a]. This rule is approximate and may be adjusted either way as the case warrants.

A_2 = area of a side view shadow projected onto a plane parallel to the bisecting plane of the sector. (in^2)

A_3 = For 90° and 120°, area of a section plane that is tangent to the disc bore and perpendicular to the bisecting plane of the sector. For 180°, area of a section plane through the diameter plus the projected area of the disc bore on the section plane. (in^2)

A_4 = area of a section plane showing the tangential face of the disc. A_4 is the same for all sector sizes. (in^2)

3. References

1. "The Containment of Disc Burst Fragments By Cylindrical Shells." A. C. Hagg and G. O. Sankey. ASME Paper No. 73-WA/PWR2 August 1, 1973

Appendix A

Position of Mass Center of Sector

The disc profile may be divided into a number of thin circular arcs of radial thickness t_i, thickness through the plane b_i and mean radius R_i. The arc size of pieces of a sector is 2α. See Figure A1.

For a single thin ring of radial thickness t, width b, mean radius $\bar{R}$ and arc size 2α, the position of the center of area on the plane face and thus the CG of the mass is at

$$\bar{y} = \bar{R} \frac{\sin \alpha}{\alpha}$$

The weight of a single section is

$$W = 2\alpha \bar{R} t b \gamma$$

Using the technique for finding the center of mass of a composite compute $\bar{Y}$ as follows:

[ ]a

where I is recognized as the second moment of area of the tangential face cross section and S is the first moment of the same area, both about the center of the disc. See Figure A2.

The value $I/S(=\bar{R})$ can be identified as the radius of a thin ring whose sector will have the same mass center as the disc sector. It must be distinguished from the radius to the center of area of the tangential face which is

$$\bar{R}_A = \frac{\sum \bar{R}_i t_i b_i}{\sum t_i b_i} = \frac{S}{A}$$

[

]a

Figure A1
RADIAL DISC SECTION

[

]a

Figure A2
DISC INTEGRATION

For a parallel sided disc segment, the summations may be integrated, yielding

[ ]^a

For convenience in the missile calculation, it is desirable to have factors that can be determined for a complete disc and applied to sectors of any size.

For any sector size

[ ]^a

and weight

$$W = 2\alpha(\sum \overline{R}_i t_i b_i)\,\gamma$$

so that the weight moment is

$$W\overline{y} = \frac{\sin \alpha}{\alpha}\,(2\alpha)\,(\sum \overline{R}_i^{\,2} t_i b_i)\,\gamma = \frac{\sin \alpha}{\alpha}\,[\gamma(2\alpha)I]$$

For a full circle, the value of $W\overline{y}$ will be $(\frac{2\pi}{2\alpha})$ times as great, although without physical meaning. Let $[\gamma(2\pi)I]$ be then identified as the weight of a full ring times a radius value $\overline{R}$, i.e., $W\overline{R}$, such that when $\overline{R}$ is multiplied by a sector size function $(\sin \alpha/\alpha)$, the result is the distance to the mass center $\overline{y}$ for that sector.

[ ]^a

For composite bodies, i.e., disc plus blades, a similar development is possible by adding more components.

For sum of rotor disc and blades:

[ ]^a

Relation between centrifugal force, K_3, K_1, I, $W\bar{R}$, and σ_{AT}:

The fundamental definition of $CF = \frac{W}{g} \omega^2 \bar{R}$

$$\therefore CF = \frac{W}{g} \left(\frac{N}{60} \times 2\pi\right)^2 \bar{R} = \left[\frac{N^2}{g} \times \left(\frac{\pi}{30}\right)^2\right] W\bar{R}$$

$$\text{Define } K_1 = \left[\frac{N^2}{g} \left(\frac{\pi}{30}\right)^2\right]$$

[ ]^a

[ ]^a

The commonly used equation for disc σ_{AT} is

[ ]^a

For body force and external loading fractions

$$\sigma_{AT1} = \frac{2K_3 I}{A} = \frac{2K_3(2\pi I)}{2\pi A} = \frac{(\gamma K_1)(2\pi I)}{2\pi A} = \frac{K_1 (W\bar{R})}{2\pi A}$$

Similarly for the external load $\sigma_{AT2} = \frac{K_1(W\bar{R})}{2\pi A}$

Therefore $\sum \sigma_{AT} = \frac{K_1 \sum \overline{WR}}{2\pi A}$

The value of $\overline{WR}$ for a row of blades is found from the fundamental relation.

$$\overline{WR} = \frac{\text{Row CF}}{K_1}$$

Appendix B

Disc Fragment Velocity Augmentation Factor

When a disc fragment rotating about its mass center fragments into two parts, one fragment has higher velocity than the other. For a 180° sector fragmenting into 90° sectors, the development is given in Reference 1. This concept may be extended to a fragment of any size subdividing into sectors of arbitrary size.

Let the initial fragment size be angle β with mass center at CG_β. See Figure B1. The distance from "O" to CG_β.

$$\bar{y}_\beta = \frac{\sin(\beta/2)}{(\beta/2)}\bar{R} \quad , \beta \text{ radians} \quad (\text{See Appendix A for definition of } \bar{R})$$

For the potential subfragment with angle θ the distance is

$$\bar{y}_\theta = \frac{\sin(\theta/2)}{(\theta/2)}\bar{R} \quad , \theta \text{ radians}$$

$$\bar{y}_\theta > \bar{y}_\beta \text{ always}$$

The angle between the radius vectors through $\bar{y}_\beta$ and $\bar{y}_\theta$ is

$$\beta - \beta/2 - \theta/2 = \frac{(\beta-\theta)}{2} = \frac{\phi}{2} \text{ radians}$$

The distance between CG_β and CG_θ is

$$D^2 = \bar{y}_\beta^{\,2} + \bar{y}_\theta^{\,2} - 2\bar{y}_\beta\,\bar{y}_\theta \cos(\phi/2)$$

See Figure B2.

Also $\bar{y}_\theta^{\,2} = D^2 + \bar{y}_\beta^{\,2} - 2D\bar{y}_\beta \cos\alpha$

or $\cos\alpha = \dfrac{D^2 + \bar{y}_\beta^{\,2}\ \bar{y}_\theta^{\,2}}{2D\bar{y}_\beta}$

Let angle $\gamma = \frac{\pi}{2} - \alpha$ radians

The rotations of the fragment with angle β about CG_β during the time required for refracture is

$$\delta = \frac{\omega l}{U}$$

where ω = angular velocity, radians/sec.
l = radial length of crack path, inches
U = crack growth velocity, inches/sec.

The position of the CG's and vectors then moves from the position shown in Figure B2 to that shown in Figure B3, which is the position when the θ fragment becomes free. The velocity components of CG_θ in Figure B3 are

$$V_x = \omega\bar{y}_\beta - \omega D\sin(\gamma-\delta)$$

$$V_y = \omega D\cos(\gamma-\delta)$$

or using relations for difference of angles,

$$V_x = \omega\bar{y}_\beta - \omega D\cos(\alpha+\delta)$$

$$V_y = \omega D\sin(\alpha+\delta)$$

$$V_{CG\theta} = V_x \overrightarrow{+} V_y$$

Since K_V is the augmentation factor applied to the simplistic velocity of CG_θ

$$K_V = \frac{V_{CG\theta}}{\omega\bar{y}_\theta}$$

[

][a]

Figure B1

DISC FRAGMENT

[[

][a]][a]

Figure B2 *Figure B3*

CG RELATIONSHIPS

The mass radius $\bar{R}$ and rotational speed ω appear in all the various quantities except δ is such a way that K_V is independent of $\bar{R}$ and dependent on ω only in determining δ.

Figure B4 shows how K_V varies with fragment size for a typical $l = 26$ inches at 1800 RPM ($\omega = 188.5$), at 1.2 x 1800 RPM ($\omega = 226.2$), and at 1.9 x 1800 RPM ($\omega = 358.15$) for $\beta = \pi$ and $\beta = 2\pi/3$.

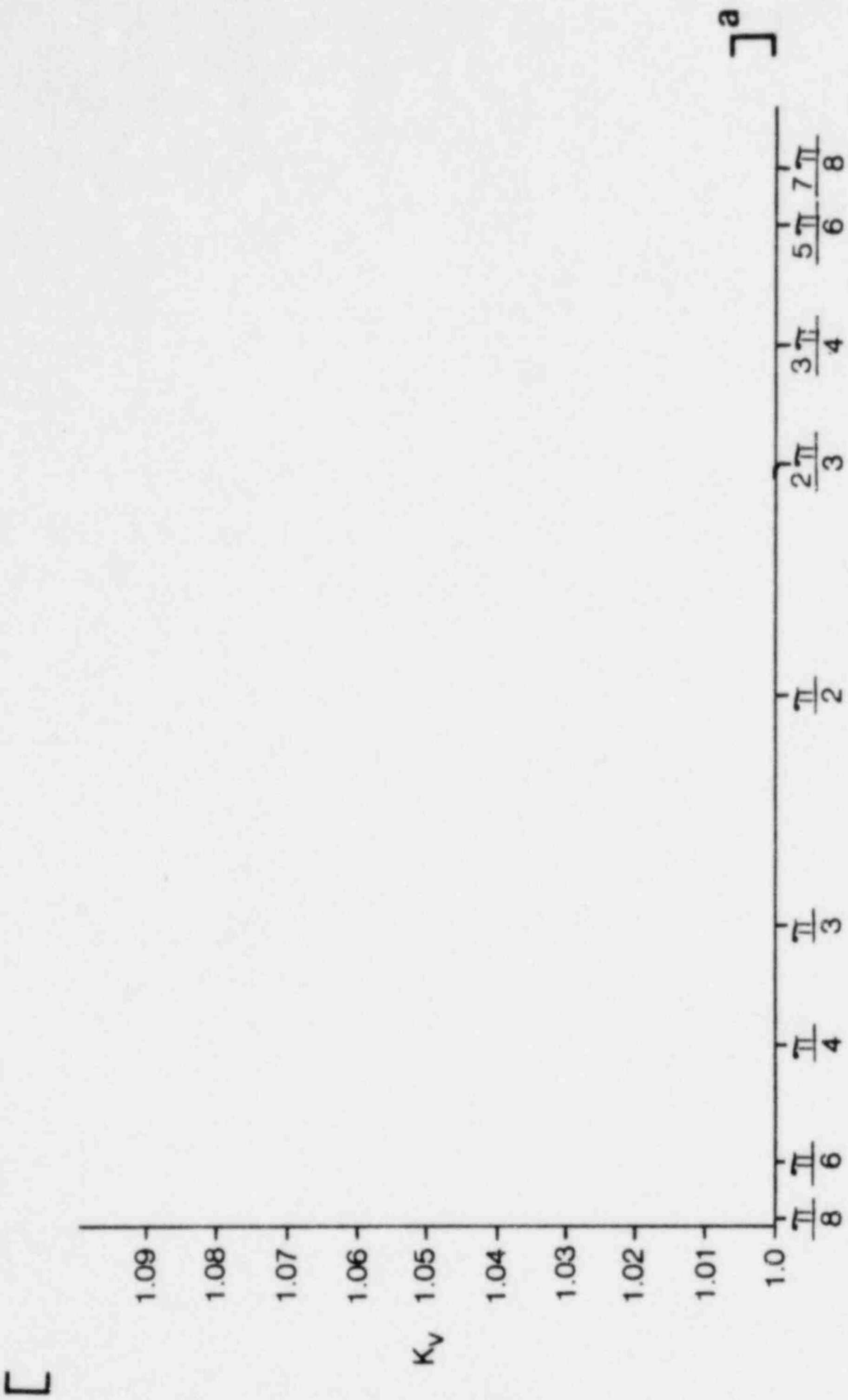

Figure B4

VARIATION OF K_V WITH FRAGMENT SIZE

Appendix C

Fragment Subdivision Study

The analytical basis for the tendency of fragments of arbitrary size to break down into smaller fragments is now described.

Assume that a disc is rotating about its center with angular velocity ω. Because of a pre-existing crack, the disc fractures in a [ ][a]. In this situation the disc stresses are completely [ ][a]. [ ][a]

Depending on the angular size of the fragment under study, the fragment will continue to rotate about the original center because it is captured on the rotor ($\beta > 180$) or will translate and rotate about the CG of the free fragment ($\beta < 180$).

The highest elastic stress in the original and fragmented states is at the bore of the disc. The disc is assumed to have pre-existing cracks of nearly critical size distributed equally around the bore. Since the first failure would be due to a crack in an elastic stress field, if the elastic stress at any point around the bore of the fragment equals or exceeds the original whole disc bore stress, a second failure to a smaller size can be assumed equally likely to occur.

The test for refracture then will be the ratio of total elastic stress at the bore after fracture to the whole disc bore stress. Any angular position where the ratio $\geq$ 1.0 is a likely failure site.

Case 1 - Partial Disc of Sector $\beta > 180^0$

Fragment rotates about center "O". See Figures C1 and C2.

The stress at point P has a direct force component and a bending component.

Radius to CG_θ, $\bar{y}_\theta = \frac{\sin(\theta/2)}{\theta/2}\bar{R}$

Weight of θ sector $W_\theta = W(\frac{\theta}{2\pi})$ where W is weight of full disc, including blades, if applicable.

CF of sector $CF_\theta = \frac{W_\theta}{g} \times \bar{y}_\theta \times \omega^2$

$$= \frac{W\bar{R}}{g}\omega^2 \frac{\sin(\theta/2)}{\pi}$$

$$= K_1 (W\bar{R}) \frac{\sin(\theta/2)}{\pi}$$

The forces normal and parallel to the stress plane are

$W_{\theta N} = CF_\theta \times \sin(\theta/2)$

$F_{\theta S} = CF_\theta \times \cos(\theta/2)$

Direct stress $\sigma_D = \frac{F_{\theta N}}{A_T}$

Bending moment on disc tangential face

$$M = F_{\theta s}\, \bar{y}_{\theta} \sin \theta/2 - F_{\theta N}\, (\bar{y}_{\theta} \cos \theta/2 - \bar{r}_A)$$

where $\bar{r}_A$ is radius to center of area of tangential face

Since the disc is a beam of high curvature, the bending stress is determined from curved beam equations

$$\text{Let } H = \frac{A_T}{\int \frac{dA}{r}}$$

Bending stress at P, radius R_i

$$\sigma_B = \frac{M}{A_T} \frac{(H-R_i)}{R_i(\bar{r}_A-H)} \qquad \bar{r}_A > H$$

Total stress at P

$$\sigma = \sigma_D + \sigma_B$$

Case 2 - Partial Disc of Sector $\beta < 180$

Fragment rotates about CG_β. See Figure C3.

The stress at P has a direct force component and a bending component.

Radius to CG_θ, $\bar{y}_\theta = \frac{\sin(\theta/2)}{\theta/2}\bar{R}$

Radius to CG_β, $\bar{y}_\beta = \frac{\sin(\beta/2)}{\beta/2}\bar{R}$

From Figure C1, where θ is the size of the trailing piece, ϕ is the size of the leading piece. The angle between the radius vectors through CG_β and CG_θ is

$$\beta - {}^{\beta}/_{2} - {}^{\theta}/_{2} = \frac{\beta-\theta}{2} = {}^{\phi}/_{2}$$

CASE 1

FRAGMENT $\beta \geq 180°$

[[

]^{a}]^{a}

Figure C1 *Figure C2*

CASE 2

FRAGMENT $\beta < 180°$

[

ANGLE BETWEEN CF_{θ} & $F_{\theta N}$, THE NORMAL TO THE STRESS PLANE = $\left(\frac{\phi}{2} - \frac{\theta}{2}\right) - (90° - \alpha)$

]^{a}

Figure C3

The distance between CG_β and CG_θ

$$D^2 = \bar{y}_\beta^{\,2} + \bar{y}_\theta^{\,2} - 2\bar{y}_\beta \bar{y}_\theta \cos \varphi/2$$

Since the β fragment is assumed to be rotating about CG_β, the CF of the θ portion is directed along line $CG_\beta \rightarrow CG_\theta$. The angle between the CF vector and the normal to the stress plane is δ, where

$$\delta = (\frac{\varphi}{2} - \frac{\theta}{2}) - (\frac{\pi}{2} - \alpha)$$

Through manipulation of various angle relations

$$\alpha + \gamma + {}^{\varphi}/_{2} = \pi$$

$$\gamma + {}^{\varphi}/_{2} - \frac{\pi}{2} = \frac{\pi}{2} - \alpha$$

$$\delta = ({}^{\varphi}/_{2} - {}^{\theta}/_{2}) - (\gamma + {}^{\varphi}/_{2} - {}^{\pi}/_{2})$$

$$\delta = \frac{\pi}{2} - \gamma - {}^{\theta}/_{2}$$

$$\bar{y}_\beta^{\,2} = D^2 + \bar{y}_\theta^{\,2} - 2D\,\bar{y}_\theta \cos \gamma$$

$$\cos \gamma = \frac{D^2 + \bar{y}_\theta^{\,2} - \bar{y}_\beta^{\,2}}{2D\bar{y}_\theta}$$

Calculate δ from above.

The weight of the θ segment is

$$W_\theta = W(\frac{\theta}{2\pi})$$

The CF of the θ segment is

$$CF_\theta = \frac{W_\theta}{g}\,\omega^2 D = \frac{W_\theta}{2\pi g}\,\omega^2 D$$

Resolved on the stress plane

$$F_{\theta N} = CF_{\theta} \cos \delta$$

$$F_{\theta s} = CF_{\theta} \sin \delta$$

The direct stress $\sigma_D = \dfrac{F_{\theta N}}{A_T}$

Vector $F_{\theta N}$ intersects the stress plane at radius $y_{\theta} \cos \theta/2$. The moment of $F_{\theta N}$ is

$$M = -F_{\theta N} (y_{\theta} \cos {}^{\theta}/_{2} - \bar{r}_A)$$

The moment for $F_{\theta s}$ is

$$M = F_{\theta s} \, \bar{y}_{\theta} \sin {}^{\theta}/_{2}$$

The total moment

$$M = F_{\theta S} \left(\frac{\sin^2 {}^{\theta}/_{2}}{{}^{\theta}/_{2}} \bar{R}\right) - F_{\theta N} \left(\frac{\sin {}^{\theta}/_{2} \cos {}^{\theta}/_{2}}{{}^{\theta}/_{2}} \bar{R} - \bar{r}_A\right)$$

Then the bending stress at disc bore is

$$\sigma_B = \frac{M}{A_T} \frac{(H - R_i)}{R_i(\bar{r}_A - H)} \text{ as for } \beta > \pi$$

Total stress at P

$$\sigma = \sigma_D + \sigma_B$$

Appendix D

HP Rotor Ultimate Strength Limits

The upper limit of HP rotor ultimate strength to be used for all HP rotor failure speed calculations were determined by surveying the population of rotors already manufactured. The breakdown of rotors and materials is shown below:

HP TYPE	NO.	MAT. SPEC	NO. OF SPECIMENS
[	]b	[	]b
[	]b	[	]b
		[	]b
[	]b	[	]b
Total specimens		[	]b
		[	]b

The specimens were sorted by location and ranked by strength range in excess of minimum specification value. The results are charted on Figures D1 and D2. From this data it was decided to use a [ ]b increment to the specification minimum as the uniform estimate of the maximum expected ultimate.

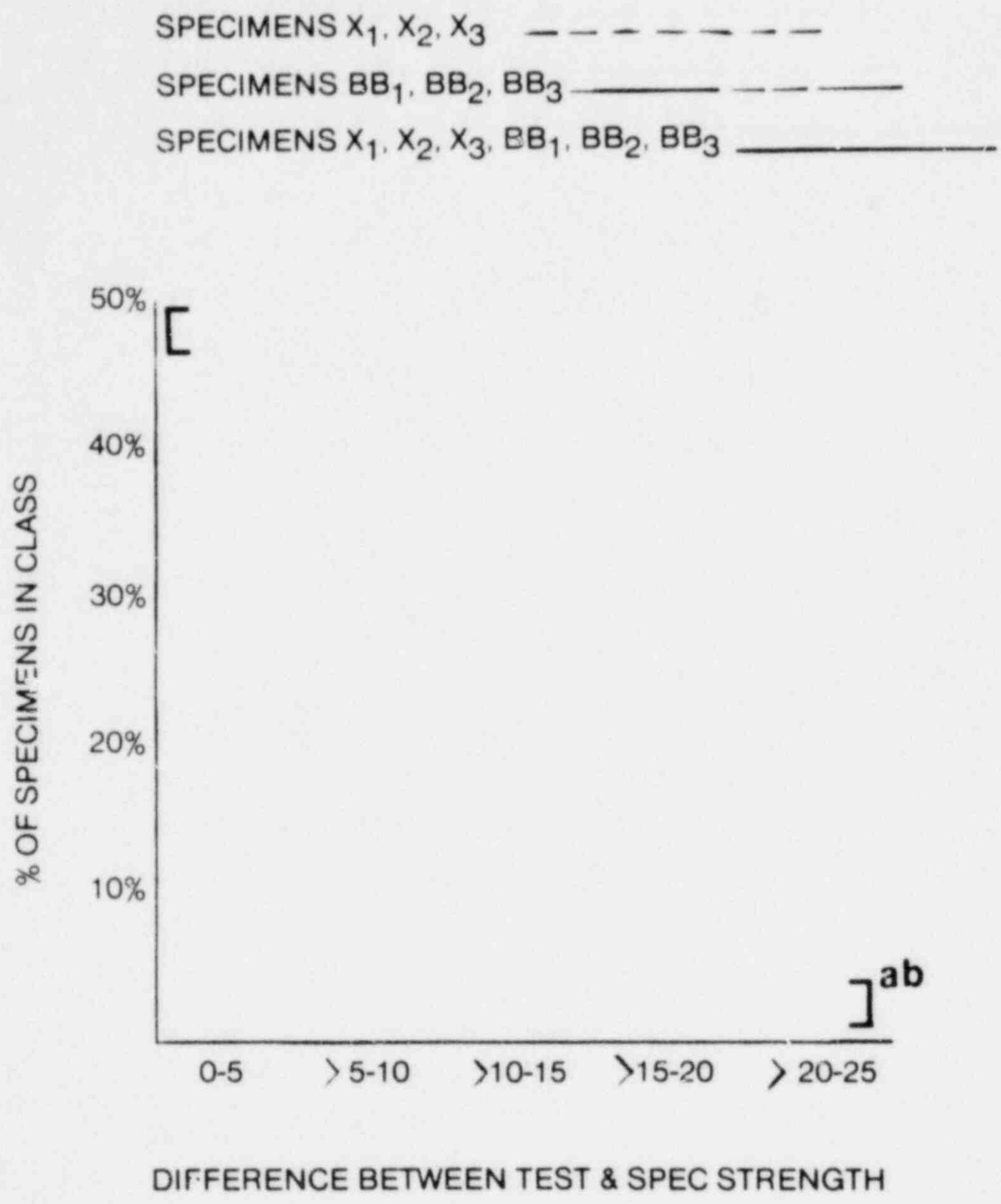

Figure D1
HP ROTOR FORGING ULTIMATE STRENGTHS MTL A

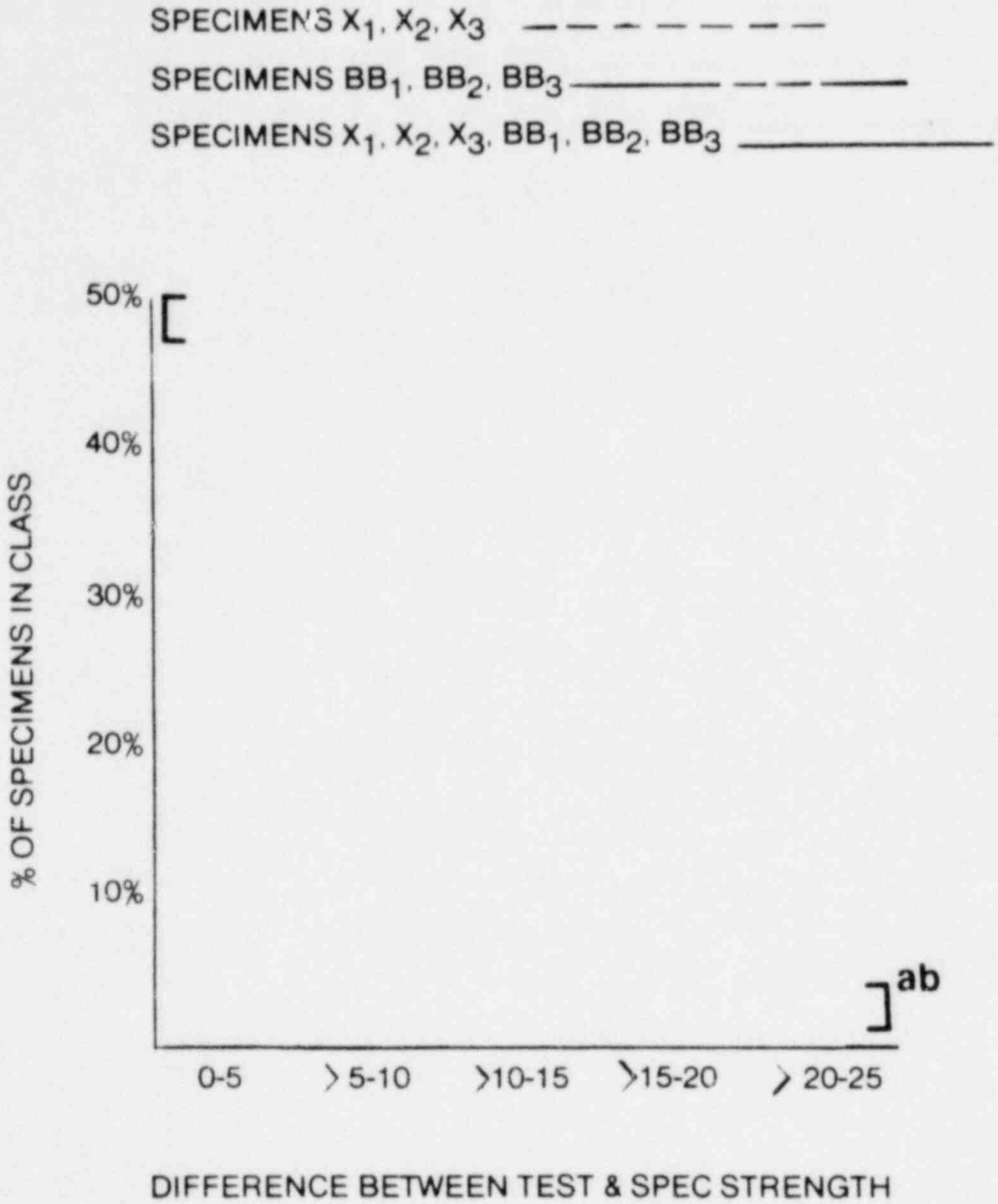

Figure D2
HP ROTOR FORGING ULTIMATE STRENGTHS MTL B

PART B

TABLE OF CONTENTS

PART B

LIST OF FIGURES

PART B

LIST OF TABLES

TABLE NO.	TITLE	PAGE NO.

PART B
NOMENCLATURE AND UNITS

All nomenclature used in this part are defined as they appear in the text. Equations as written in this part are based on a system of units that are defined as follows:

TERM	UNITS
Energy and work	ft-lb
Mass	lbm
Velocity	ft/sec
Strength	lb/in^2
Strain	dimensionless
Volume	in^3
Length, thickness, distance, radius	in
Angle	radians
Area	in^2
Density, ρ	lb/in^3 (.283 unless known to be otherwise)
Gravitational constant, g	32.2 ft/sec^2

1.0 INTRODUCTION

Part B is concerned with the determination of whether or not a disc burst will result in missiles being ejected from the turbine casing, and if so, the external kinetic energy properties of those missiles.

During the late 1960's, when work commenced in this area, it became evident that the existing body of literature, although extensive, was still evolutionary. For refinement purposes a series of spin-burst tests were performed with discs and cylindrical shells at the Westinghouse Research Laboratories. These relatively simple tests of plain and symmetrically flanged shells were used to develop semi-empirical calculation methods to correlate the test results and provide predictive analytical methods(1)*. The analytical methods were extrapolated by engineering judgment to be used for predictive calculations of the actual, more complex, turbine structures.

There was, of course, a desire to learn more about the actual behavior of missiles and targets in other typical turbine configurations. This resulted in additional testing during 1979 of shells struck along their edges (termed asymmetric impact) and cylindrical rings of various configurations, both with and without blade grooves. The tests confirmed some of the existing calculation methods, and provided new insights. As a result, a review of all the missile calculation techniques was done by a review panel, and a more complete, sophisticated set of calculation procedures was formulated, incorporating the most recent information available. This section B is a result of that review effort, providing the most comprehensive set of detailed calculation methods released to date for predicting the energy absorption of turbine disc fragments colliding with turbine casing structures.

*Refers to reference numbers at the end of this part.

2.0 FUNDAMENTALS OF MISSILE ENERGY ABSORPTION BY CIRCULAR SHELLS (THE HAGG-SANKEY METHOD)

2.1 THE CONTAINMENT AND PENETRATION PROCESSES

To determine whether disc fragments can be contained or will penetrate a cylindrical structure, two separate sequential stages of impact must be considered. In Stage 1 the consideration is whether or not the impacting fragments punch a hole through the structure with only very localized damage. This is essentially the type of failure which occurs when a high speed projectile, such as a bullet, perforates a sheet of glass, making only a hole large enough to allow passage of the projectile.

If localized penetration does not occur in Stage 1, the structure must be assessed to see if it will fail in a gross sense by a tensile mode of deformation known as Stage 2. In this stage, usually larger volumes of material are involved in the deformation, not just at the local impact area as in Stage 1.

There are specific energy related criteria which are used to evaluate the outcome of the two stages of containment or penetration and they are presented in the sections that follow.

2.2 INITIAL DISC FRAGMENT ENERGY

It has been observed and reported that only the translational kinetic energy of a disc fragment should be used to determine containment or penetration. With respect to the rotational energy, large friction forces act to dissipate this energy component as evidenced by heating and smearing of metal which have been observed over the contact surfaces of shell and fragment. The friction force at each contact area combines with the radial impact force to incline the shear direction. The increase in shear resistance of the material matches the increase in applied force, and therefore the friction force neither helps nor hinders perforation (1).

The initial translational kinetic energy of the disc fragment is

$$KE_c = \frac{1}{2g} M_1 V_1^2$$

M_1 is the mass of the disc fragment and V_1 is the initial velocity of the fragment at its mass center of gravity.

Values of M_1 and V_1 are obtained as described in Part A.

2.3 STAGE 1 ENERGY RELATIONSHIPS

In the Stage 1 impact there is a transfer of momentum between the missile fragment (M_1) and the effective mass of the containment structure (M_2). If the fragment is contained, the fragment will be decelerated and the structure locally accelerated to a common velocity. At that point it can be said that an inelastic collision has occurred, and from the principles of conservation of momentum it is determined that the energy loss of the system is

$$\Delta KE = KE_o \frac{M_2}{M_1 + M_2}$$

In order for this loss to occur, it must be accounted for by the work of plastic deformation (U_p) required to shear out and compress the material of the impact area.

Energy of compression $\quad E_c = \frac{\sigma_d \varepsilon_c V_c}{12}$

σ_d is dynamic ultimate strength

ε_c is average compressive strain

V_c is volume of compressed material in impact zone

Energy of shear $E_s = \frac{K\tau_d A_s t}{12}$ τ_d is dynamic shear strength

A_s is the shear area

t is shell thickness

K is an experimental constant which is defined by $K\tau_d = 0.27\ \sigma_d$ for typical carbon steels.

The dynamic ultimate strength is shown as a function of the static ultimate strength for ductile steels in Figure 2.01.

Work of plastic deformation $U_p = E_s + E_c$

Stage 1 containment $U_p > \Delta KE$

Stage 1 perforation $U_p < \Delta KE$

For the long shell case shown in Figure 2.02, the equation for the velocity of the combined shell fragment and disc fragment after perforation is given here in a modified form of that derived in Reference 1.

$$V_{21} = V_1 \left\{\frac{M_1}{M_1+m_{21}} \left[1 - \frac{M_2-m_{21}}{M_1+M_2} \left(1 - \sqrt{1- \left(1 + \frac{M_1}{M_2}\right) \frac{U_p}{KE_o}}\right)\right]\right\}$$

m_{21} is the mass of the plug perforated from the shell.

2.4 STAGE 2 ENERGY RELATIONSHIPS

If Stage 1 containment is achieved based on the preceding criteria, the kinetic energy of the system at the end of Stage 1 is

$$KE_1 = KE_o \frac{M_1}{M_1 + M_2}$$

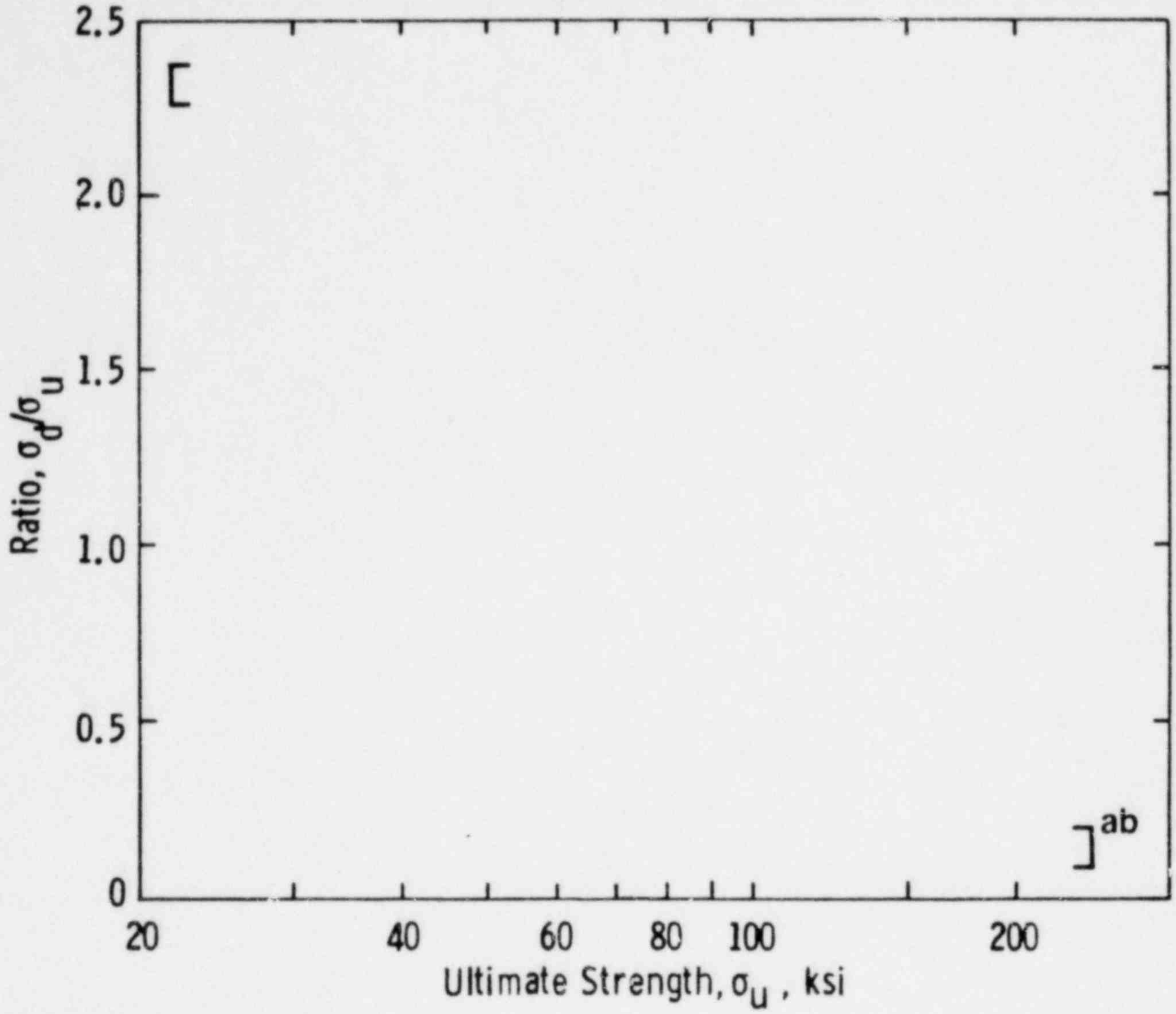

Figure 2.01

DYNAMIC ULTIMATE STRENGTH OF STEELS

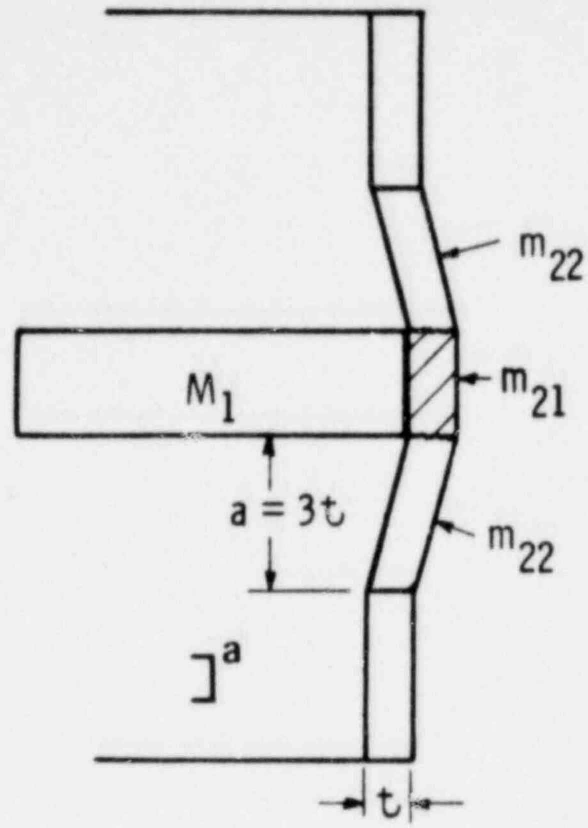

[ ][a]

Long Cylindrical Shell

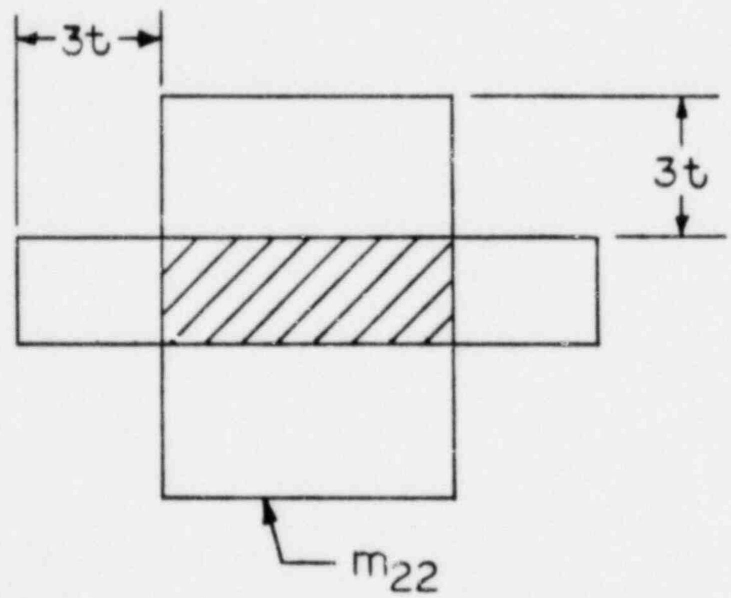

Figure 2.02
EFFECTIVE MASS OF A LONG SHELL

This energy must be absorbed by a tensile mode of deformation of the structure.

Energy of tensile deformation $E_t = \frac{\sigma_d \varepsilon_t V_t}{12}$ ε_t is average tensile strain

V_t is volume of material strained in tension

Stage 2 containment $E_t > KE_1$

Stage 2 failure $E_t < KE_1$

If Stage 2 failure occurs, the residual kinetic energy of the system is

$$KE_2 = KE_1 - E_t$$

This energy is shared by M_1 and M_2. Only a portion of it will be carried on beyond this process. The size of shell fragments is not usually well defined as with Stage 1 perforations, but rules for the selection of specific fragment sizes are given in later sections of the report.

The exit velocity after a Stage 2 failure can be obtained from

$$V_{22} = \sqrt{\frac{2g\ KE_2}{M_1 + M_2}} \quad .$$

2.5 EFFECTIVE MASS DETERMINATION OF THE CONTAINMENT SHELL

Reference 1 discusses the determination of effective mass for cylindrical containment shells in some detail. Figure 2.02 shows the major finding: for long shells, plastic hinges form at the edge of the missile boundary and at a distance of 3 times the shell thickness from the missile boundary. For this case, the effective target mass $M_2 = m_{21} + .34\ m_{22}$, where m_{21} and m_{22} are the actual total masses of the volumes depicted in Figure 2.02. For symmetrically impacted shells where $a^{(1)} < 3t$, hinges will form at the missile boundary only in the axial direction, and at the boundary and 3t in the circumferential direction (assuming that at least 6t space exists between adjacent disc impact surfaces). For shells where $a < \approx 1.2t$ in the axial direction, it is unlikely that shearing will take place in the circumferential planes; rather, it is believed that shearing will tend to occur completely across the axial shear planes.

A general expression for effective mass of an arbitrary size hinged flap when $a < 3t$ is

$$m_{22e} = K_f \, m_{22}$$

where K_f is an effectiveness factor derived from the mass moment of inertia and in simplified form is

$$K_f = \frac{\left(\frac{a}{t}\right)^2 + 1}{4\left(\frac{a}{t}\right)^2 + 1}$$

In these cases, $M_2 = m_{21} + \sum_n (m_{22e})_n$ where n represents the number of flaps.

3.0 APPLICATION OF PRINCIPLES TO ACTUAL TURBINE STRUCTURES

The basic containment and penetration criteria discussed briefly in the preceding sections and in more detail in Reference 1 are directly applicable only to the model structures for which they were derived. In reality, actual turbine structures differ in certain respects from the model utilized. Much of the revised methodology given in subsequent sections of this report reflects additional test results and the results

Note (1): "a" is the smaller dimension of the axial overhang of the shell beyond the missile <u>or</u> 3t.

of a thorough review of analytical methods to eliminate uncertainties and incorporate a precise, methodical calculation procedure.

Although the methods given here are deterministic rather than probabilistic (i.e., provide single-value results), they are not considered to be excessively conservative, but are reasonably so. When sufficient evidence of certainty is available for a particular criterion, that criterion is used in favor of possibly a more conservative one. When there is insufficient evidence or some uncertainty, the more conservative of the available options is used. It is felt that the net result of this approach is to give values that represent a realistic upper bound of exit energies and velocities.

The analysis method with the most test data is the Hagg-Sankey method for collisions with shells. These collisions do not, however, usually absorb a large amount of energy. Cylinder rings that are [ ]^{b}, are the primary energy absorbers; therefore, a great deal of the analytical effort has been devoted to the development of realistic and consistent techniques for this type of structure. The pertinent definitions, theory, and assumptions that apply to cylinder rings are described along with the analytical method that begins in the next section of this report. This same approach is used in subsequent sections that cover other collision modes.

3.1 COLLISIONS WITH RINGS - SYMMETRIC VS. ASYMMETRIC

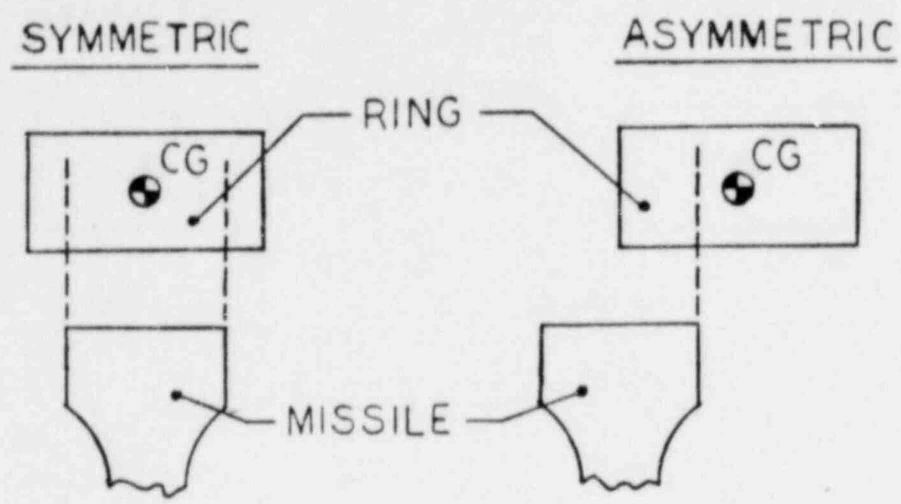

DEFINITIONS:

SYMMETRIC COLLISION - A collision in which the center of gravity of the ring structure being considered lies within the projected boundaries of the missile impact surface.

ASYMMETRIC COLLISIONS - A collision in which the center of gravity of the ring structure being considered lies outside of the projected boundaries of the missile impact surface.

RING STRUCTURE - Includes mass of separate blade ring, impacted blading, back-up ring, and wall as applicable for the case under consideration. Specific rules for symmetric and asymmetric cases are given in the analysis sections for each type.

THEORETICAL BACKGROUND:

If the center of gravity (CG) of a body [ ]b of a pushing surface, the bearing distribution between the two can achieve a center of pressure that [ ]b with the CG, thereby imparting a uniform translational velocity to the impacted body. If the CG is [ ]b of the pushing surface, a force couple is established that tends to [ ]b being impacted. The impacted body will attain a [ ]b and a [ ]b at its CG lower than the velocity of the missile.

3.1.1 SYMMETRIC COLLISIONS

3.1.1.1 BASIS OF ANALYSIS

Establish that the case under considerat' is indeed symmetric. The shaded areas in Figures 3.01 to 3.04 are typical of the cross-sections to be used for calculating the CG for symmetrical cases. Flat radial walls are considered to be [ ]b to their outer limit. Conical walls are [ ]b to the point where they intercept another wall or a wrapper (shell).

For first collisions, the disc segment is assumed to be oriented such that one corner of the segment is [ ]a for purposes of analysis. This is a conservative assumption that limits the amount of available shear strain energy in Stage 1 since it is assumed that [ ]a at the horizontal joint. In addition, the amount of available tensile [ ]a at that location, as is the effective target mass M_2.

For collisions subsequent to the first, any structural material that is perforated as a plug is assumed [ ]a the previous missile mass and be [ ]a of the missile. The missile in these collisions also is assumed to be aligned with the horizontal joint.

[

][a]

Figure 3.01
TARGET MASS FOR SYMMETRIC IMPACT
(TYPICAL FOR LP TYPE I)

[

][a]

Figure 3.02
TARGET MASS FOR SYMMETRIC IMPACT
(TYPICAL FOR LP TYPE II)

[

]a

Figure 3.03
TARGET MASS FOR SYMMETRIC IMPACT
(TYPICAL FOR LP TYPE III)

[

]a

Figure 3.04
TARGET MASS FOR SYMMETRIC IMPACT
(TYPICAL FOR LP TYPE IV)

In the first collision, the disc segment will strike a cylinder ring with its rim. A target mass m_{21} directly impacted by the disc is defined [ ]a of the disc rim. The arc length is specified to be calculated at the top of the [ ]a on the centerline of the disc. On the "Disc Properties" data sheet, this is given as "Missile Outer Radius" [Section A, Figure 16]. An additional amount of target mass m_{22} is obtained from the overhanging part of the ring between the disc impact locations. This is shown schematically in Figure 3.05. The amount of overhang considered for m_{22} is based on [ ]a the effective thickness of the ring or [ ]a the distance to the next m_{21}, whichever is less.

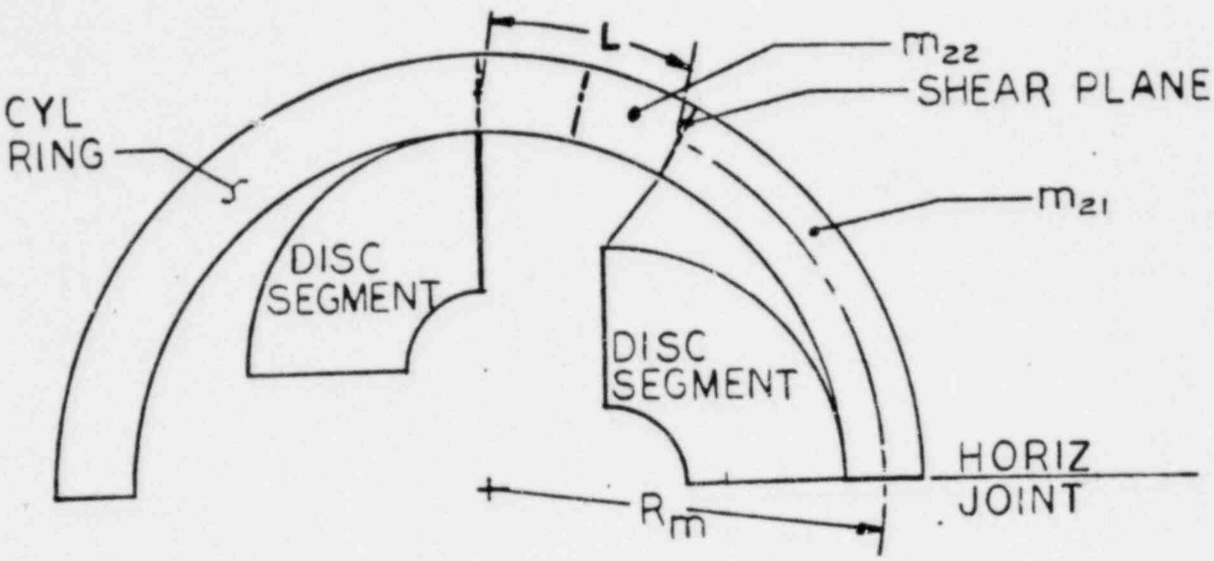

Figure 3.05
TARGET MASS

3.1.1.2 FIRST COLLISION GEOMETRIC PARAMETERS

Since cylinder rings have a complex cross-section, a method was devised to obtain an effective thickness which is based on the shearing properties of the section.

EFFECTIVE THICKNESS

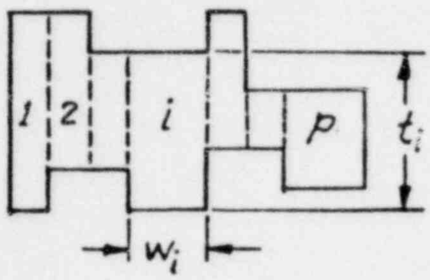

[ ][a]

NOTES: (1) Only material effective in shear is used in this calculation. If a section is a composite of two or more half-rings, each half-ring is calculated independently.

(2) [ ][a] that are part of the blade unit and are [ ][a] together, are assumed not to have an overhang effect. [ ][a] that are [ ][a] do have the overhang effect.

(3) More complex shapes with slanted surfaces can be calculated more precisely.

The pertinent parameters associated with Stage 1 of the first collision are determined by the equations that follow and by referring to Figure 3.06.

<u>90° DISC SEGMENT</u> $\Theta_D = \frac{\pi}{2}$

Arc length of disc rim $L_D = \frac{\pi}{2} R_D$

[

]a

Figure 3.06
SYMMETRIC COLLISION GEOMETRIC PARAMETERS

Arc length of disc is transferred to inside of [

]^a by compressive contact. The contact angle subtended is

$$\Theta_c = \frac{\pi}{2} \times \frac{R_D}{Ri} \qquad (\Theta = \text{radians unless other specified})$$

The angle asociated with the involved overhanging material is designated Θ_G, and is the smaller of the two following possibilities:

(1) $\Theta_{Gn} = \frac{\pi}{4}\left(1 - \frac{R_D}{R_i}\right)$

or

(2) $\Theta_{Gn} = \frac{3\ t_{en}}{R_{mn}}$ where R_{mn} = radius to CG of x-section of ring "n" (n=1, 2...)

$$t_{en} = \frac{(\sum w_i t_i^2)_n}{A_n}$$

and A_n = x-sect. area of ring "n"

R_D = radius to top of [ ]^a ("Missile outer radius")
R_i = inner radius of first ring shearing material contacted

<u>120° DISC SEGMENT</u> $\Theta_D = \frac{2\pi}{3}$

Arc Length of Disc Rim $L_D = \frac{2\pi}{3} R_D$

Subtended contact angle $\Theta_c = \frac{2\pi}{3} \times \frac{R_D}{R_i}$

Overhang angle (smaller of the two)

(1) $\Theta_{Gn} = \frac{\pi}{3}\left(1 - \frac{R_D}{R_i}\right)$ or (2) $\Theta_{Gn} = \frac{3\ t_{en}}{R_{mn}}$ (n=1, 2....)

3.1.1.3 EFFECTIVE MASS MATERIAL

EFFECTIVE MASS MATERIAL OF RINGS

Includes separate [

]^a (if impacted by the disc).

Circumferential effective mass is defined by angle $\Theta_{Kn} = \Theta_c + K_{fn}\Theta_{Gn}$

where K_{fn} is determined as follows:

For overhang Case (1), $L_{on} = \Theta_{Gn} R_{mn}$ (n=1, 2....)

Calculate $K_{fn} = \dfrac{\left(\dfrac{L_o}{t_e}\right)_n^2 + 1}{4\left(\dfrac{L_o}{t_e}\right)_n^2 + 1}$ or obtain from Figure 3.07.

For overhang Case (2), $K_{fn} = .34$

EFFECTIVE MASS OF RINGS $M_{2R} = \sum_n \Theta_{Kn} R_{mn} A_n \rho$ (n=1, 2....)

If a Stage 1 or 2 perforation occurs, the mass of the perforated plug is assumed to be represented by a piece of ring over the angle Θ_c. Although a piece of this size may not always result, it is conservative to assume that such occurs and is carried on to the next collision.

MASS OF PERFORATED FRAGMENT

$$m_{21} = M_{2B} + \rho\Theta_c \sum_n R_{mn} A_n \quad (n=1, 2....)$$

where M_{2B} is defined as follows.

EFFECTIVE MASS MATERIAL OF BLADING - M_{2B}

Only [ ][a] that are directly impacted by the disc segment are considered as part of M_2.

The mass of [ ][a] is calculated over the angle θ_c .

EFFECTIVE MASS MATERIAL OF A WALL

Circumferential effective mass angle $\theta_w = \theta_{Kn} = \theta_c + K_{fn}\ \theta_{Gn}$

where subscript n refers to the attached back-up ring.

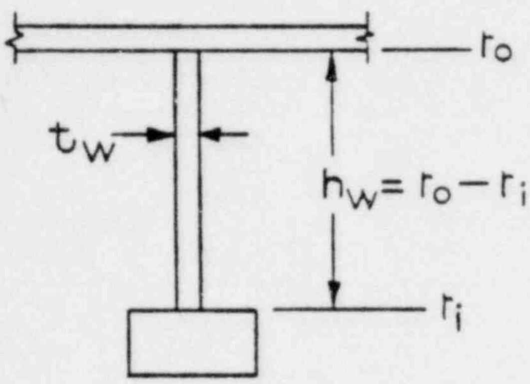

Radial dimension:

Use h_w as shown at the left.

EFFECTIVE MASS

$$M_{2w} = \theta_w \left(\frac{r_o + r_i}{2}\right) h_w t_w \rho$$

SPECIAL CASE - Offset center

When the true center of the wall radius r_o' is offset from the rotor center by a distance d, a fictitious on-center radius r_o is calculated. It is taken to be the distance from the rotor center to the outer edge along a line at the angle $\frac{1}{2}\theta_c$, shown as r_o below. It can be determined by trigonometric relationships using the known dimensions and specified angle.

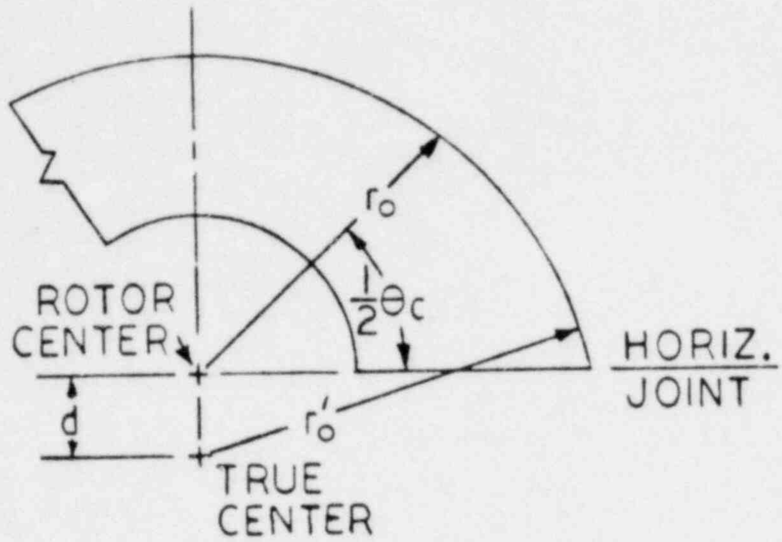

TOTAL EFFECTIVE TARGET MASS

$$M_2 = M_{2R} + M_{2B} + M_{2w}$$

3.1.1.4 ENERGY LOSS IN STAGE 1

The maximum energy that can be absorbed in Stage 1 due to an inelastic collision is

$$\Delta KE = KE_o \frac{M_2}{M_1 + M_2}$$ where KE_o = energy of missile entering the collision

and M_1 = mass of the missile

This energy loss is achieved under two conditions:

(1) If two adjacent disc segments strike the ring so closely spaced that there is insufficient overhanging mass between the segments to develop shearing action, then that ring will not have any possibility of Stage 1 failure and will cause a Stage 1 energy loss of ΔKE. A conservative evaluation decided that this condition exists when

$$L \leq 2t_e \quad \text{(Refer to Figure 3.05)}$$

or

$$L_o \leq t_e$$
for the innermost ring

(2) Stage 1 containment is also achieved for $L > 2t_e$ when the sum of the energies that can be dissipated in shear and compression are such that

$$U_p = E_s + E_c > \Delta KE$$

Shear strain energy $E_s = \frac{0.27}{12} \sum_n [\sigma_d \sum_1^p w_i t_i^2]_n$ for the "n" rings across one shear plane at σ_c

Notes: There may be occasional instances where a symmetric ring case may have an additional shear plane in the circumferential direction resulting from an attached shell or offset wall. These cases will usually be obvious and the shear energy is calculated as described in Section 3.1.2.4 for SA_1 mode.

Walls attached to rings being sheared are [ ][a]

Compression strain energy $E_c = \frac{0.07}{12} [\sum_n (\sigma_d \Theta_c R_{cm} A_c)_n + \sigma_{dB} \frac{M_{2B}}{\rho}]$

where A_c = area of cross-section that is in compression (M_{2B} material considered separately)

R_{cm} = radius to centroid of A_c

The compression cross-section is defined by the [ ][a] the confines of the missile width (see Figure 3.08). It extends radially to the [ ][a] involved in the collision. If the width reduces due to an undercut, it remains at the reduced width beyond that point.

The dynamic strength of the blading, σ_{dB}, is usually taken to be the same as a cast blade ring (a conservative assumption).

If $U_p < \Delta KE$, Stage 1 failure occurs, and the disc and cylinder fragments exit from the collision with a velocity

[ ][a]

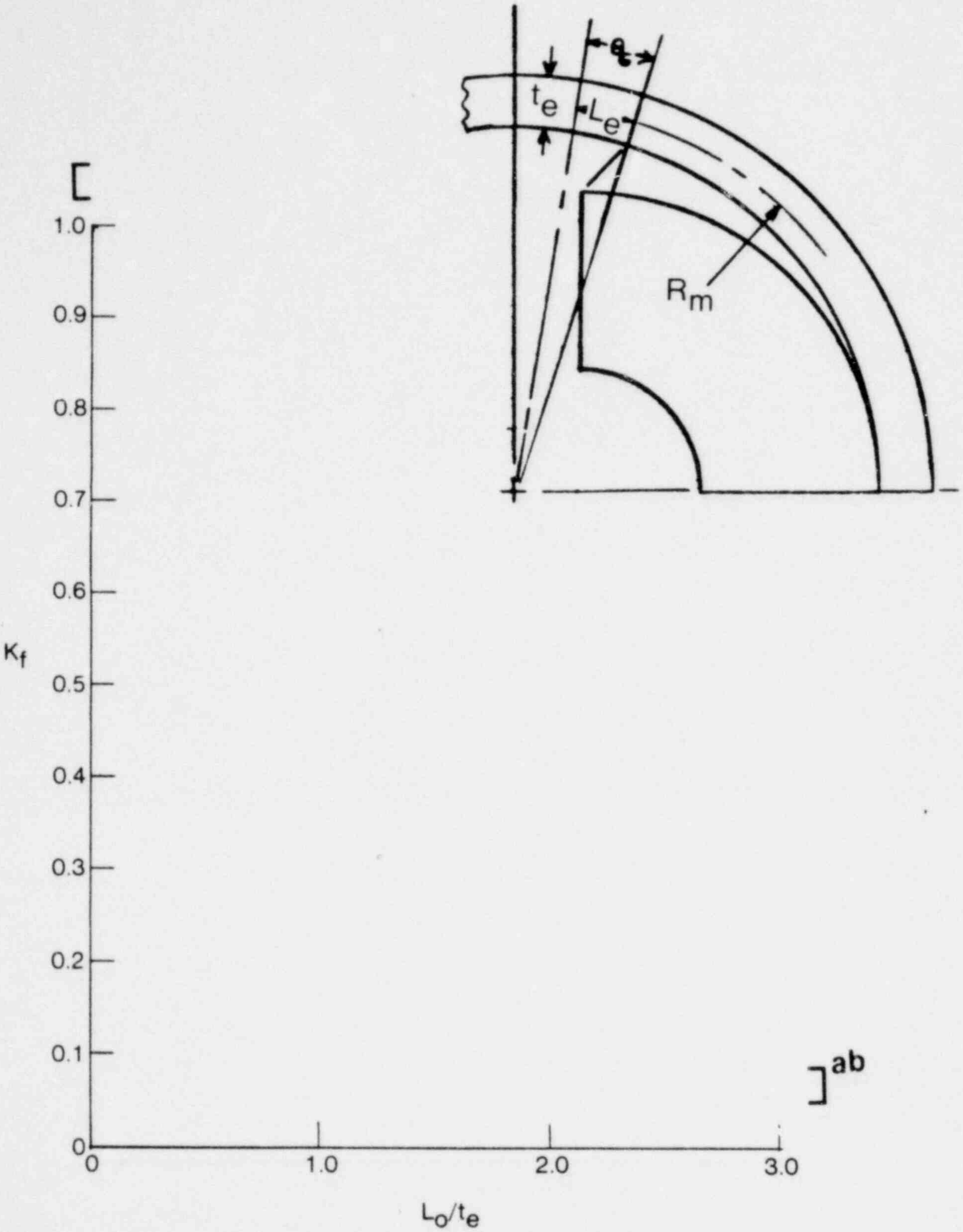

Figure 3.07
EFFECTIVE MASS FACTOR, K_F, FOR FREE END FLAP

[

][a]

Figure 3.08

EXAMPLES OF COMPRESSION STRAIN VOLUME

and kinetic energy [ ][a]

If $U_p > \Delta KE$ and Stage 1 containment is achieved, the kinetic energy of the system is

[ ][a]

3.1.1.5 ENERGY LOSS IN STAGE 2

Overall containment at the end of Stage 2 is obtained if the available tensile strain energy exceeds the system kinetic energy at the end of Stage 1:

$$E_t > KE_1$$

If $E_t < KE_1$, Stage 2 failure occurs, and the system kinetic energy is

$$KE_2 = KE_1 - E_t = KE_o - \Delta KE - E_t$$

Tensile strain energy, E_t:

Continuous

[ ]a are the only structural elements asumed to be capable of absorbing tensile strain energy.

The horizontal joint is assumed to provide [ ]a continuity such that tensile strain is [ ]a at that location.

Based on minimum test results, the tensile strain value used is [ ]a throughout ring cross-section, from the location at $\frac{1}{2}\theta_c$ to the far end of the θ_G overhang. From the $\frac{1}{2}\theta_c$ location, the strain is assumed to decrease linearly from [ ]a at the horizontal joint. (See Figure 3.09).

The same strain pattern is assumed to exist in the radial walls in the circumferential direction. However, the strain level diminishes in the radial direction, such that an effective radial height is determined over which the strain is assumed uniform (see derivation in Appendix A). The angle θ_G of a wall is the same as that of the ring to which it is attached.

[

]a

Figure 3.09
CIRCUMFERENTIAL TENSILE STRAIN DISTRIBUTION

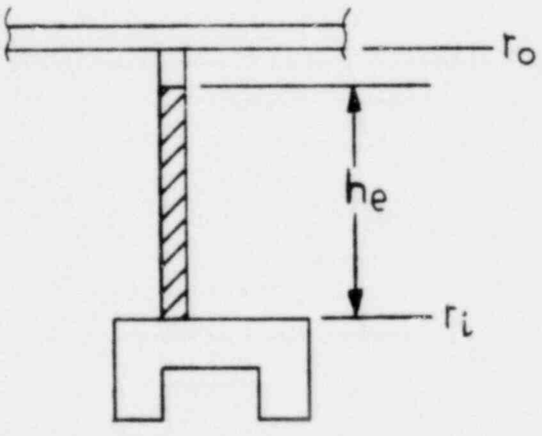

Figure 3.10
EFFECTIVE HEIGHT OF RADIAL WALL

EFFECTIVE HEIGHT OF RADIAL WALL $$h_e = r_i \frac{r_o^2 - r_i^2}{r_o^2 + r_i^2}$$ (See Figure 3.10)

EFFECTIVE TENSILE STRAIN VALUE (Calculated for each tensile element)

[ ][a]

TENSILE STRAIN ENERGY

$$E_t = \frac{1}{12} \sum_n [\sigma_{dn} \varepsilon_{tn} (\Theta_{Cn} + \Theta_c) R_{mn} A_n] \quad (n=1, 2....)$$

Note: For a wall, $A = h_e t_w$

and $R_m = r_i + \frac{1}{2} h_e$

The resulting velocity from a Stage 2 failure is

[ ][a]

and the kinetic energy of the fragments continuing as a missile is

[ ][a]

3.1.1.6 SECOND AND SUBSEQUENT COLLISION CONSIDERATIONS

After a first symmetric collision with a ring assembly that results in Stage 1 or 2 failure, it is assumed that the [ ][a] (unless specified elsewhere) will [ ][a] to any subsequent collisions. The outside radius of the outermost part becomes the new value of R_D for calculating the new angles of target mass involvement. Similarly, the previous θ_C becomes the new θ_D . If the subsequent collision is a symmetric ring collision (highly unlikely), it is then handled as on the preceding pages, using the [ ][a] as the [ ][a]

Most collisions subsequent to a symmetrical ring collision will be cylinder walls in collision with cylinder wrappers. This type of collision is dealt with in Section 3.2.2.

3.1.2 ASYMMETRIC COLLISIONS

3.1.2.1 BASIS OF ANALYSIS

The first step is to establish that the case under consideration is indeed asymmetric. In many cases this will be quite obvious, but in some cases it may be necessary to first locate the CG using the assumptions associated with symmetric collisions. If the CG is [ ]a, the collision is considered to be asymmetric, and a different set of rules and assumptions are applied.

Just as for symmetric collisions, the disc segment is assumed to be oriented such that one corner of the segment is aligned with the [ ]a

When a collision is asymmetric, the target mass of the ring structure is determined as though it is a curved beam [ ]a. From the mass moment of inertia, the actual mass, and the eccentricity of the impact, an effective mass is found to use in the basic energy relationships of Stage 1 and Stage 2.

Unless otherwise specified, definitions of symbols given in Section 3.1.1 are also applicable hereafter.

3.1.2.2 FAILURE MODE CONSIDERATIONS

The potential for a number of different failure modes in Stage 1 require that the analyst first be able to identify the [ ]a in order to assess the analytical approach to be used in determining effective mass and other energy considerations. The true Stage 1 shear failure modes have been categorized as being of three types, designated SA_1, SA_2, and SA_3*.

SA_1 This mode is represented by two shear planes: a circumferential plane that intersects a radial plane that coincides with the disc corner (see Figure 3.11). A large radial resistance away from the impact zone usually yields this shear failure mode.

SA_2 This mode is represented by a circumferential shear plane that is continuous around a half-ring (see Figure 3.12). This mode occurs similarly to SA_1 when the adjacent disc segments strike closely together.

SA_3 This mode is identical to the usual symmetrical mode failure, that is failure by a radial shear plane across the entire ring structure. This mode is most common when there is no offset radial resistance (see Figure 3.13).

Brittle Fracture Mode:

The 1979 test series revealed another mode that may also exist. For rings with grooves struck as shown in Figure 3.14, a brittle bending failure occurs that by-passes the usual Stage 1/Stage 2 energy approach. The pattern of failure is similar to an SA_1 shear mode, but the energy absorption is usually considerably less. This is largely due to the fact that almost no momentum is transferred to the material outside the perforated fragment.

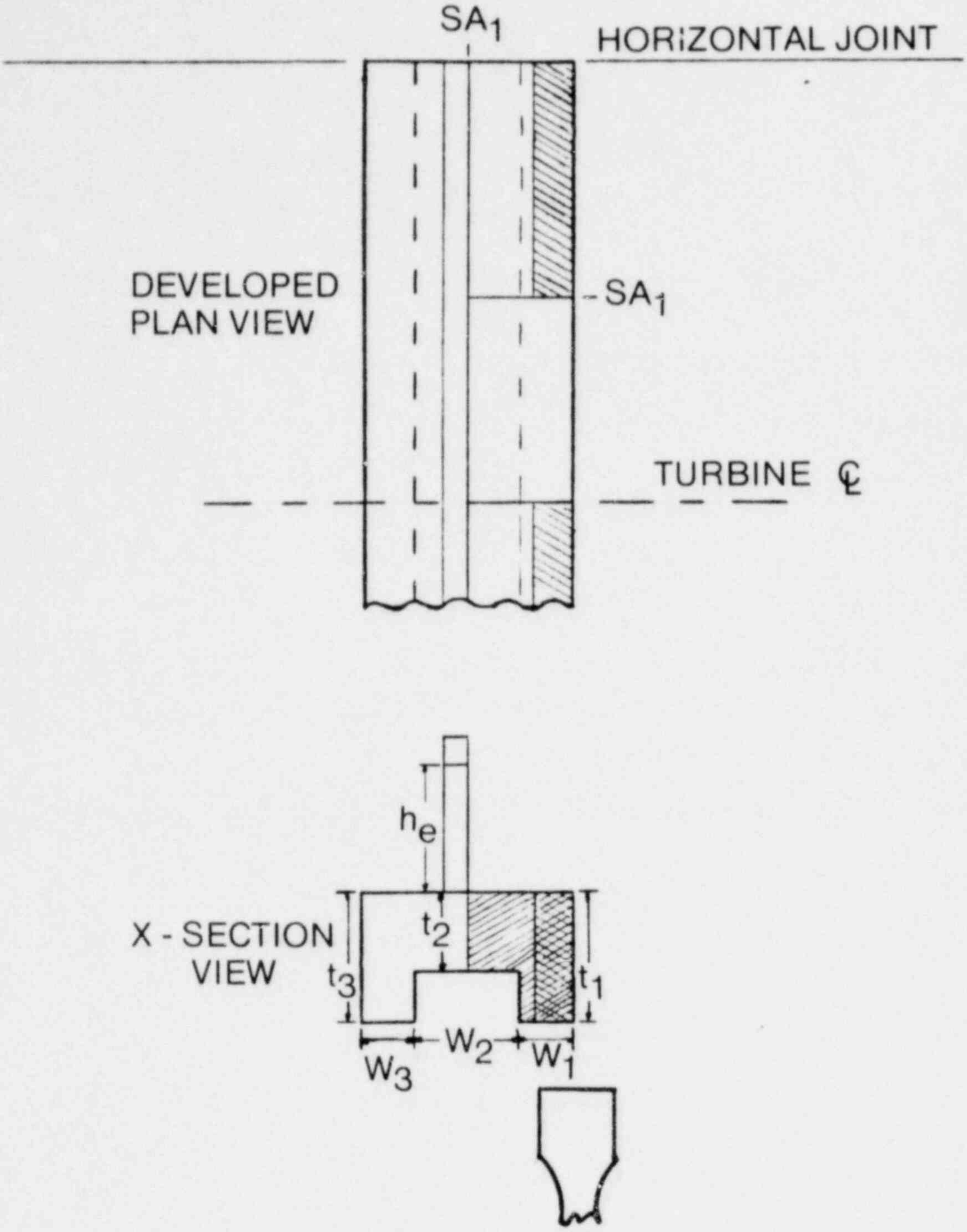

Figure 3.11

SA_1 SHEAR FAILURE MODE

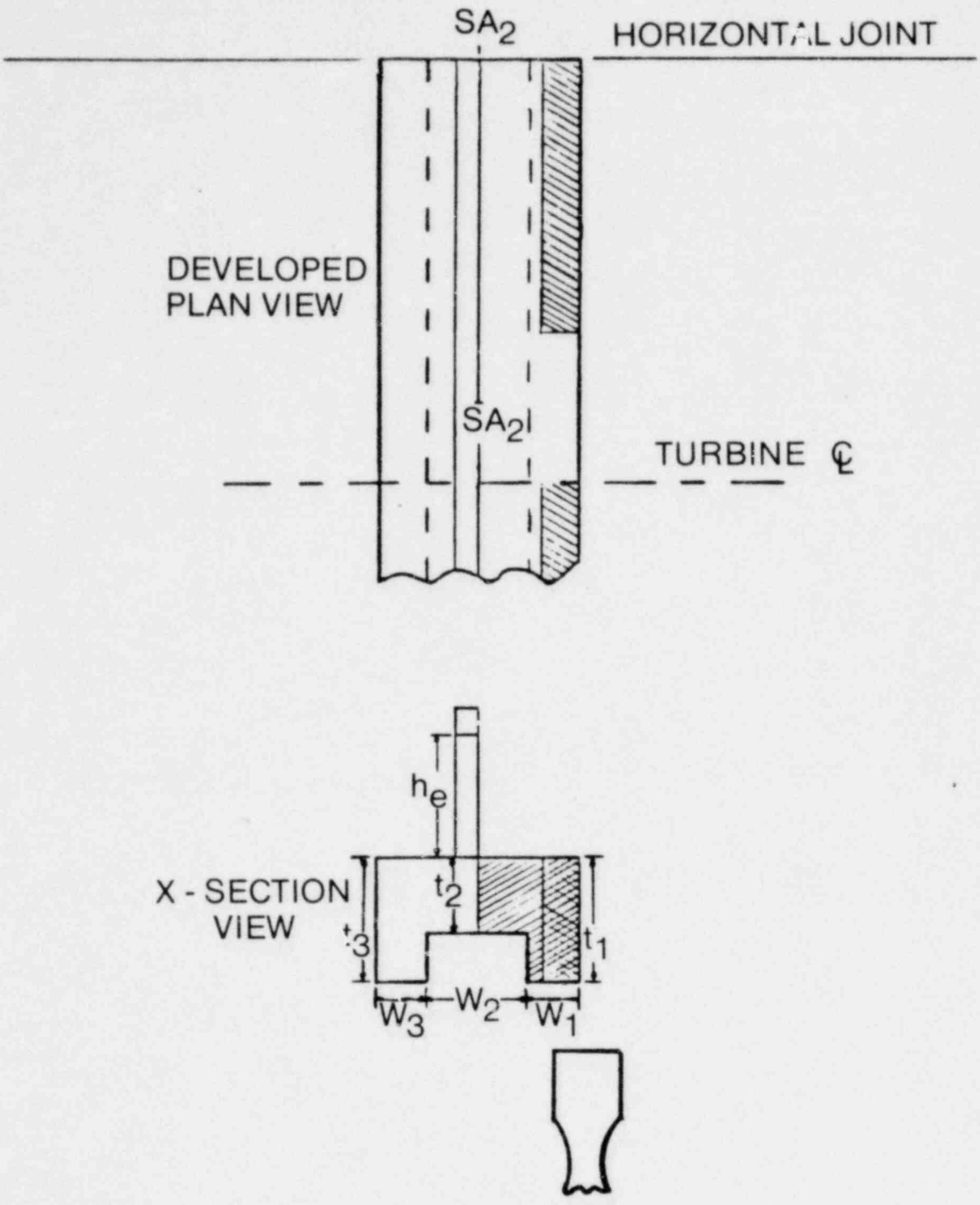

Figure 3.12

SA_2 SHEAR FAILURE MODE

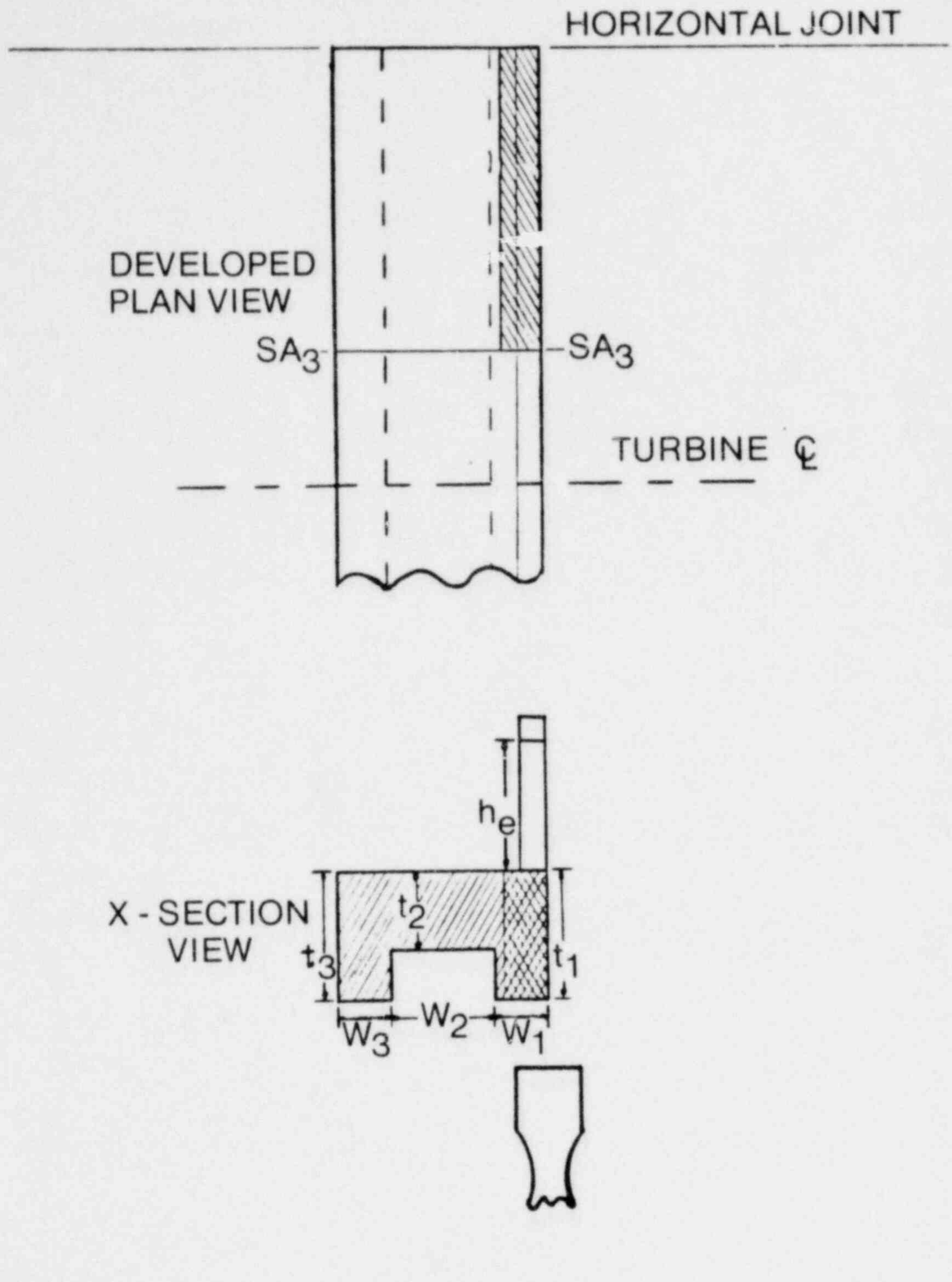

Figure 3.13

SA_3 SHEAR FAILURE MODE

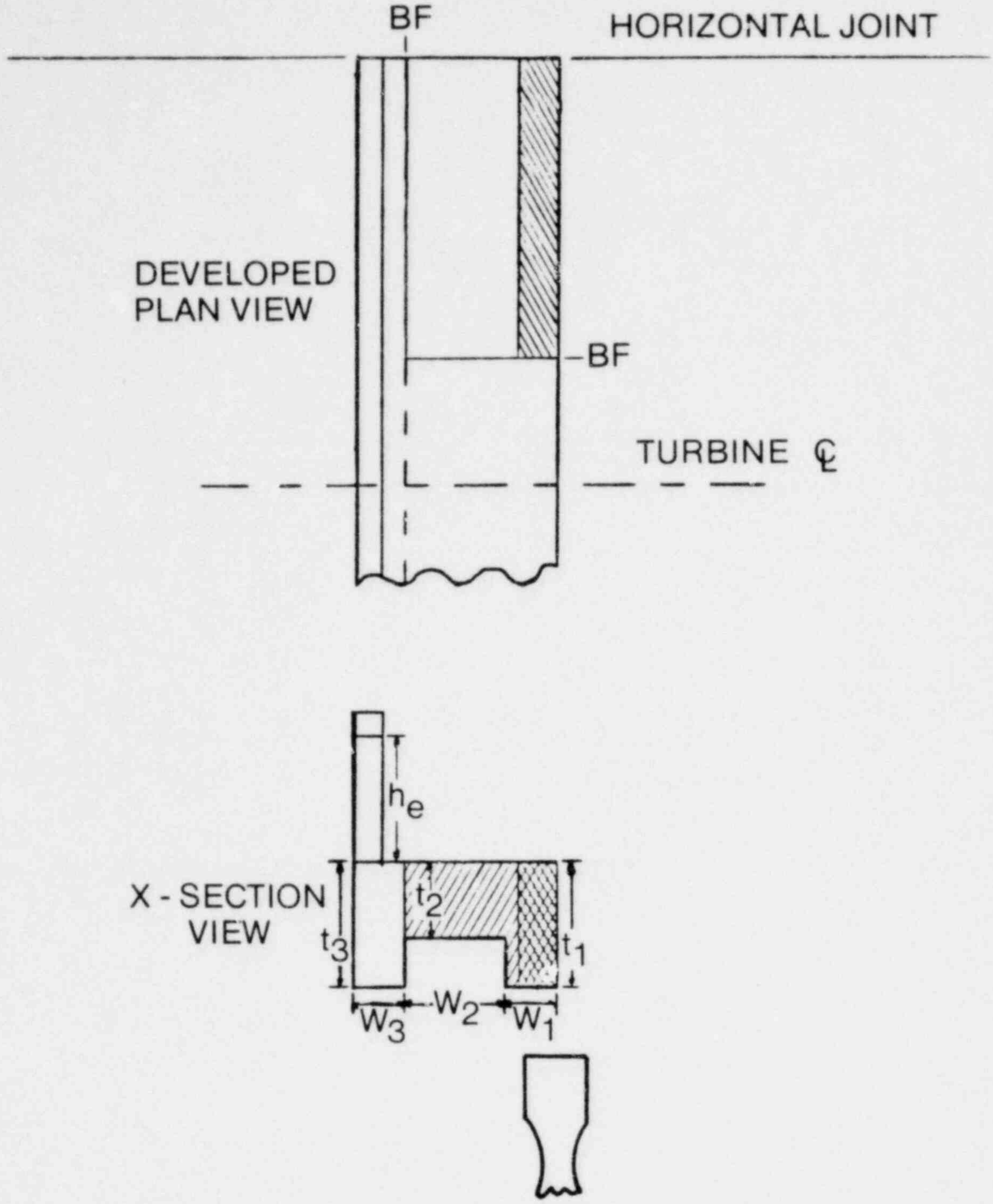

Figure 3.14
BRITTLE FRACTURE MODE

Determination of Mode for Common Turbine Structures

Fabricated Back-Up Ring and Wall Assembly:

If a ring is backed by a
[ ]a will influence the possible shear perforation modes.

1) [ ]a is located within the bounds shown by positions "A" and "B", SA_1 and SA_2 are the only shear modes considered possible, provided that the portion of m_2 mass to the left of the shear plane is greater than that to the right of the plane.

2) [ ]a is to the right of position "A", SA_3 is the most likely failure mode, although SA_1 and SA_2 should also be checked at or near section "C-C", i.e., on the other side of the [ ]a

3) [ ]a is to the left of position "B", brittle fracture mode will govern.

For cases 1) and 2) above, M_2 is based on the entire ring cross-section and effective [ ]a of height h_e.

For case 3) above, M_2 is based only on the fracture fragment.

In all cases, the [ ]a is considered to provide no shear resistance effect in Stage 1.

Separate Blade Ring with Fabricated Back-up Ring and Wall:

This structural situation can also provide any of the three shear failure modes or the brittle fracture mode. Figures 3.15 and 3.16 show some of the different possibilities. All three shear failure modes and the brittle fracture mode are possible. The same principles are used in deciding which mode pertains in a particular case. Blade ring and back-up ring are [ ]a for calculation of M_2.

Impacts on Corners of Blade Roots:

A fairly common asymmetric impact situation is one in which the disc corner overlaps the [ ]a held in a separate [ ]a (see Figure 3.17). Usually the overlap is relatively small [ ]a, and the 1979 tests showed that the disc segment merely smeared the corner of the [ ]a and impacted solidly on the [ ]a. Therefore, for most cases it is assumed that the disc impacts the primary ring and that the [ ]a is left behind and is not involved in the collision as an energy absorber or as part of M_2. The exceptions to this are cases where it is evident that the overlap is large or where the [ ]a must be impacted in order for the primary ring to participate in the collision (see Figure 3.18). Both ring elements are considered in strain energy calculations and are [ ]a in the calculation of M_2.

3.1.2.3 EFFECTIVE MASS OF RINGS IMPACTED ASYMMETRICALLY WITHOUT BRITTLE FRACTURE FAILURE

If an evaluation has been made of the asymmetric ring structure assembly and it has been determined that the brittle fracture mode does not govern, the effective target mass is determined by the following procedure. [

]a

[

][a]

Figure 3.15

SA_1 OR SA_2 SHEAR FAILURE MODE ON SEPARATE BLADE RING

[

][a]

Figure 3.16
BRITTLE FRACTURE MODE
ON SEPARATE BLADE RING

[

]a

Figure 3.17
MISSILE SHIFT FOR SMALL BLADE ROOT OVERLAP

[

]a

Figure 3.18
NO MISSILE SHIFT FOR LARGE BLADE ROOT OVERLAP

Using the same relationships as for symmetric collisions, the following values are calculated for each ring element:

$$t_e \quad \theta_c \quad \theta_G \quad L_o \quad \theta_K \quad \theta_W$$

The effective height of any attached wall is found by

$$h_e = r_i \left[\frac{r_o^2 - r_i^2}{r_o^2 + r_i^2} \right]$$

where h_e is interpreted as shown in Figure 3.10 for the simplest configuration.

When a ring is impacted asymmetrically, it is
[
]a. However, the relatively flexible attached wall is unlikely to rotate much except locally at the point of attachment to the ring. Therefore, the wall is
[ ]a as shown in Figure 3.19, and its mass effect can be [ ]a that will develop at the joint of the wall and ring.

PROCEDURE:

1. Calculate mass of effective wall $m_w = \theta_w \left(\frac{r_e + r_i}{2}\right) h_e t_w \rho$

2. The mass of the wall is lumped along the [ ]a shown in Figure 3.19. The lumped mass is most easily represented by a very small square area with a very high fictitious density:

$$\rho^* = \frac{m_w}{A_w^* \theta_w r_i}$$ where A_w^* is the fictitious area (suggest $.1 \times .1 = .01$ in^2)

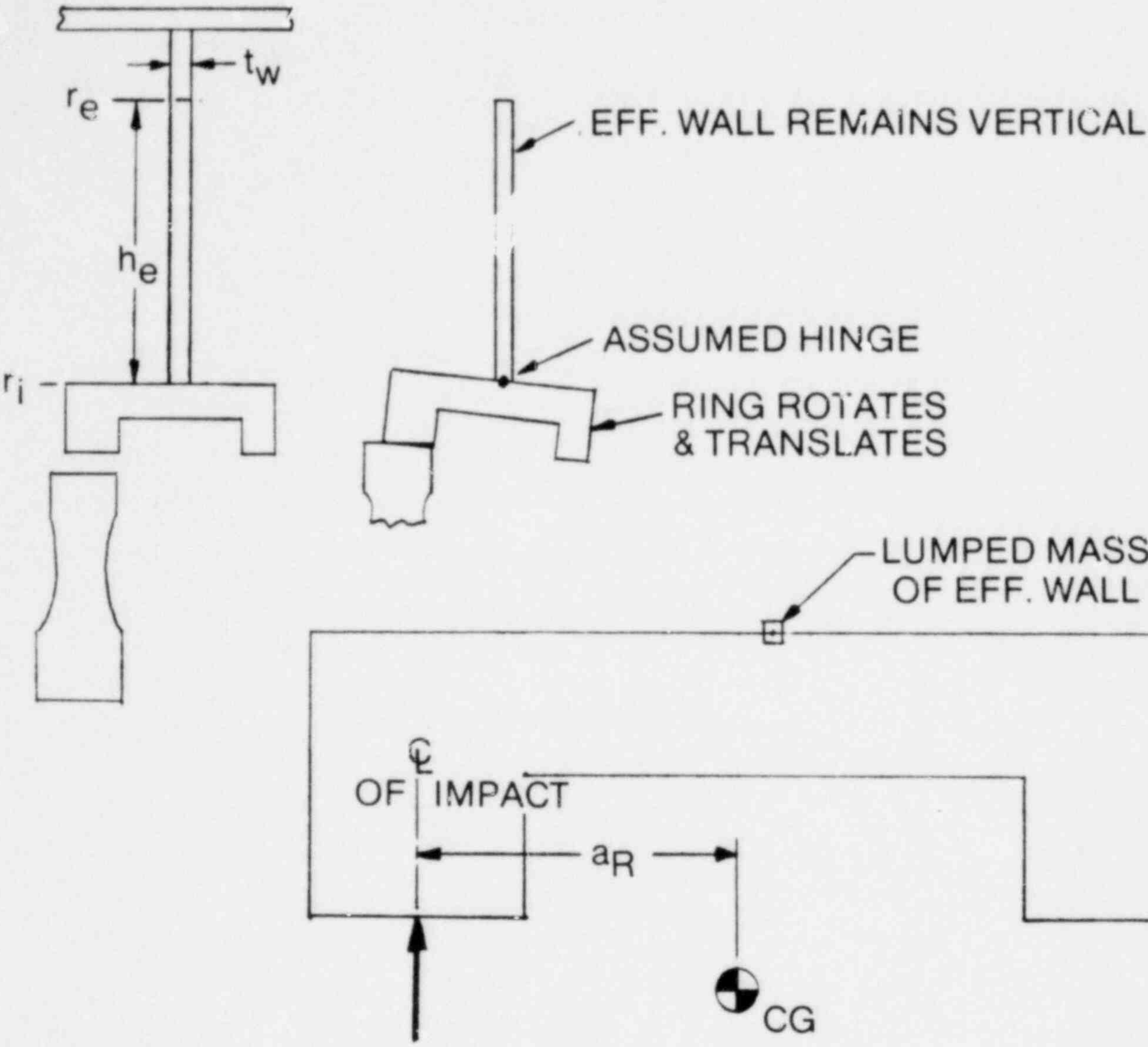

Figure 3.19

ASYMMETRIC IMPACT EFFECTIVE MASS DETERMINATION

3. The mass and moment of inertia properties of the ring with the lumped wall are then determined:

$$m_2 = \sum_n [\rho_{Kn} R_{mn} A_n \rho] + m_w + M_{2B}$$

I_{CBM} = mass moment of inertia of all the elements acting as a curved beam (taken about CG of curved beam mass). This value can be calculated by hand for simple structures using relationships shown in Appendix B.

Effective target mass $M_2 = \dfrac{m_2 I_{CBM}}{m_2 a_R^2 + I_{CBM}}$

where a_R = the horizontal distance between the centerline of impact and the CG of the m_2 mass.

The relationship of the masses can be expressed by the ratio $K_c = \dfrac{M_2}{m_2}$ where

$$K_c = \frac{I_{CBM}}{m_2 a_R^2 + I_{CBM}} .$$

The value K_c is used in subsequent calculations.

SPECIAL CASES OF ASYMMETRIC EFFECTIVE MASS DETERMINATION

In some cases, a missile may strike one ring which is separated from a second by a short wall. The wall continues above the second ring as shown in Figures 3.20 and 3.21. In these cases, the effective wall height h_e is interpreted as shown. Each of the two rings is considered [

][a] are shown in Figures 3.20 and 3.21. The value of $(M_2)_{R1}$ is the value used in the initial collision calculations. A special technique is also used to assess the effects of the initial collision on $(M_2)_{R2}$, which is described in Section 3.1.2.7.2.

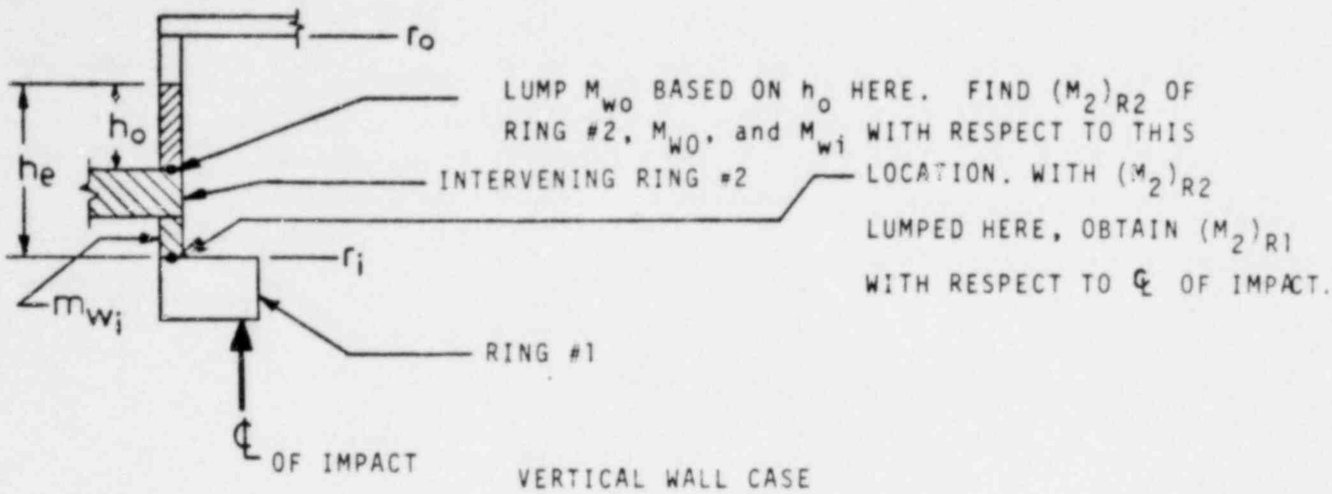

VERTICAL WALL CASE

Figure 3.20
VERTICAL WALL CASE

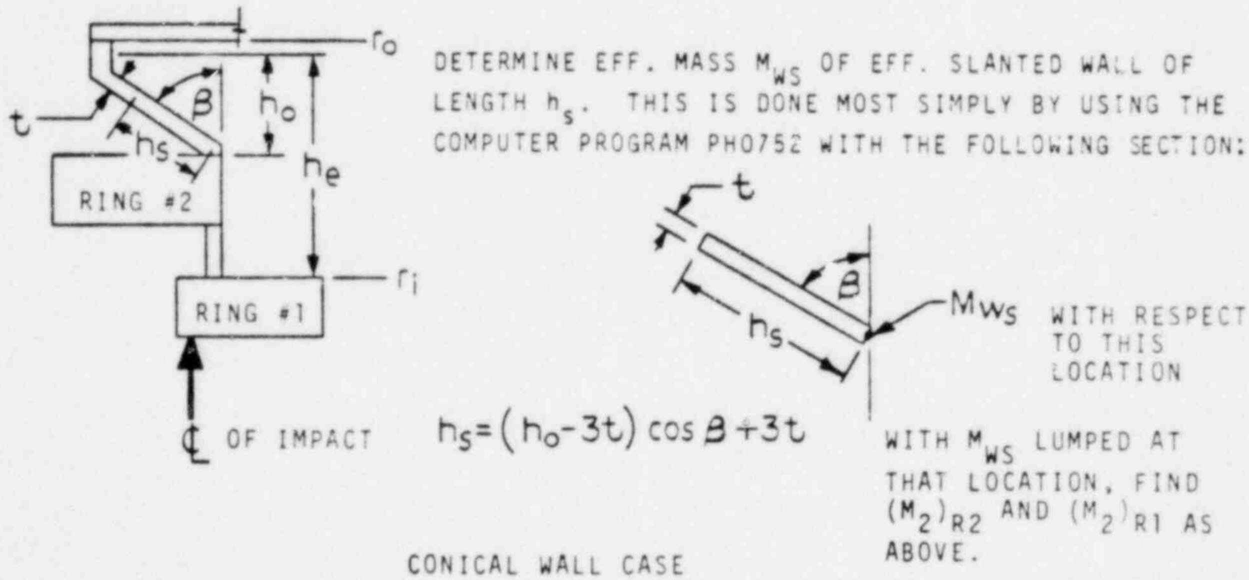

CONICAL WALL CASE

Figure 3.21
CONICAL WALL CASE

PROCEDURE FOR DETERMINING ASYMMETRIC EFFECTIVE
MASS WITH RINGS SEPARATED BY A WALL

3.1.2.4 ENERGY LOSS IN STAGE 1

As for symmetric cases, the maximum possible Stage 1 energy loss is

$$\Delta KE = KE_o \frac{M_2}{M_1 + M_2}$$

where KE_0 and M_1 are as before, and M_2 is the effective mass of the asymmetric target as determined on the page immediately preceding. This energy loss can be achieved under the following conditions:

If SA_3 is the lowest energy shear mode and is an allowable mode according to the guidelines given, then the energy loss in Stage 1 will be [ ][a]

If SA_1 or SA_2 is the lowest energy of the allowable shear modes in a particular case, then the energy loss in Stage 1 will be [ ][a]

If Stage 1 containment is achieved, the kinetic energy of the system (M_1 and M_2) is

[ ][a]

Calculation of shear strain energy:

SA_1 mode [ ][a] for the simple case shown in Figure 3.11. Obviously, for more complex cases the calculation may not be quite so simple, but the principle is the same.

SA_2 mode [ ][a] for the simple case shown in Figure 3.12.

SA_3 mode [ ][a] for the simple case shown in Figure 3.13.

Calculation of compression strain energy E_c:

Same as for symmetric cases; see page B28. Some particular interpretation examples are shown in Figure 3.08.

Strain energy of Stage 1: $(U_p)_{SAn} = E_{SAn} + E_c$ (n=1,2,3)

If $\Delta KE > (U_p)_{SAn}$ for the mode of least energy being considered, Stage 1 perforation will occur in that mode. The kinetic energy of the system (M_1 and M_2) at the end of Stage 1 is [ ][a] The velocity of the system at the centerline of impact is

[ ][a]

3.1.2.5 ENERGY LOSS IN STAGE 2

If containment is achieved in all the possible Stage 1 modes, the system progresses into Stage 2. The criterion for overall containment at the end of Stage 2 is the same as for symmetric cases: $E_t > KE_1$

If $E_t < KE_1$, Stage 2 failure occurs, and the system kinetic energy is

[ ][a]

Calculation of tensile strain energy E_t:

Continuous

[

]^a are the only structural elements assumed to be capable of absorbing tensile strain energy.

The horizontal joint is assumed to provide

[ ]^a such that tensile strain is assumed to be [ ]^a at that location.

Based on minimum test results, the tensile strain value used is [ ]^a in the area of maximum tensile straining, from the angular location $\frac{1}{2}\Theta_c$ to the end at $\Theta_c + K_f\Theta_G$. In the direction from $\frac{1}{2}\Theta_c$ to the horizontal joint, the maximum tensile strain is assumed to decrease from

[ ]^a

In contrast to symmetrical ring cases where the tensile strain energy of each structural element could be calculated on the basis of assumed uniform strain across any section, there is no such straightforward technique for evaluating the tensile strain energy in an asymmetrically impacted ring. The tensile strain tends to be greatest on the edge near the impact and least on the edge away from the impact. Some involved theoretical approaches were considered as to how to obtain E_t under these circumstances, but a relatively simple approach was finally adopted which states that the effective volume in tension is

[ ]^a

This formula is based on the logic that the effective mass M_2 represents a reasonable expectation of the participation of the entire mass m_2 in the straining process. It can be seen that this formula essentially leads to the same result as the symmetric case if the eccentricity of the impact is allowed to go to [ ]^a

From the basic equation $E_t = \frac{1}{12}\sigma_d V_t \varepsilon_t$ the form for asymmetric use is developed.

EFFECTIVE TENSILE STRAIN VALUE

[ ]a

TENSILE STRAIN ENERGY

$$E_t = \frac{\sigma_d}{12} \frac{M_2}{\rho} \varepsilon_t$$

One problem with the above equations is what to do when the target mass M_2 is composed of [ ]a separate ring elements, since there is only provision for one value each of σ_d and ε_t. The approach that has been adopted in these instances is to use [ ]a of σ_d based on the proportional masses of the different materials. For establishing ε_t, the values of Θ associated with the major ring element (usually a blade ring) are used.

Another problem occurs if M_2 is composed of [ ]a These do not participate in tensile straining; therefore M_2 is recalculated for tensile straining by leaving out the [ ]a

The resulting velocity at the centerline of impact at the end of Stage 2 is [ ]a if containment is not achieved.

3.1.2.6 DETERMINATION OF FRAGMENT SIZES, ENERGIES, AND VELOCITIES AFTER IMPACT

Regardless of failure mode, the exiting fragment will be different in size from the total target mass, m_2.

Fragments from Stage 1 failures:

SA_1 mode - Fragment of arc θ_c with circumferential shear boundary as shown in Figure 3.11.

SA_2 mode - Fragment continuous in the circumferential direction with a shear boundary as shown in Figure 3.12. This failure mode leads to a special form of Stage 2, which is studied later.

SA_3 mode - Fragment of arc θ_c consisting of entire ring section without the effective wall h_e.

Fragments from Stage 2 failures:

A failure that results after Stage 1 containment produces a fragment of arc θ_c, consisting of the entire ring section without the effective wall h_e.

A failure that results from the continuation of a Stage 1 SA_2 shear mode produces a fragment of arc θ_c with an SA_2 circumferential boundary.

The masses of these failure fragments, designated m_3, are found in the same manner as m_2, using the revised boundaries as described.

Velocities at the CG of target masses and failure fragments:

Determination of the velocity at the CG of the target mass m_2 at the end of a collision is a reasonably easy calculation if the preceding calculations have all been done. The procedure is equally applicable to results from Stage 1 or Stage 2 as long as the proper data is used.

1. Designate $V_2 = V_{21}$ or V_{22} as the case may be.

2. The velocity of the CG of the entire target mass m_2 is

   [ ]a

3. Occasionally the rotational velocity of the target is also desired:

   [ ]a

4. If the CG of the failure fragment lies inside the missile impact zone, the fragment is
   [
   ]a The kinetic energy of the combined exiting missile would be

   [ ]a

5. If the CG of a failure fragment is outside the missile impact zone as shown in Figure 3.22, the fragment will [
   ]a and its translational velocity can be found by linear interpolation as follows:

   [ ]b Note that d_{CG} is positive if the CG of the fragment is between the CG of the target mass and the centerline of impact. d_{CG} is negative if the CG of the fragment is farther from the centerline of impact than the CG of the target mass.

[

]a

Figure 3.22

DIMENSIONS FOR FRAGMENT VELOCITY DETERMINATION

6. For closely spaced rings as shown in Figure 3.23, a kinematic study should be made to determine if ring #1 is pushed by the missile into ring #2, or whether the ring #1 fragment rotates clear of ring #2. This may be extremely difficult to determine accurately, so that some conservative assumptions may be justified as to the impact locations on the two rings. In a manner similar to that used for [ ]a the rotational energy of the ring #1 fragment is ignored in determining the initial energy of the combined missile striking ring #2. The energy of the missile combination can be found as follows:

[ ]a

The effective initial missile mass of the next collision is assumed to be

$$(M_1)_{n+1} = \left(\frac{2g\ KE_M}{V_2^{\,2}}\right)_n$$ where n refers to collision number.

7. If the study shows that the original missile will cause the failure fragment to rotate away and be left behind, the continuing missile energy will be

[ ]a

The ring failure fragment is assumed to follow the missile through the holes created without further loss of energy. The exit energy of such a ring fragment will then be

[ ]a

[

]ab

Figure 3.23
EXAMPLE OF TWO RINGS COLLIDING

3.1.2.7 SPECIAL CASES OF ASYMMETRIC COLLISIONS

3.1.2.7.1 STAGE 2 DEVELOPMENT AFTER AN SA_2 STAGE 1 FAILURE

As noted earlier, if an asymmetric case results in an SA_2 mode failure during Stage 1, the disc segments are still enveloped within a complete band of material, so that the segments will continue to deform the sheared band of material by tensile straining. The means by which this additional strain energy is accounted for are as follows:

1. Determine the mass properties of the sheared-off band as a target mass over the angle θ_K based on t_e of the band and establish if the band is symmetric or asymmetric with respect to the missile segments as per previous criteria. Actual target mass = m_{3K}.

2. If the fragment band is <u>symmetric</u>, calculate the Stage 2 tensile energy absorption capability $(E_t)_{SA2}$ for the band segment as one would for an ordinary symmetric ring. Since the fragment is symmetric, its overall velocity at the beginning of Stage 2 is taken to be V_{21} (see page B52). The missile energy at the end of Stage 1 to be absorbed in Stage 2 is

   [ ]a

   If $(E_t)_{SA2} > KE_{1Df}$, Stage 2 containment is achieved.

   If $(E_t)_{SA2} < KE_{1Df}$, $KE_2 = KE_{1Df} - (E_t)_{SA2}$

   [ ]a

   Missile energy after Stage 2 [ ]a where m_{3C} is the tensile failure fragment over the angle θ_C

3. If the fragment band is asymmetric, obtain from the original target mass [ ][a] and then calculate [ ][b] for the fragment band. Determine an effective mass M_{3K} to be used for calculating tensile strain energy: [ ][a]

The effective tensile strain value ε_t for the fragment band is calculated as on page B54, and the tensile strain energy is

[.][a]

The kinetic energy in a fragment such as this is composed of both a translational term and a rotational term. If we assume that the fragment continues to rotate at the same velocity as the original target mass, then

[ ][a]

The kinetic energy of the fragment band at the end of Stage 1 is then

[ ][a]

The disc or initial missile energy at the end of Stage 1 is

[ ][a]

Thus, the energy at the end of Stage 1 to be absorbed in Stage 2 is

[ ][a]

If $(E_t)_{SA2} > KE_{1Df}$, Stage 2 containment is achieved.

If $(E_t)_{SA2} <$ [ ][a]

[ ][a]

Kinetic energy of initial missile after Stage 2

[ ][a]

The fragment band produces a tensile failure fragment of the same cross-section over the angle Θ_c which is designated m_{3c} and has effective mass

[ ][a]

Velocity of m_{3c} fragment CG [ ][a]

Kinetic energy of m_{3c} fragment after Stage 2

[ ][a]

KE_{2D} and KE_{2f} are combined or left separate based on next collision considerations as described on page B58.

3.1.2.7.2 WALL CONNECTED RINGS

The method used to determine the effective target mass for these configurations (see Figures 3.20 and 3.21) was discussed on page . The assessment of Stage 1 shearing depends on the location of the impact and the relationship of the rings and connecting wall. Examples are shown in Figures 3.24 and 3.25.

For the example shown in Figure 3.24, all three rings are used to obtain $(U_p)_{SA3}$, since the
[ ][a]
the wall while they are shearing through in the SA_3 mode. The two inner rings are treated as a unit for M_2 mass calculation, while the outer ring and walls are lumped as shown for the M_2 calculation. If a Stage 1 failure occurs, the missile will continue unimpeded to a
[ ][a]

[

]a

Figure 3.24
WALL CONNECTED RINGS THAT SHEAR AS A UNIT

[

]a

Figure 3.25
WALL CONNECTED RINGS THAT
SHEAR SEPARATELY

For the example shown in Figure 3.25, the eccentricity between the connecting wall and the missile edge leads to the usual SA_1 mode for Stage 1 assessment. Examples of this type usually will have a Stage 1 failure of the end overhang of Ring #1. As this occurs, kinetic energy is being transferred through the connecting wall to Ring #2, causing that ring to attain some calculable translational and rotational velocities. This means that Ring #2 can be considered as [ ][a] from the shear fragment being produced in Stage 1 of Ring #1.

The question of whether or not the shear fragment and missile [ ][a] depends on what happens to Ring #2 as a result of the energy imparted to it during Stage 1 of the collision. As Ring #2 moves outward from the velocity imparted to it, [ ][a] of the ring occurs just as in a Stage 2 situation. If sufficient [ ][a] energy is available in Ring #2, the ring will hold in tension and its velocity will [ ][a] The missile from the Ring #1 shear failure will then strike Ring #2 and a second collision process must be evaluated. If there is not sufficient available tensile strain energy, Ring #2 will fail in tension and allow the missile to pass through unimpeded. Since the tension failure in this case is not preceded by any shear cutting of Ring #2, the tension break will probably occur at only one arbitrary location; thus it is assumed that the Ring #2 will remain attached to other stationary structure and not produce any reportable fragments.

The above assumed collision scenario is expressed by the following calculations.

1. Assess the outcome of the Stage 1 collision with Ring #1 (R1). If as usual there is Stage 1 SA_1 failure, then $(KE_1)_{R1}$ and $(V_{21})_{R1}$ are obtained as shown on page B52. The velocity of the CG of the entire target mass is

   [ ][a]

Note that while $(\ )_{R1}$ refers to Ring #1 data, this data is with the lumped data of Ring #2 included.

2. Determine the velocity at the centerline of the connecting wall:

   [ ]a (See Figure 3.25)

3. Calculate the radially directed kinetic energy of Ring #2 (R2) at the end of Stage 1 of the R1 collision:

   [ ]a

4. Determine the tensile strain energy capability of R2 in the first collision: [ ]a

   where $(\varepsilon_t)_{R2}$ is the effective tensile strain of R2 as determined on page B54.

5. If $(E_{t1})_{R2} < (KE_1)_{R2}$, R2 will fail in tension and allow the first collision missile to pass through unimpeded. The missile will be composed of the disc segment, M_D, and the R1 shear fragment, $(m_f)_{R1}$, and the energy of the combined pieces will be

   [ ]a

6. If $(E_{t1})_{R2} > (KE_1)_{R2}$, R_2 will hold in tension. The missile from the R1 shear failure will strike R2 and a second collision must be evaluated, where the missile initial energy is

   [ ]a

7. In the second collision with R2, it is assumed that the connecting wall has broken from the remaining stationary part of R1. Therefore, R2 will appear as shown in Figure 3.26 during the second collision. Note that the angle Θ_c must be adjusted by the standard procedure for second collisions struck by first collision fragments. A normal Stage 1 calculation is then made with the known information. SA_3 is the most likely shear mode.

8. If $(\Delta KE)_{R2} > (U_p)_{R2}$, Stage 1 perforation of R2 occurs with a resulting additional fragment based on the R2 ring body only. The fragment will probably be an asymmetric type and its characteristics are determined as shown on pages B55 to B58. The disc plus the R1 shear fragment will continue on to a piercing collision with the outer cylinder with combined energy

   [ ][a]

   The R2 fragment is reported as exiting the turbine with kinetic energy and velocity as determined in this collision.

9. If $(\Delta KE)_{R2} < (U_p)_{R2}$, Stage 1 containment is obtained and R2 proceeds into Stage 2 for the second time. It is assumed that the tensile strain energy capability has been reduced by the kinetic energy absorbed in tension by the ring during the first collision. The tensile strain energy capability of R2 in the second collision is then

   [ ][a]

   where ( )* are the quantities based on angles of the second collision and $(KE_1)_{R2}$ was calculated in Step 3.

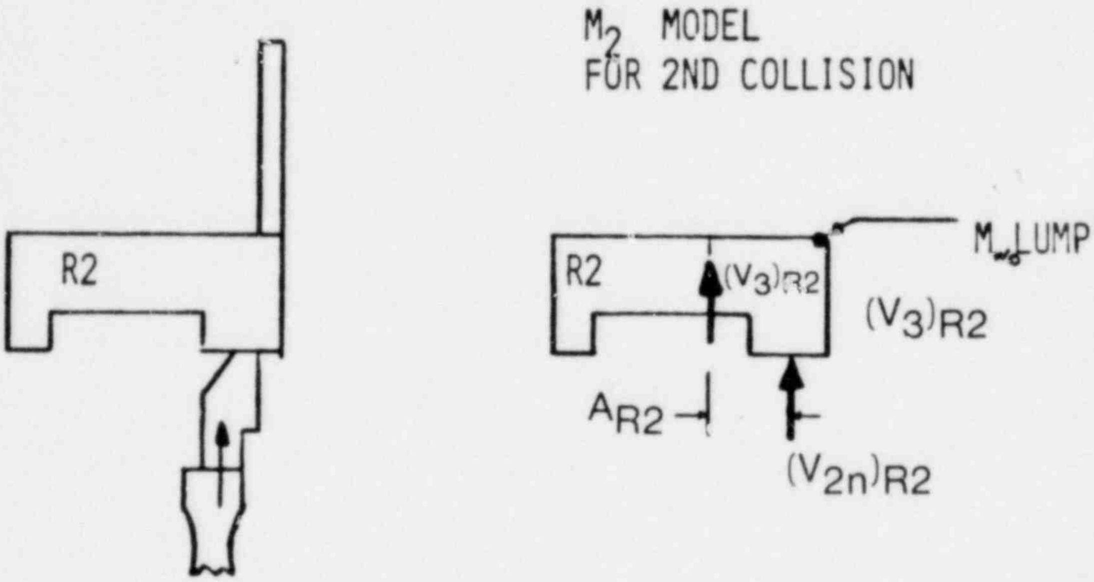

Figure 3.26
WALL CONNECTED RINGS - 2ND COLLISION

10. The kinetic energy of the system after Stage 2 is

[ ]a

If $(KE_2)_{R2} < 0$, overall containment has been achieved.

If $(KE_2)_{R2} > 0$, the disc segment and R1 shear fragment will continue on to a piercing collision with the outer cylinder with combined energy

[ ]a

The R2 ring fragment will be as determined on pages B55 to B58 and be reported as exiting the turbine with kinetic energy and velocity as determined in this collision.

3.1.2.7.3 BRITTLE FRACTURE

As stated earlier, tests have shown that
[ ]b type will occur at locations like section A-A of Figure 3.14 when impacted as shown. The wall location must be as defined on page . The most energy that can be absorbed in this type of collision is the energy of brittle fracture, E_b, which is defined below and is related to the momentum transfer energy and the energy of SA_1 Stage 1 failure. There is no Stage 2 energy absorption relative to this mode of failure.

The procedure to use is as follows:

1. Determine the possible SA_1 mode Stage 1 strain energy absorption value based on the fragment defined by the shaded area, A_b. The shear strain energy is calculated as on page B51 and the compression strain energy as on page B28. Then the possible plastic strain energy of the brittle fracture is

   [ ]a

It will be assumed that this value is one possible limit of the [ ]a energy loss; i.e., the energy loss cannot exceed that which would be lost by Stage 1 type failure.

2. Determine the mass of the ring fragment, m_{2b}, that would result from [ ]a

$m_{2b} = A_b \theta_c R_{mb} \rho$ where R_{mb} is the radius to the centroid of the A_b area.

3. Determine the eccentricity coefficient, K_b, of the fracture fragment:

$$K_b = \frac{(I_{CBM})_b}{m_{2b} a_b^2 + (I_{CBM})_b}$$

where a_b is the distance from the centerline of impact to the CG of m_{2b} and $(I_{CBM})_b$ is the mass moment of inertia of m_{2b}.

The effective mass of the fragment is $M_{2b} = K_b m_{2b}$

4. The maximum energy loss due to an inelastic collision is

[ ]a

It will be assumed that this is the other possible limit of brittle fracture energy loss.

5. Therefore, the energy of brittle fracture is the lesser of the two limits:

$$E_b = \text{the lesser of} \begin{cases} U_{pb} \\ \Delta KE_b \end{cases}$$

6. The energy of the system after the collision is

   $KE_1 = KE_0 - E_b$

   and the velocity at the center of impact is

   [ ]a

7. Since the fragment is asymmetric, its CG velocity [ ]a

   and translational kinetic energy [ ]a

   The missile energy is [ ]a

3.1.2.7.4 HUB COLLISIONS

Disc hubs may collide with rings that were not previously impacted by the rim of the disc. This possibility should be investigated as part of the sequence of collisions as the disc moves outward (see Figure 3.27). As done with rim collisions, a slight overlap of the disc hub on the blade roots is ignored and the impact relationship of hub to back-up ring is assumed to be as depicted in Figure 3.28. The compressed volume is obtained as shown and the shear or brittle fracture energy is obtained in accordance with the location of the backing wall. The radius of the hub at the impact location is used to determine the arc length needed for the various parameters used in energy calculations. All calculations and decisions then follow previously established procedures. NOTE: Any stationary remnant of a previously impacted ring or other cylinder structure will not be considered as capable of sustaining a hub collision because of the uncertainty of its final location and energy absorption capability remaining after the preceding collision.

[

]a

Figure 3.27
TYPICAL HUB COLLISION

[

]a

Figure 3.28
HUB COLLISIONS
COMPRESSED VOLUME & IMPACT LOCATION

3.1.3 SIMULTANEOUS COLLISIONS WITH TWO ADJACENT RINGS

3.1.3.1 BASIS OF ANALYSIS

Collisions of this type are quite common at certain locations in Low Pressure (LP) turbines. The primary difference between these collisions and the previously discussed symmetric and asymmetric collisions with [ ]a is that the incoming kinetic energy must be apportioned between the adjacent rings and then the Stage 1 and Stage 2 concepts must be considered for each of the two rings. To discuss all possible combinations of collision types would require a rather lengthy treatise, so only the common cases that have been discovered in existing turbines will be covered here.

3.1.3.2 COLLISION INVOLVING SYMMETRIC IMPACT AND BRITTLE FRACTURE

The most common example of this type collision is the one shown in Figure 3.29, which is the [ ]a impacting the [ ]a (symmetric impact) and the [ ]a (brittle fracture). However, other examples exist in some of the LP turbines. The procedure for calculation is somewhat tedious but relatively straightforward.

Procedure:

Perform steps 1 to 3 of Section 3.1.2.7.3 for the brittle fracture fragment by itself.

4. Determine the target mass of the symmetric ring structure, M_{2S}, based on the procedure of Section 3.1.1.3. For the flow guide structure shown, to simplify accounting for the $3t_c$ flap on the cone, increase the mass directly impacted by the addition of an equivalent piece t_c wide beyond the impact edge.

[

]a

Figure 3.29
COMBINED SYMMETRIC IMPACT & BRITTLE FRACTURE

5. The maximum possible kinetic energy loss of the brittle fracture fragment by itself is

[ ]a where $M_2 = M_{2b} + M_{2S}$

and the energy loss of brittle fracture is

E_b = the lesser of $\begin{matrix} U_{pb} \\ \Delta KE_b \end{matrix}$

6. Compute $U_{pS} = E_{cS} + E_{sS}$ for the symmetric ring structure. For the flow guide structure shown, an SA_1 type failure mode will govern.

7. Determine the maximum possible Stage 1 energy loss of the combined impacted masses:

[ ]a

8. Determine the Stage 1 result:

(a) If $\Delta KE > E_b + U_{pS}$, Stage 1 perforation occurs and the system energy at the end of the collision is

[ ]a (Go to Step 10)

(b) If $\Delta KE < E_b + U_{pS}$, Stage 1 containment is achieved and leads to Stage 2 (Step 9).

9. If Step 8(b) governs, obtain the tensile strain energy of the symmetric ring structure, E_{tS}. For the flow guide example, the t_c effective part of the cone is considered to be part of the tensile cross-sectional area. The system energy at the end of Stage 2 is

[ ]a

If $KE_2 < 0$, overall containment has been achieved.

If $KE_2 > 0$, Stage 2 perforation has occurred (go to Step 10).

10. If perforation occurs in either Stage 1 or Stage 2, the system velocity in the line of impact is

V_{2n} = [ ]a where n refers to Stage 1 or 2 as applicable.

11. The major missile (disc segment + symmetric fragment) continues to the next collision at velocity V_{2n} and kinetic energy

[ ]a where m_{21S} is the mass of the symmetric ring fragment bounded by the shear planes.

12. The brittle fracture fragment exits with a CG velocity [ ]a

and translational kinetic energy [ ]a

3.1.3.3 COLLISION INVOLVING SYMMETRIC IMPACT AND ASYMMETRIC IMPACT WITHOUT BRITTLE FRACTURE

Collisions of this type have been found to occur in certain locations of some [ ][a] (for example, see Figure 3.30). As with the preceding example, the principles are relatively straightforward, but the calculations are still more complex because of the greater number of possible failure combinations.

Procedure:

1. Evaluate the effective target mass for each of the two ring structures: M_{2S} = symmetric target mass

   M_{2A} = asymmetric target mass

   $M_2 = M_{2S} + M_{2A}$

2. Calculate the maximum Stage 1 energy loss associated with each of the two ring structures:

   Symmetric [ ][a]

   Asymmetric [ ][a]

3. For each of the two ring structures, calculate the Stage 1 energy of plastic deformation:

   Symmetric $U_{pS} = E_{cS} + E_{sS}$ based on the appropriate modes

   Asymmetric $U_{pA} = E_{cA} + E_{sA}$ described in earlier sections

[

][a]

Figure 3.30
COMBINED SYMMETRIC & ASYMMETRIC IMPACTS

4. Determine the outcome of the Stage 1 processes:

(a) If ΔKE_S < [ ]a

(b) If ΔKE_S > [ ]a

(c) If ΔKE_S > [ ]a

(d) If ΔKE_S < [ ]a

5. Consider the meaning of the Stage 1 results in Step 4:

(a) This Stage 1 result says both ring structures provide Stage 1 containment; therefore the two ring structures enter Stage 2 and the final result is

[ ]a where E_{ts} and E_{tA} are determined as shown in previous sections.

If $KE_2 < 0$, overall containment has been ac..ieved.

If $KE_2 > 0$, under most conditions (see page B58 for exception) the original missile plus the symmetric plug fragment will continue

together alone at the velocity [ ]a and with combined

kinetic energy [ ]a

The asymmetric fragment created by Stage 2 failure will then have velocity V_{3f} a' defined in Step 5, Section 3.1.2.6, and KE_f as defined in Steo 7, Section 3.1.2.6.

(b) This is the result when both ring structures have Stage 1 failure. What happens after that is a function of the Stage 1 asymmetric failure mode.

SA_1 or SA_3 mode:

[ ]a

Kinetic energy of original missile and fragment from symmetric structure:

[ ]a

Kinetic energy of fragment from asymmetric structure:

Fragment <u>symmetric</u> (see Step 4, Section 3.1.2.6)

[ ]a

In this case, the missile into the next collision would consist of $M_1 + m_{21S} + m_3$ and total kinetic energy would be $KE_{DSf} = KE_{DS} + KE_f$

Fragment <u>asymmetric</u> (see Step 5, Section 3.1.2.6)

[ ]a

In most cases, this would be an exiting fragment as in Step 7, Section 3.1.2.6, but the possibility of Step 6, Section 3.1.2.6 should be considered.

SA_2 mode:

[ ][a]

Kinetic energy of original missile and fragment from symmetric structure at the end of Stage 1:

[ ][a]

The asymmetric structure at the end of Stage 1 has formed the continuous band typical of SA_2 failures. Refer to Section 3.1.2.7.1 of this report.

o If the fragment band is <u>symmetric</u> at the end of Stage 1, $V_{3f} = V_{21}$ and kinetic energy of the band is

[ ][a] where m_{3K} is the fragment band mass over the angle θ_K determined on the basis of t_e of that fragment.

The available missile kinetic energy at the end of Stage 1 then is [ ][a]

Calculate the tensile strain energy capability of the band as for a symmetric ring: $(E_t)_{SA2}$.

If $(E_t)_{SA2} > KE_{1DSf}$, Stage 2 containment is achieved.

If $(E_t)_{SA2} < KE_{1DSf}$, $KE_2 = KE_{1DSf} - (E_t)_{SA2}$

[ ][a]

The missile leaving the collision will be $M_1 + m_{21S} + m_{3c}$ where m_{3c} is the tensile failure fragment from the band over the angle ϕ_c. The missile energy leaving the collision will be

[.][a]

- If the fragment band is <u>asymmetric</u> at the end of Stage 1, first obtain

the CG velocity of the asymmetric target mass: [ ][a]

Fragment band velocity [ ][a]

Obtain $(E_t)_{SA2}$ and KE_{1f} as given in Step 3, Section 3.1.2.7.1.

KE_{1DS} is the same as the preceding case.

Energy at end of Stage 1, $KE_{1DSf} = KE_{1DS} + KE_{1f}$

If $(E_t)_{SA2} > KE_{1DSf}$, Stage 2 containment is achieved.

If $(E_t)_{SA2} < KE_{1DSf}$, $KE_2 = KE_{1DSf} - (E_t)_{SA2}$

[ ][a]

Energy of initial missile and symmetric fragment at end of Stage 2,

[ ][a]

The asymmetric fragment band is handled the same as on page B61, giving KE_{2f}.

KE_{2DS} and KE_{2f} are combined or left separate based on next collision considerations as described on page B58.

(c) In this case, there is Stage 1 failure of the symmetric ring structure and Stage 1 containment at the asymmetric ring structure. The entire asymmetric ring structure then enters Stage 2 tensile straining. The system kinetic energy at the end of Stage 1 is reduced by the amount of kinetic energy transferred to the symmetric structure outside of the shear plane. The reduced value is the kinetic energy available for Stage 2 absorption. The kinetic energy of the new system at the end of Stage 2 is

[ ][a]

where [ ][a]

and E_{tA} is obtained from M_{2A} as on page B54.

If $KE_2 < 0$, overall containment is achieved.

If $KE_2 > 0$, there is Stage 2 failure with a velocity of the original missile and the symmetric plug fragment

[ ][a] and combined kinetic energy

[.][a]

The asymmetric fragment created by Stage 2 failure will then have velocity V_{3f} as defined in Step 5, Section 3.1.2.6 and KE_f as defined in Step 7, Section 3.1.2.6. KE_{2DS} and KE_f are combined or left separate based on next collision consideration on page B58.

(d) In this case, there is Stage 1 failure of the asymmetric ring structure and Stage 1 containment at the symmetric ring structure. The Stage 2 behavior depends on the Stage 1 asymmetric failure mode.

SA_1 or SA_3 mode:

[ ]^a

Kinetic energy of fragment from asymmetric structure:

Fragment symmetric (see Step 4, Section 3.1.2.6)

[ ]^a

Fragment asymmetric (see Step 5, Section 3.1.2.6; V_{3f} is denoted as V_{31f} here.)

[ ]^a

Kinetic energy of symmetric structure and original missile at the end of Stage 1 [ ]^a

Available kinetic energy at the end of Stage 1 to be absorbed in Stage 2

[ ][a]

where KE_{1f} is the appropriate value from the preceding page.

System kinetic energy at the end of Stage 2

[ ][a] where E_{tS} is determined as before.

If $KE_2 \leq 0$, there is Stage 2 containment.

If $KE_2 > 0$, there is Stage 2 failure with a velocity of the original missile and the symmetric plug fragment

[ ][a] where [.][a]

The kinetic energy of the original missile and the plug from the symmetric structure is

[ ][a]

and the kinetic energy of the fragment from the asymmetric structure is

[ ][a] where [.][a]

KE_{2DS} and KE_{2f} are combined or left separate based on next collision considerations as described on page B58.

SA2 mode:

[ ]a

Kinetic energy of symmetric structure and original missile at the end of

Stage 1 [ ]a

o If the SA_2 fragment band is symmetric at the end of Stage 1, $V_{3f} = V_{21}$ and the kinetic energy of the band is [ ]a (see Section 3.1.2.7.1)

Available missile kinetic energy at the end of Stage 1

[ ]a

Calculate tensile strain energy capability [ ]a as described previously.

System kinetic energy at the end of Stage 2

[ ]a

If $KE_2 \leq 0$, there is Stage 2 containment.

If $KE_2 > 0$, there is Stage 2 failure and the original missile, the symmetric structure plug, and the fragment from the SA_2 band all have velocity

[ ]a

and combined kinetic energy

[ ]a

- If the SA_2 fragment band is <u>asymmetric</u> at the end of Stage 1, obtain V_{31f} from V_{21} as in Step 3, Section 3.1.2.7.1, and

$$M_{3K} = \frac{V_{31f}}{V_{21}} m_{3K} .$$

[ ]a

Determine KE_{1f} from Step 3, Section 3.1.2.7.1. Kinetic energy of symmetric structure and original missile at the end of Stage 1

[ ]a

Available kinetic energy at the end of Stage 1

[ ]^a

Tensile strain energy capability [ ]^a

System kinetic energy at the end of Stage 2

[ ]^a

If $KE_2 < 0$, there is Stage 2 containment.

If $KE_2 > 0$, there is Stage 2 failure and the original missile and the symmetric plug have a velocity

[ ]^a

and combined kinetic energy

[ ]^a

The fragment from the asymmetric band is handled as on page B62, giving KE_{2f}. KE_{2DS} and KE_{2f} are combined or left separate based on next collision considerations on page B58.

3.1.3.4 OTHER POSSIBLE SIMULTANEOUS COLLISIONS OF ADJACENT RINGS

Other combinations of simultaneous collisions are possible, such as:

Asymmetric impact and brittle fracture

Asymmetric impact and asymmetric impact

Symmetric impact and symmetric impact.

However, none of these combinations has been discovered in existing low pressure turbine cylinders, so analytical approaches for these cases have not been developed.

3.2 COLLISIONS INVOLVING CYLINDER WRAPPERS (SHELLS)

3.2.1 BASIS OF ANALYSIS

The current analysis development assumes that in most cases a blunt (Hagg-Sankey) type collision with a cylinder wrapper (shell) will occur only if the first collision is a symmetric case with a radial backing wall in the path of the disc. In such a case, all subsequent collisions will be of blunt orientation; however, the circumferential edge of the radial wall will be the blunt surface since it is assumed that the wall remains erect.

If a disc is involved in an asymmetric ring collision first, any subsequent collisions with cylinder wrappers are considered to be piercing orientation.

The procedure used for blunt collisions is a slightly modified version of the basic Hagg-Sankey procedure for long shells as described in Section 2.0 of this report.

The method used for piercing collisions is based on observation of the EPRI missile test of this type to which conservative assumptions are applied (2).

3.2.2 BLUNT (HAGG-SANKEY) SHELL COLLISIONS

There are two different conditions under which this type of collision will occur:

- The collision is caused by an attached wall that is torn through from the preceding collision (see Figure 3.31). In this case the circumferential arc length of the contact zone is

  $L_c = (r_{01} + \frac{t}{2})\,\theta_{c1}$ where θ_{c1} is established in the preceding collision.

- The collision is caused by an unattached wall that has continued on from a previous perforation (see Figure 3.31). In this case the circumferential arc length of the contact zone is

  $L_c = \frac{r_{o2}}{r_{o1}}(r_{o1} + \frac{t}{2})\,\theta_{c2}$ where θ_{c2} and r_{o2} are established from the originating collisions.

  In the event of an offset center or two center wrapper, it is sufficiently accurate to use the local radius for r_{o1}.

Assumptions:

1. One radial edge of the wall fragment is [ ][a]

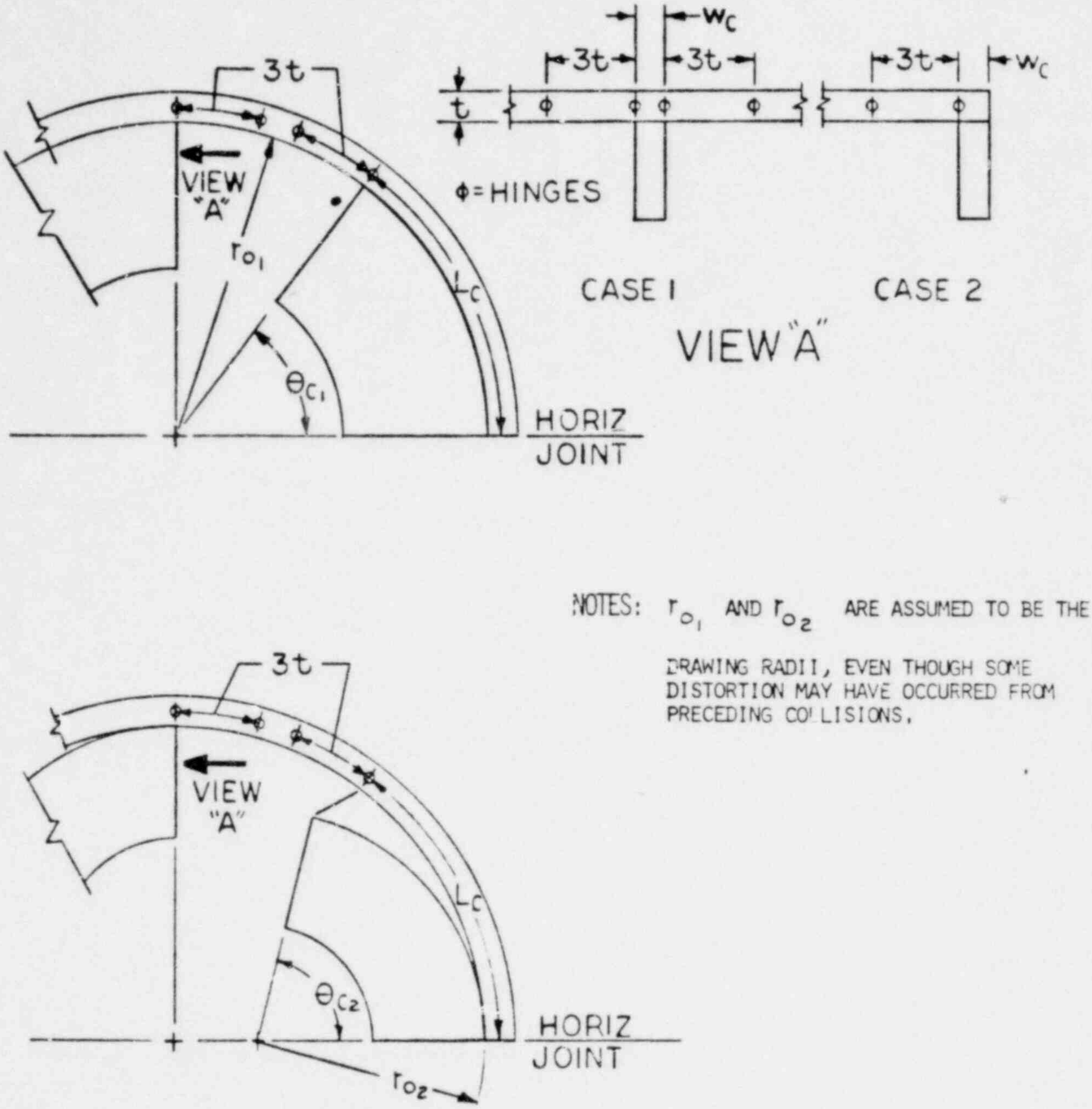

Figure 3.31
BLUNT COLLISIONS WITH CYLINDER WRAPPERS

2. The horizontal joint is assumed to provide no shear resistance, but there is sufficient tensile restraint to develop full tensile strain of the shell over the region specified below.

3. The derivation is based on a gap between impacting fragments that is greater than [ ]a, which will usually be the case.

4. If they should happen to occur, the procedure is also applicable to blunt hits by discs or rings not preceded by walls.

5. There are two basic shell configurations that normally occur in practice. These are shown in Figure 3.31. Case 1 is handled in typical Hagg-Sankey fashion, assuming [ ]a tensile strain over the M_2 elements in Stage 2. Case 2 is assumed to be capable of sustaining only [ ]a tensile strain in much the same manner as a ring. Tensile strain in Stage 2 is taken as [ ]a over the m_{21} element plus [ ]a at the short side and [ ]a along the long side.

Calculation Procedure:

CASE 1: Biaxial tension case

Stage 1 [ ]a

[ ]a

$$U_p = E_s + E_c$$

$$M_2 = \rho\,[(2\,L_c + w_c)\,t^2 + L_c w_c t] \qquad m_{21} = \rho\,L_c w_c t$$

[ ][a]

If U_p < ΔKE, Stage 1 perforation occurs and system velocity after the collision is found from

[ ][a]

The K.E. of the continuing missile is

[ ][a]

If U_p > ΔKE, Stage 1 containment is achieved and Stage 2 occurs.

[ ][a]

K.E. of system at end of Stage 2 is

[ ][a]

Containment is achieved if $KE_2 < 0$.

If $KE_2 > 0$, Stage 2 failure occurs with the following results:

K.E. of continuing missile where wall was attached [ ][a]

K.E. of continuing missile where wall was not attached [ ][a]

Velocity at end of Stage 2

[ ][a]

CASE 2: Uniaxial tension case

<u>Stage 1</u> [ ][a]
[ ][a] $U_p = E_s + E_c$

$M_2 = \rho[(L_c + w_c)\, t^2 + L_c w_c t]$ $m_{21} = \rho\, L_c w_c t$

Remainder of Stage 1 calculations are the same as Case 1.

<u>Stage 2</u> $U_p > \Delta KE$

[ ][a]

Remainder of Stage 2 calculations are the same as Case 1.

3.2.3 PIERCING COLLISIONS WITH SHELLS

If a piercing collision is called for as per Section 3.2.1, it will be assumed to occur as described here and shown in Figure 3.32.

[

]a

DEFINITIONS:

[

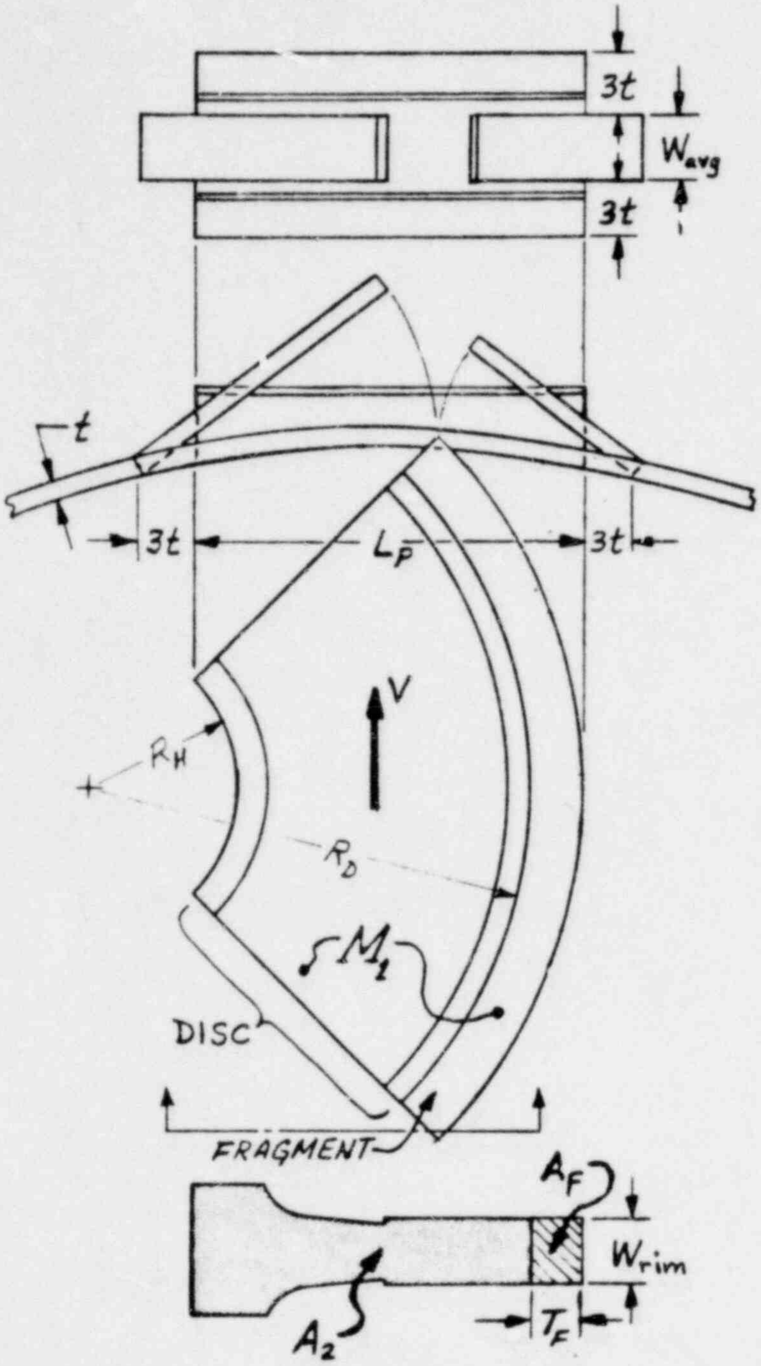

]a

NOTE: The disc will carry a previously perforated fragment only if that fragment achieved a symmetric status during the collision that produced it.

Figure 3.32
PIERCING COLLISION

EFFECTIVE MASS OF IMPACTED SHELL

$$M_2 = \rho [W_{avg} L_p t + 2 (W_{avg} + L_p) t^2 \text{ or } = \rho [(A_2 + A_F) t + 2 (W_{avg} + L_p) t^2]$$

MISSILE VELOCITY AFTER COLLISION

[ ]a

MISSILE KINETIC ENERGY AFTER COLLISION

[ ]a

If this is the last collision (i.e., outer cyl.), missiles are reported as separate components, i.e., disc and previously perforated fragment. The pierced shell is considered to produce no reportable fragments.

3.2.4 SECONDARY COLLISIONS WITH PREVIOUSLY PERFORATED SHELLS

A wrapper that has failed as a result of a Hagg-Sankey type collision caused by a radial wall (see Figure 3.33) may also be subsequently impacted by the ring(s) and/or disc rim if the hole created by the initial perforation is not large enough to allow those items to pass through unimpeded. The 3t flaps are assumed to have been previously accelerated and may possibly be missing, so that only shell material beyond the outer 3t boundary is considered for the additional collision. The analysis procedure used is simply to assume conservation of momentum in a totally in collision.

For a flat-top cross-section, the method is quite simple. An m_{21} area is defined by the width w and the arc length $R_1\theta_c$. The m_{22} is obtained from 3t flaps at one end and along one or both circumferential edges as applicable.

[ ][a]

Velocity after collision [ ][a]

The structure depicted in Figure 3.33 strikes the shell again with the sloped surface of the blade ring, as shown in Figure 3.34. The average radius $\frac{1}{2}(R_1 + R_2)$ is used to obtain the appropriate arc length.

[

][a]

Figure 3.33
SECONDARY COLLISION
SINGLE RADIUS EXAMPLE

[

][a]

Figure 3.34
SECONDARY COLLISION
VARYING RADIUS EXAMPLE

3.3 REPORTING OF EXITING MISSILE FRAGMENTS

The missile analysis process assumes that fragments created symmetrically [ ][a] as it proceeds through the sequence of collisions. This is a generally conservative method of obtaining total exit energies and velocities. Since the disc segments and various fragments [ ][a] upon exiting from the turbine, they are reported as [ ][a] items. Fragments created asymmetrically are not generally carried through the remaining collisions unless they are trapped between the missile and the next structure impacted. Asymmetric fragments are therefore reported with the conditions that they have at the end of the last collision in which they are known to participate.

The following properties are reported for all exiting missile fragments:

Fragment weight - lb (rounded to nearest 5 lb)

Exit velocity - ft/sec (rounded to nearest 1 ft/sec)

Exit translational kinetic energy - 10^6 ft-lb (rounded to nearest 0.01 x 10^6 ft-lb)

Other comments related to specific types of fragments are given below.

DISC SEGMENTS: The exiting mass of the disc segment is assumed to be the [ ][a]
Dimensional parameters are reported as shown in Figure 18 of Section A.

CYLINDER FRAGMENTS: Exiting blade ring and cylinder fragments vary significantly in shape. Fragments with equivalent rectangular areas are reported rather than furnishing detailed sketches and tables of dimensions (see Figure 3.35). Arc length at the centroid of the cross-sectional area is also given. The methods of calculating the equivalent dimensions are as follows:

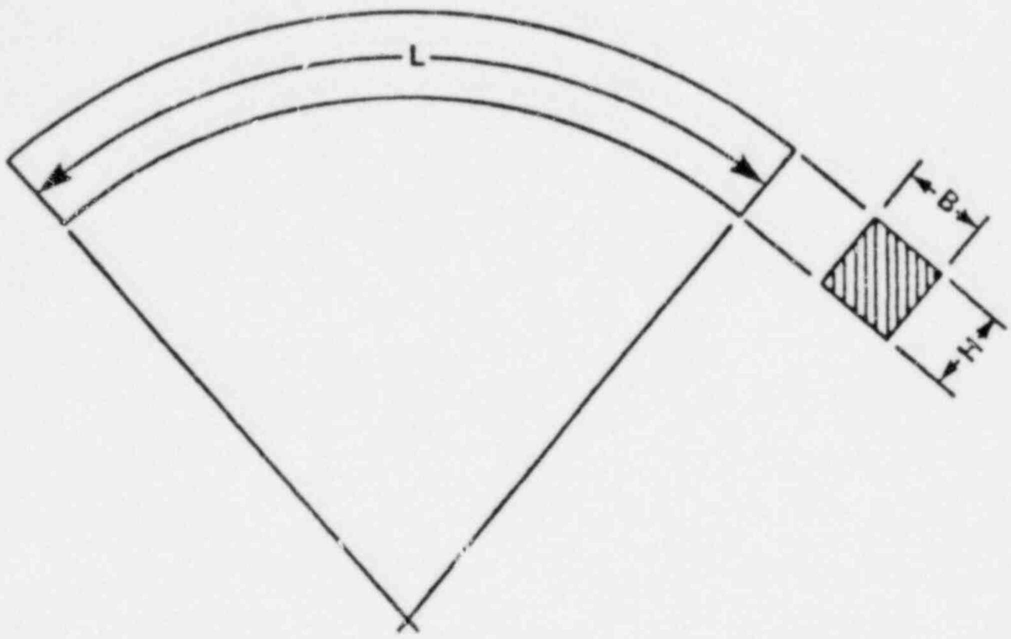

Figure 3.35
L.P. CYLINDER & BLADE RING FRAGMENTS EQUIVALENT RECTANGULAR DIMENSIONS

A. Ring fragments without included stationary blades (see Figure 3.36)

1. Select a characteristic dimension of the ring, usually the overall width of the ring fragment, B_2, rounded to the nearest 0.1 inch.

2. Calculate the equivalent thickness, H_2, from the known cross-sectional area, A_2, and the characteristic width, B_2:

$$H_2 = \frac{A_2}{B_2}$$

(Round H_2 to the nearest 0.1 inch).

3. From the actual mass of the fragment, m_{f2}, calculate the characteristic arc length, L_2:

$$L_2 = \frac{m_{f2}}{\rho B_2 H_2}$$

(Round L_2 to the nearest 0.1 inch).

For symmetric fragments, m_{f2} is the individual ring element part of m_{21} as defined on page B24.

For asymmetric fragments, m_{f2} is the individual ring element part of m_3 as defined on page B55.

When m_3 has two or more ring elements, the translational velocity for each element is assumed to be that of the integrated ring mass at its CG.

[

]a

Figure 3.36
GEOMETRY USED TO OBTAIN RING FRAGMENT DIMENSIONS

B. Ring fragments with included stationary blades (see Figure 3.36):

1. Calculate the arc length at the centroid of the cross-section (do not include stationary blading in this cross-section):

$$L_1 = R_{m1} \theta_c$$

(Round L_1 to nearest 0.1 inch)

2. From the mass of the fragment including blades, m_{f1}, calculate the equivalent thickness, H_1, using a characteristic dimension of the ring fragment width as B_1 (rounded to the nearest 0.1 inch):

$$H_1 = \frac{m_{f1}}{\rho B_1 L_1}$$

(Round H_1 to the nearest 0.1 inch)

For symmetric ring fragments, m_{f1} is the individual ring element part of m_{21} including stationary blading. For asymmetric fragments, m_{f1} is the individual ring element part of m_3 including stationary blading. Velocity is determined as in paragraph "A" preceding.

CYLINDER WRAPPER PIECES: Report as part of any wall to which they are welded in a symmetric collision case. An unattached wrapper that is blunt impacted creates an m_{21} fragment if Stage 1 perforation occurs, and no fragment if Stage 2 failure occurs.

LOW ENERGY MISSILES: Exit velocity and kinetic energy are not reported for missile fragments that have an exit kinetic energy calculated to be less than [ ][a]

EJECTION ANGLES of the disc missiles are given by the following guidelines (refer to Figure 3.37):

- o Discs 1 to N-1: ±5 degrees measured from the vertical radial plane passing through the disc.

- o Disc N: 5 degrees to 25 degrees measured from the vertical radial plane passing through the disc. Fragments from this disc will eject only towards the cylinder end wall.

  (N is the number of discs in a single flow half).

These guidelines are based on results reported in reference 1.

SAMPLE PAGES: Examples of the format in which fragment data is presented in customer reports are shown in Tables 3.01 through 3.03

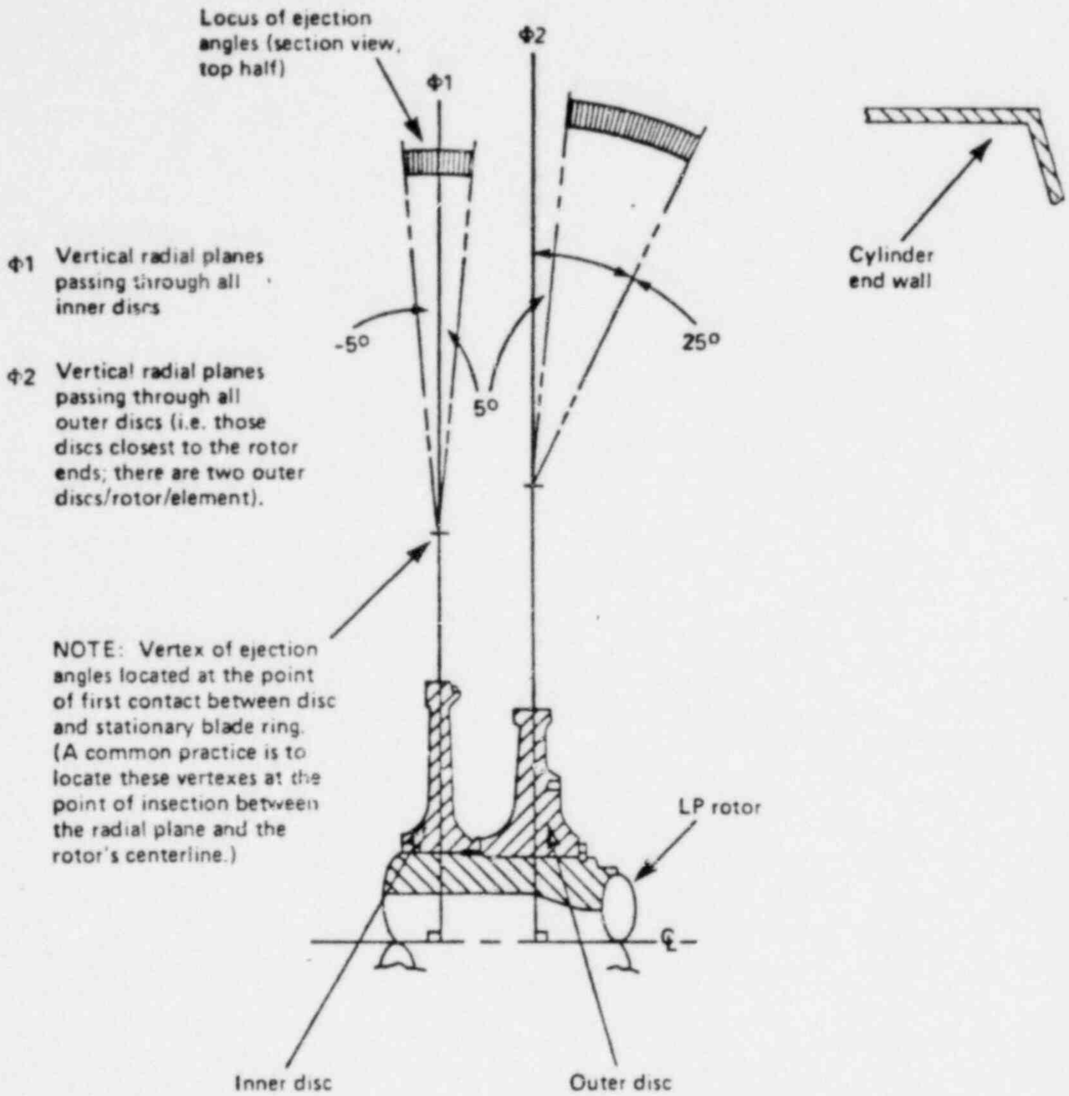

Figure 3.37
EJECTION ANGLES FOR L.P. DISCS

Table 3.01

LP CYLINDER AND BLADE RING FRAGMENT DIMENSIONS

(Refer to Figure 3.35)

FRAGMENT NUMBER	L (in) 90° SEGMENT	L (in) 120° SEGMENT	B (in)	H (in)

[

]a

Table 3.02
INTERNAL DISC SEGMENT PROPERTIES FOR LP DISCS 1 THROUGH 6

		100% SPEED		132% SPEED		DESTRUCTIVE OVERSPEED	
	WEIGHT (lb)	VELOCITY (ft/sec)	ENERGY (10^6 ft-lb)	VELOCITY (ft/sec)	ENERGY (10^6 ft-lb)	VELOCITY (ft/sec)	ENERGY (10^6 ft-lb)
90° DISC SEGMENT							
DISC No. 1	[						
DISC No. 2							
DISC No. 3							
DISC No. 4							
DISC No. 5							
DISC No. 6							
DISC No. 6*							]ab
120° DISC SEGMENT							
DISC No. 1	[						
DISC No. 2							
DISC No. 3							
DISC No. 4							
DISC No. 5							
DISC No. 6							
DISC No. 6*							]ab

*Weight change due to loss of blades prior to reaching destructive overspeed.

B111

Table 3.03
EXIT MISSILE PROPERTIES FOR NO. 2 LP DISC AND FRAGMENTS

		100% SPEED		132% SPEED		DESTRUCTIVE OVERSPEED	
	WEIGHT (lb)	VELOCITY (ft/sec)	ENERGY (10^6 ft-lb)	VELOCITY (ft/sec)	ENERGY (10^6 ft-lb)	VELOCITY (ft/sec)	ENERGY 10^6 ft-lb)
90° DISC BURST							
DISC No. 2	[						
FRAGMENT No. 2.1							
FRAGMENT No. 2.2							]ab
120° DISC BURST							
DISC No. 2	[						
FRAGMENT No. 2.1							
FRAGMENT No. 2.2							]ab

*Exit missile energies of less than 100,000 ft-lb are not reported.

B112

4.0 REFERENCES

1. "The Containment of Disk Burst Fragments by Cylindrical Shells, Hagg, A.C., and Sankey, G.O.; ASME Paper No. 73-WA/PWR-2 August 1, 1973

2. "Preliminary Results of Turbine Missile Casing Tests, "Yoshimura, H.R. and Schamaun, J.T.; Electric Power Research Institute Project 399, Preliminary Report, October, 1978.

5.0 Appendices

Appendix A: Derivation of Effective Height of a Radial Wall for Tensile Straining and Mass Moment of Inertia

Appendix B: Mass Moment of Inertia of Curved Beams

Appendix C: Values of Dynamic Ultimate Strength for Common Westinghouse Structural Materials

APPENDIX A: Derivation of Effective Height of a Radial Wall for Tensile Straining and Mass Moment of Inertia

The effective height concept for use in missile absorption calculations involving radial walls is based on the method used for finding circumferential stresses in a thick-walled cylinder with internal pressure. The equations used are from Formulas for Stress and Strain, Roark and Young, 5th Ed., Table 32, Case 1, page 504. Figure A.1 on the next page shows the dimensional parameters used and the assumed distribution of loading.

The derivation is also based on the following additional assumptions:

1. [

]a

2. [

]a

3. [

]a

q = internal radial pressure from the ring

Maximum circumferential stress at radius r_i

$$\sigma_{c\ max} = q \frac{r_o^2 + r_i^2}{r_o^2 - r_i^2}$$

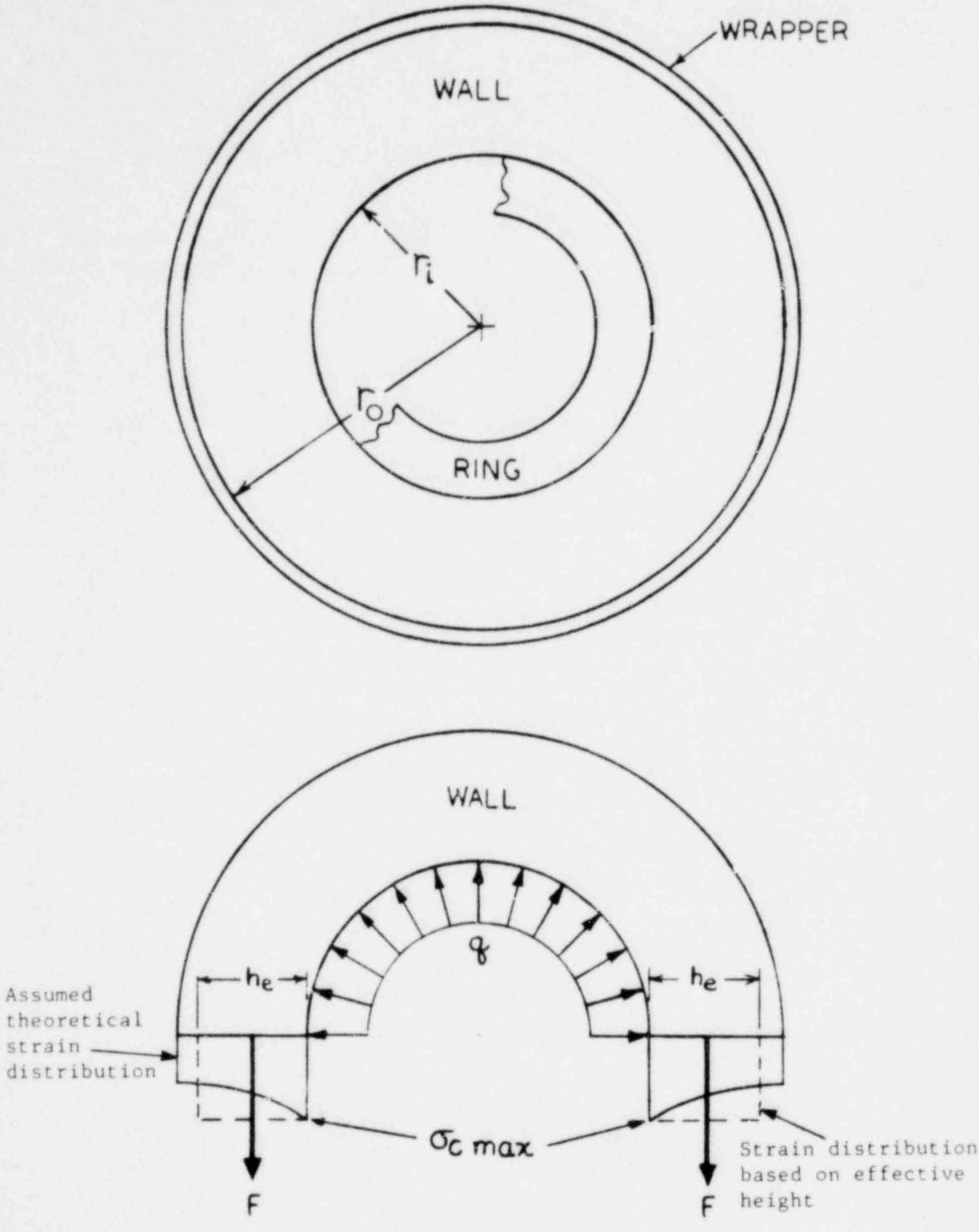

Figure A.1

DIMENSIONS & ASSUMED LOADING FOR EFFECTIVE HEIGHT OF A WALL

The total circumferential force is found from the free-body in Figure A.1:

$$2F = 2r_i q \rightarrow F = r_i q$$

The effective height h_e is defined as the radial dimension outward from the ring that provides the same circumferential force at the maximum stress level as does the varying distribution over the full wall height:

$$h_e\,\sigma_{c\,max} = F = r_i q$$

$$q\,\frac{r_o^2 + r_i^2}{r_o^2 - r_i^2}\,h_e = r_i q$$

EFFECTIVE HEIGHT $\quad h_e = r_i\,\dfrac{r_o^2 - r_i^2}{r_o^2 + r_i^2}$

SPECIAL CASES

Figures A.2 and A.3 depict the method to be used when a wall is interrupted by an intervening ring or its direction changes from radial to conical. Essentially it has been conservatively assumed that the intervening ring has no effect on the determination of h_e and that the conical direction affects only the effective height h_s as used in asymmetric collisions.

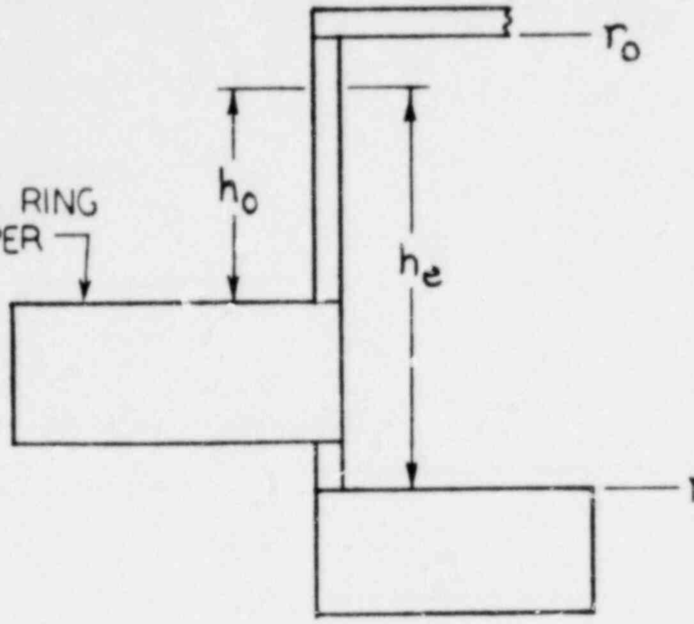

Figure A.2

INTERVENING RING

(TYPICAL, LP TYPE II & IV LAST EXTRACTION)

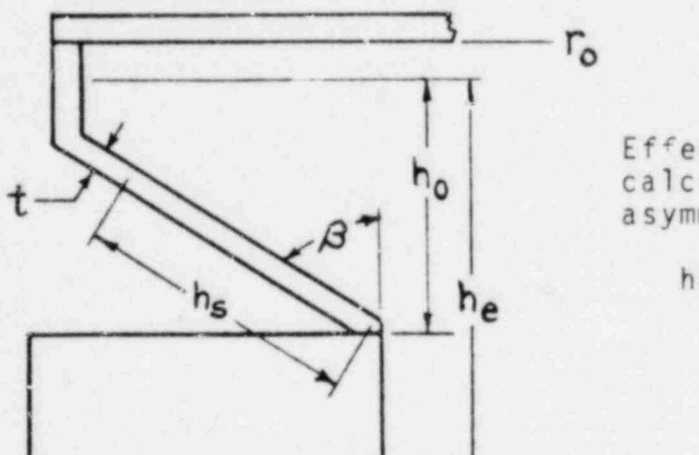

Effective wall to use in calculating properties of asymm. struck rings.

$$h_s = (h_o - 3t)\cos\beta + 3t$$

EFFECTIVE HEIGHT OF WALL FOR SPECIAL CASES

Figure A.3

CONICAL WALL

(TYPICAL, LP TYPE I LAST EXTRACTION)

APPENDIX B: Mass Moment of Inertia of Curved Beams

When a ring element is impacted asymmetrically, there is good reason to believe that the impacted mass behaves as a curved beam attempting to rotate out of its plane about an axis through the center of gravity of the affected arc (see Figure B.1). This being the case, it is essential to know the mass moment of inertia of the curved beam section to determine the effective target mass M_2 for use in missile calculations. One method of deriving the equations for this purpose is given below for relatively simple cross-sections which can be approximated by a group of rectangles.

Reference: Formulas for Stress and Strain, Roark and Young, 5th Ed., Table 1, Case 19, page 69.

First consider the properties of the plane face area shown in Figure B.2. The angle α, the radius R, and the thickness t are known. The face area is then

$$A = \alpha t\,(2R-t)$$

NOTE: α is in radians in the equations

Location of centroid

$$\bar{y} = R\left[1 - \frac{2\sin\alpha}{3\alpha}\left(1 - \frac{t}{R} + \frac{1}{2 - t/R}\right)\right]$$

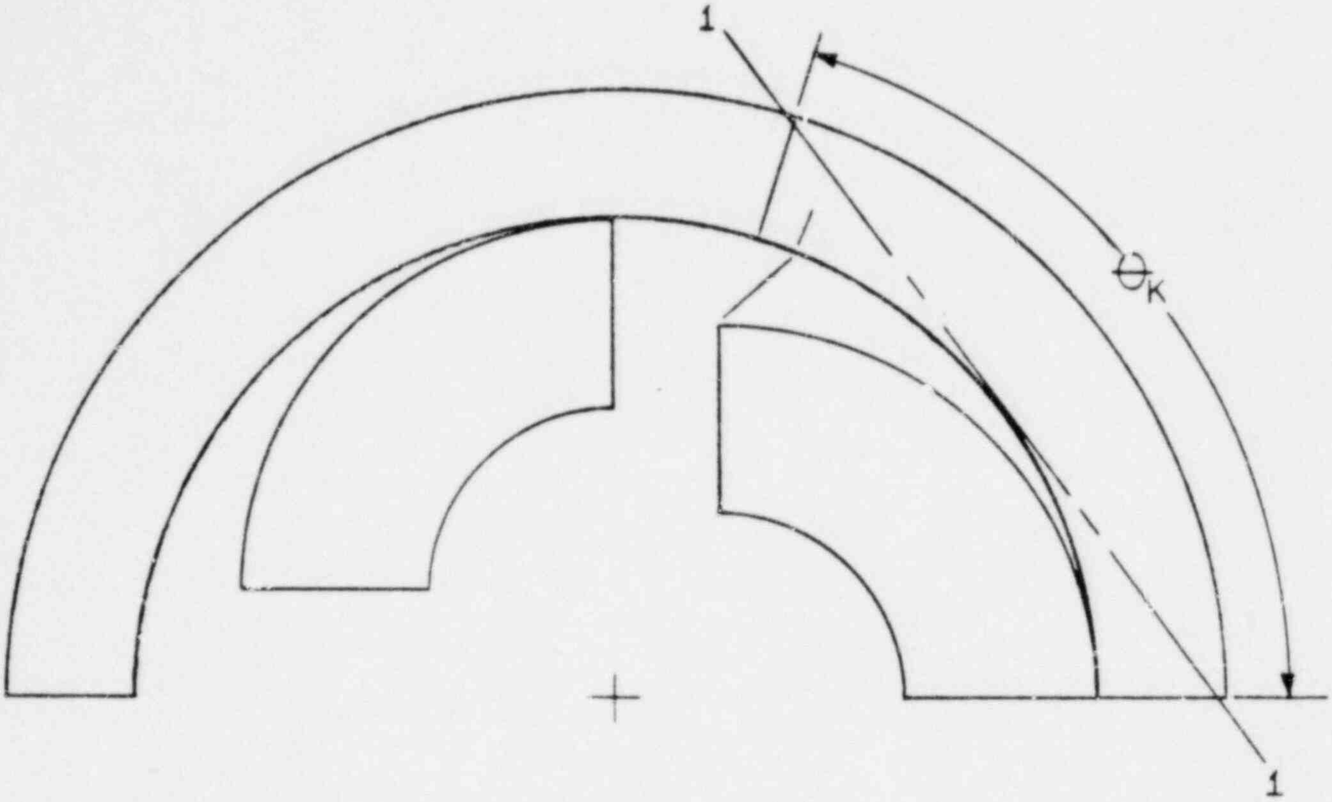

Figure B.1
AXIS OF CURVED BEAM MOMENT OF INERTIA

Area moment of inertia about 1-1 axis

$$I_1 = R^3 t \left[\left(1 - \frac{3t}{2R} + \frac{t^2}{R^2} - \frac{t^3}{4R^3}\right) \times \left(\alpha + \sin\alpha \cdot \cos\alpha - \frac{2\sin^2\alpha}{\alpha}\right) + \frac{t^2 \sin^2\alpha}{3R^2\alpha(2 - t/R)} \times \left(1 - \frac{t}{R} + \frac{t^2}{6R^2}\right) \right]$$

The mass moment of inertia of a very thin element (thk. = dx) about its own 1-1 axis is

$$\rho\, I_1\, dx$$

Then the total mass moment of inertia of the element about the mass center of the solid, applying the parallel axis theorem, is

$$dI_{mz} = \rho\,(I_1\, dx + A dx \cdot x^2)$$

To get the total mass moment of the solid, integrate from $-\frac{h}{2}$ to $+\frac{h}{2}$:

$$I_{mz} = \rho\left[I_1 \int dx + A \int x^2\, dx\right] = \rho\left[I_1\, x + A\,\frac{x^3}{3}\right]_{-\frac{h}{2}}^{+\frac{h}{2}}$$

MASS MOMENT OF INERTIA $\quad I_{mz} = \rho\left[I_1 h + A\,\frac{h^3}{12}\right]$

Total mass of the solid $\quad m = \rho\, A\, h$

To obtain the mass moment of inertia of a section composed of a group of rectangles (see Figure B.3 for example):

C. G. OF ENTIRE SOLID SECTION

$$\bar{y} = \frac{\sum_{1}^{n} m_i \bar{y}_i}{\sum_{1}^{n} m_i} \qquad \bar{x} = \frac{\sum_{1}^{n} m_i \bar{x}_i}{\sum_{1}^{n} m_i}$$

MASS MOMENT OF INERTIA OF ENTIRE SOLID SECTION

$$I_{mz} = \sum_{1}^{n} m_i \bar{x}_i^2 + \sum_{1}^{n} m_i \bar{y}_i^2 + \sum_{1}^{n} I_{mz_i} - m_T (\bar{x}^2 + \bar{y}^2)$$

where

m_T = mass of entire solid = $\sum_{1}^{n} m_i$

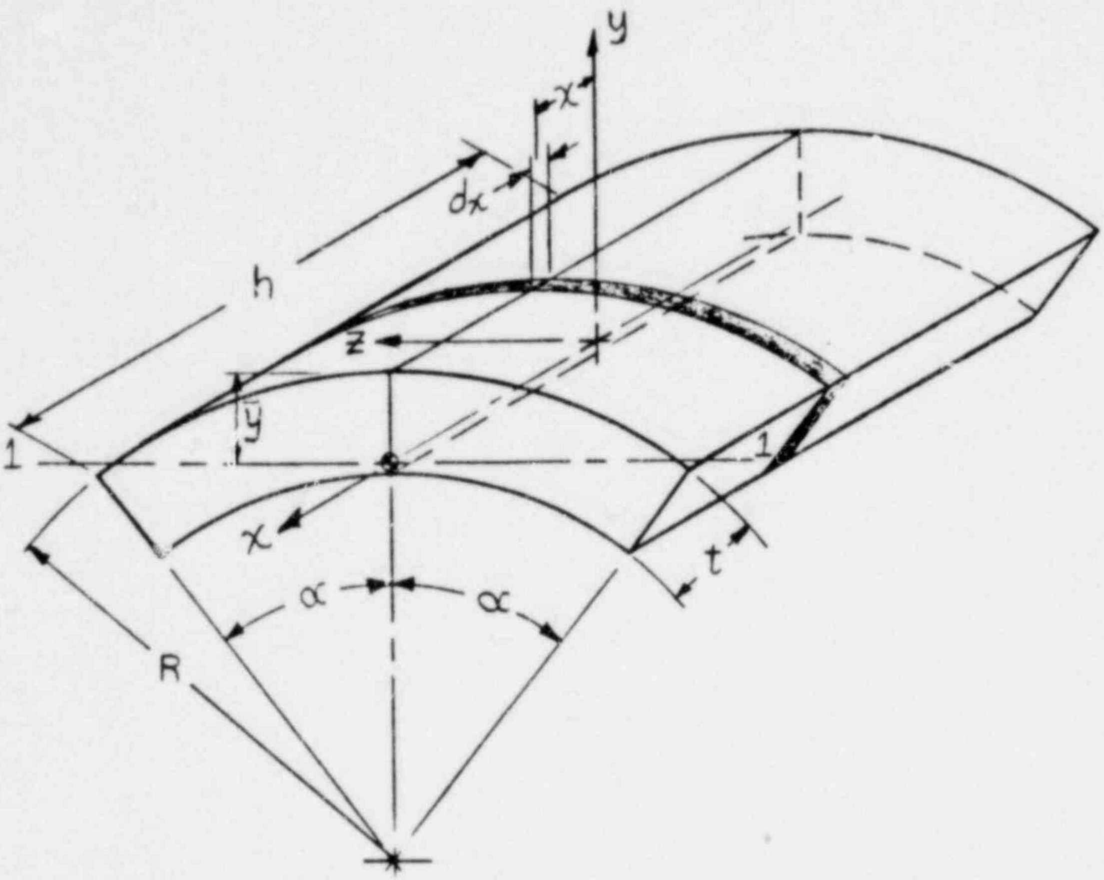

Figure B.2

GEOMETRY FOR MASS MOMENT OF INERTIA CALCULATION

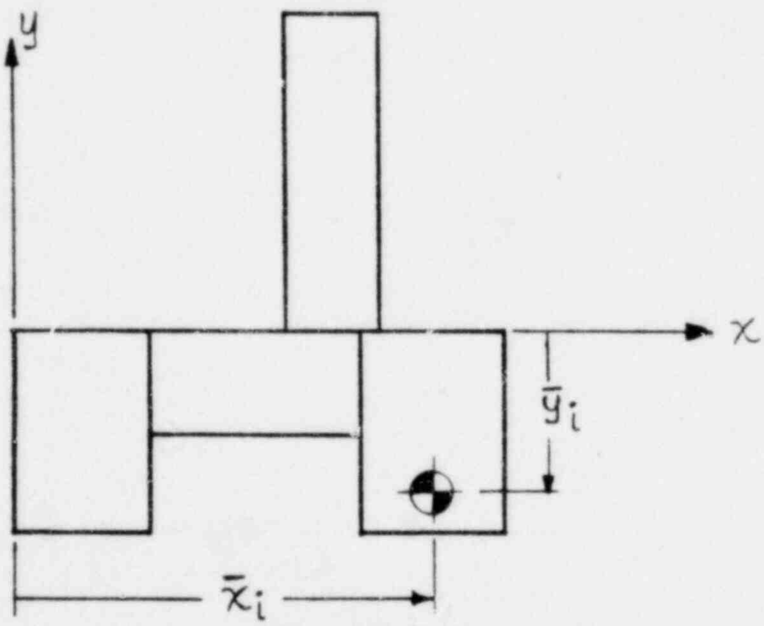

Figure B.3

SAMPLE SECTION FOR MASS MOMENT OF INERTIA CALCULATION

APPENDIX C: Values of Dynamic Ultimate Strength for Common Westinghouse Structural Materials

For consistency in calculations, the following values of dynamic ultimate strength should be used:

MATERIAL SPECIFICATION	SPECIFIED MINIMUM STATIC ULTIMATE STREN[illegible] σ_u (psi)	DYNAMIC ULTIMATE STRENGTH, σ_d (psi)
[		][a]
[		][a]
[		][a]
[		][a]

Ref.: Figure 2.01

Notes: [

][a]

[

][a]

[ ][a]

[ ][a]

*Expected minimum static ultimate strength. No specified value.

I. INTRODUCTION

1. Part C contains methods and procedures for evaluating the effects of rotor fragments hitting the blade rings and outer cylinders of nuclear HP turbines. The effects of rotor fragments hitting at four locations around the outer cylinder are analyzed.

PART C
Table of Contents

PART C
LIST OF FIGURES

PART C

NOMENCLATURE AND UNITS[†]

SYMBOL	TERM, UNITS
[	]a
[	]a
ε	Strain, in/in.
[	]a
[	]a
R_D	Radius of rotor, in.
R_i	Inside radius of blade ring or section of outer cylinder, in.
θ_c	Included angle, radians.
A	Cross-sectional area, in^2.
w	Width of section, in.
t	Thickness of section, in.
R_m	Radius to center of gravity of cross-section of blade ring, in.
t_{eq}	Equivalent thickness, in.
θ_{22}	Angle associated with overhanging material, radians.
[	]a
[	]a
L	Length, in.
V_{21}	Volume of material associated with θ_c, in^3.
[	]a
V_c'	Volume of material for compression, in^3.
R_m'	Radius to center of gravity of cross-section of blade ring for compression volume, in.
V_{21b}	Compression volume of blades, in^3.
[	]a
$V_{360°}$	Volume of blades for 360°, in^3.
[	]a
V_{22D}	Volume per end associated with overhanging material on blade rings, in^3.
W_{22D}	Effective weight per end associated with overhanging material on blade rings, lbf.

[†]Listed in order of appearance.

[ ][a]

W_{22c}	Effective weight in circumferential direction, lbf.
V_{22c}	Volume of overhanging material in circumferential direction, in^3.
W_{22A}	Effective weight in axial direction, lbf.
W_{22Ai}	Effective weight per end and per section in axial direction, lbf.
V_{22Ai}	Volume per end and per section in axial direction, in^3.
V_i	Volume of section of outer cylinder, in^3.
W_i	Weight of section of outer cylinder, lbf.
W_{22ci}	Effective weight of section of outer cylinder in circumferential direction, lbf.

[

][a]

W_T	Total effective weight, lbf.
θ_h	Angle from joint to center of rotor fragment for a particular section, radians.
θ_H	Angle from joint to center of rotor fragment, radians.
ε'	Strain at $\theta_c/2 + \theta_{22}$, in/in.
ε_T	Average tension strain, in/in.
θ_f	Angle from joint to top of flange, radians.
ΔR_c	Change in radius of section of outer cylinder, in.

[ ][a]

$V_{c\text{-}cyl.}$	Total volume of outer cylinder for compression, in^3.
A_s	Shear area, in^2.
τ_d	Dynamic shear strength, psi.
E_s	Shear energy, ft-lbf.
U_{pc}	Summation of shear energy and compression energy, ft-lbf.
$E_{c\text{-}cyl.}$	Compression energy of outer cylinder, ft-lbf.
$E_{c\text{-}rings}$	Compression energy of blade rings, ft-lbf.
$E_{sc\text{-}sect.0}$	Shear energy of section 0 of outer cylinder, ft-lbf.
$E_{sc\text{-}sect.11}$	Shear energy of section 11 of outer cylinder, ft-lbf.
ΔKE	Energy loss of inelastic collision, ft-lbf.
U_{pcA}	Summation of shear energy and compression energy for case of $2L > 2t_{eq}$, ft-lbf.

$E_{scA-sect.0}$ Shear energy of section 0 of outer cylinder for $2L > 2t_{eq}$, ft-lbf.

$E_{scA-sect.11}$ Shear energy of section 11 of outer cylinder for $2L > 2t_{eq}$, ft-lbf.

$E_{sA-cyl.}$ Shear energy of outer cylinder in axial direction for $2L > 2t_{eq}$, ft-lbf.

$E_{sA-rings}$ Shear energy of blade rings in axial direction for $2L > 2t_{eq}$, ft-lbf.

$E_{s-sect.0}$ Shear energy of section 0 for modified procedure, ft-lbf.

$E_{s-sect.11}$ Shear energy of section 11 for modified procedure, ft-lbf.

U_p Summation of shear energy and compression energy by modified procedure, ft-lbf.

$E_{T-cyl.}$ Tension energy of outer cylinder, ft-lbf.

$E_{T-ring\ 1}$ Tension energy of blade ring No. 1, ft-lbf.

$E_{T-ring\ 2}$ Tension energy of blade ring No. 2, ft-lbf.

KE_R Kinetic energy of rotor fragment after collision, ft-lbf.

[ ][a]

W_R Weight of rotor fragment, lbf.

$W_{cyl.}$ Effective weight of cylinder, lbf.

$W_{ring\ 1}$ Effective weight of blade ring No. 1, lbf.

$W_{ring\ 2}$ Effective weight of blade ring No. 2, lbf.

h Height of horizontal joint flange on outer cylinder, in.

s Flange dimension, in.

[ ][a]

[ ][a]

V_{22f} Volume of overhanging material of flange, in^3.

W_{22f} Effective weight of overhanging material in axial direction of flange, lbf.

θ_{cav} Average included angle, radians.

θ_w Included angle of material above flange for hit above joint, radians.

V_{21w} Volume of material associated with θ_w, in^3.

W_{21w} Fully effective weight for θ_w, lbf.

V_{22wc} Wall volume of overhanging material in circumferential direction for hit above joint, in^3.

W_{22wc} Effective weight of overhanging material in circumferential direction for hit above joint, lbf.

E_{sf} Shear energy of flange, ft-lbf.

d Clearance hole diameter, in.

[ ][a]

V_{Tf} Flange ligament material, in^3.

W_{Tw} Total effective weight of cylinder wall, for hit above joint, lbf.

V_{Tw} Total volume for tension energy of outer cylinder wall for hit above joint, in^3.

E_{Tf} Tension energy of flange, ft-lbf.

E_{Tw} Tension energy of wall, ft-lbf.

E_T Total tension energy, ft-lbf.

θ_e Included angle of material, $\theta_c/2 - \theta_f$, for hit at joint, radians.

W_{21e} Fully effective weight of cylinder wall for hit at joint, lbf.

V_{21e} Volume of material of outer cylinder wall for hit at joint, in^3.

V_{22ec} Volume of overhanging material of outer cylinder wall in circumferential direction for hit at joint, in^3.

W_{22ec} Effective weight of overhanging material in circumferential direction for hit at joint, lbf.

W_{Te} Total effective weight of cylinder wall for hit at joint, lbf.

V_{Te} Total volume of outer cylinder wall for tension energy and hit at joint, in^3.

g Gravitational constant, 32.2 ft/sec^2.

V_R Velocity of rotor fragment after collision, ft/sec.

$KE_{ring\ 1}$ Fragment kinetic energy of blade ring No. 1 after collision, ft-lbf.

$KE_{ring\ 2}$ Fragment kinetic energy of blade ring No. 2 after collision, ft-lbf.

$KE_{cyl.}$ Fragment kinetic energy of cylinder after collision, ft-lbf.

B Width of blade ring or cylinder fragment, in.

H Height of blade ring or cylinder fragment, in.

1.0 NUCLEAR HP MISSILE ANALYSIS

1. The HP element is a double flow design similar to the HP double flow design shown in Figure 3.1, and consists of a forged single-piece double flow rotor, a cast steel outer cylinder, and four cast steel blade rings supported inside the outer cylinder. Steam from four control valves enters nozzle chambers at the center of the turbine element through four inlet pipes (two in the cylinder base and two in the cylinder cover). In these chambers, the steam is distributed equally to both halves of the rotor and flows axially through the blading to the exhaust chambers at each end of the HP cylinder.

2. The potential for an HP missile will be determined at four locations around the outer cylinder. Four rotor fragments per end, each fragment being a 90° section, are assumed to hit the cylinder and blade rings. The four locations are: a hit at the horizontal joint, a hit above the horizontal joint, a hit above the flange, and a hit at the top of the cylinder.

3. The calculations will be performed for rated speed and design overspeed. It is not necessary to calculate missiles at the ductile bursting speed of the HP rotor since this bursting speed is higher than the theoretical terminal speed of the unit.

4. No HP missile calculations will be performed for rotor fragments hitting below the flange of the horizontal joint.

2.0 COLLISION PROCESS

1. The HP missile analysis for nuclear turbines will be based upon a single collision process. The rotor fragment is assumed to contact both blade rings and the associated stationary blades at the same time. In turn, the blade rings contact the outer cylinder at the two blade ring fits, Figure 3.1.

2. The material between the blade ring fits on the outer cylinder and over an angle θ_c is considered fully effective, Figure 9.1.

3. Nozzle chambers are not considered available mass for reducing the translational kinetic energy of the rotor fragment.

3.0 ASSUMED FAILURE MODE

1. The nuclear HP turbine has several variations. Some typical configurations are shown on Figures 3.1 through 3.3.

2. The failure mode is for a rotor fragment to contact the two blade rings which in turn contact the blade ring fits on the outer cylinder. If the blade rings and outer cylinder are to fail, the primary failure of the outer cylinder will be near the steam inlet side of the No. 1 blade ring fit and near the steam exhaust side of the No. 2 blade ring fit. The primary failure will probably be a tension failure.

3. Since the length of the rotor fragment is longer than the length of the outer cylinder for the primary collision, the rotor fragment may make contact with additional material of the outer cylinder and nozzle chambers after the primary collision.
[

]a

4. This failure mode will be assumed for all configurations as well as for all orientations around the cylinder.

5. The ejection angle of rotor fragments is assumed to be ± 5° measured from the vertical radial plane passing through the rotor and perpendicular to the rotor longitudinal axis.

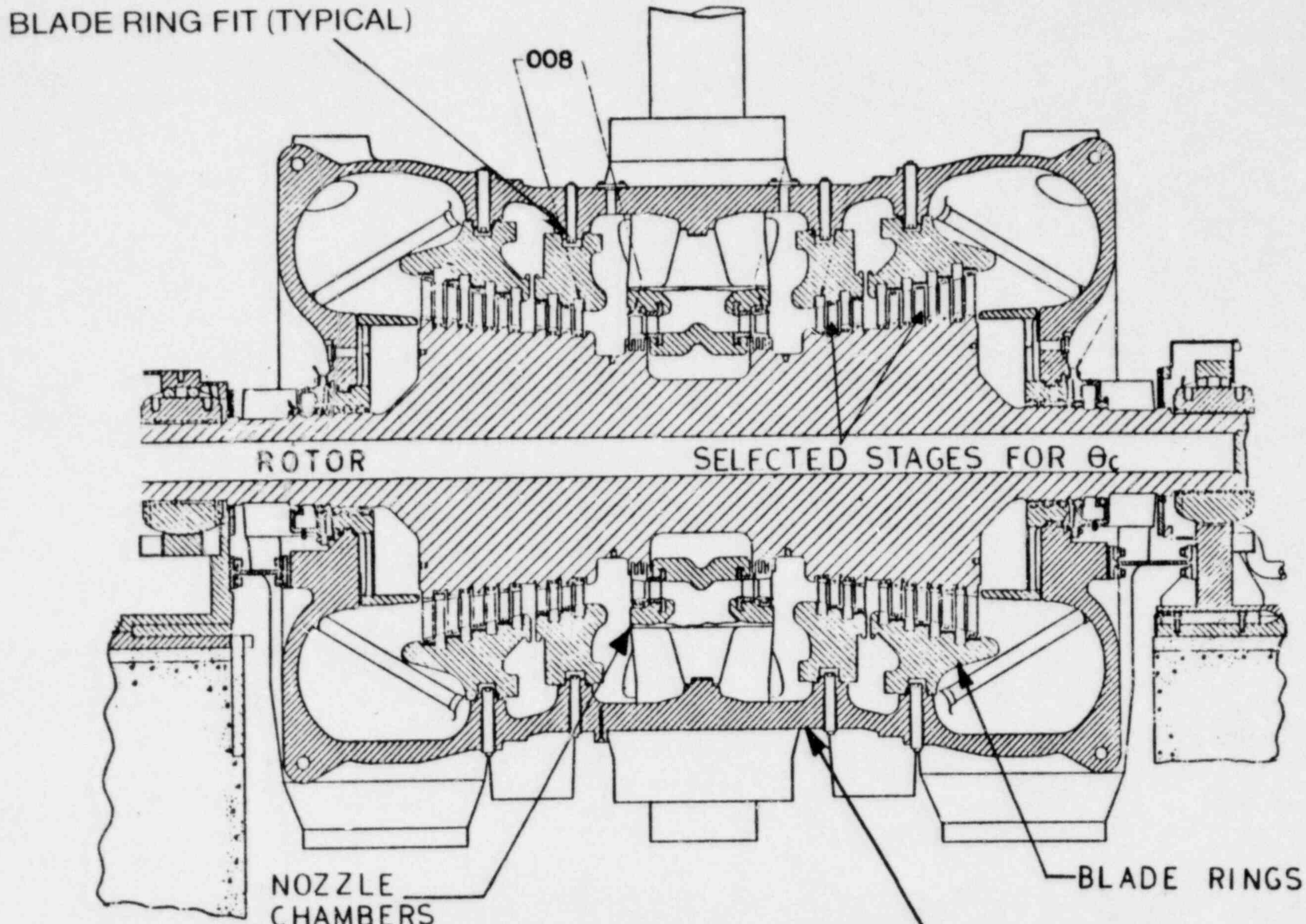

Figure 3.1

DETAILED SECTION HP TURBINE TYPE II

C 10

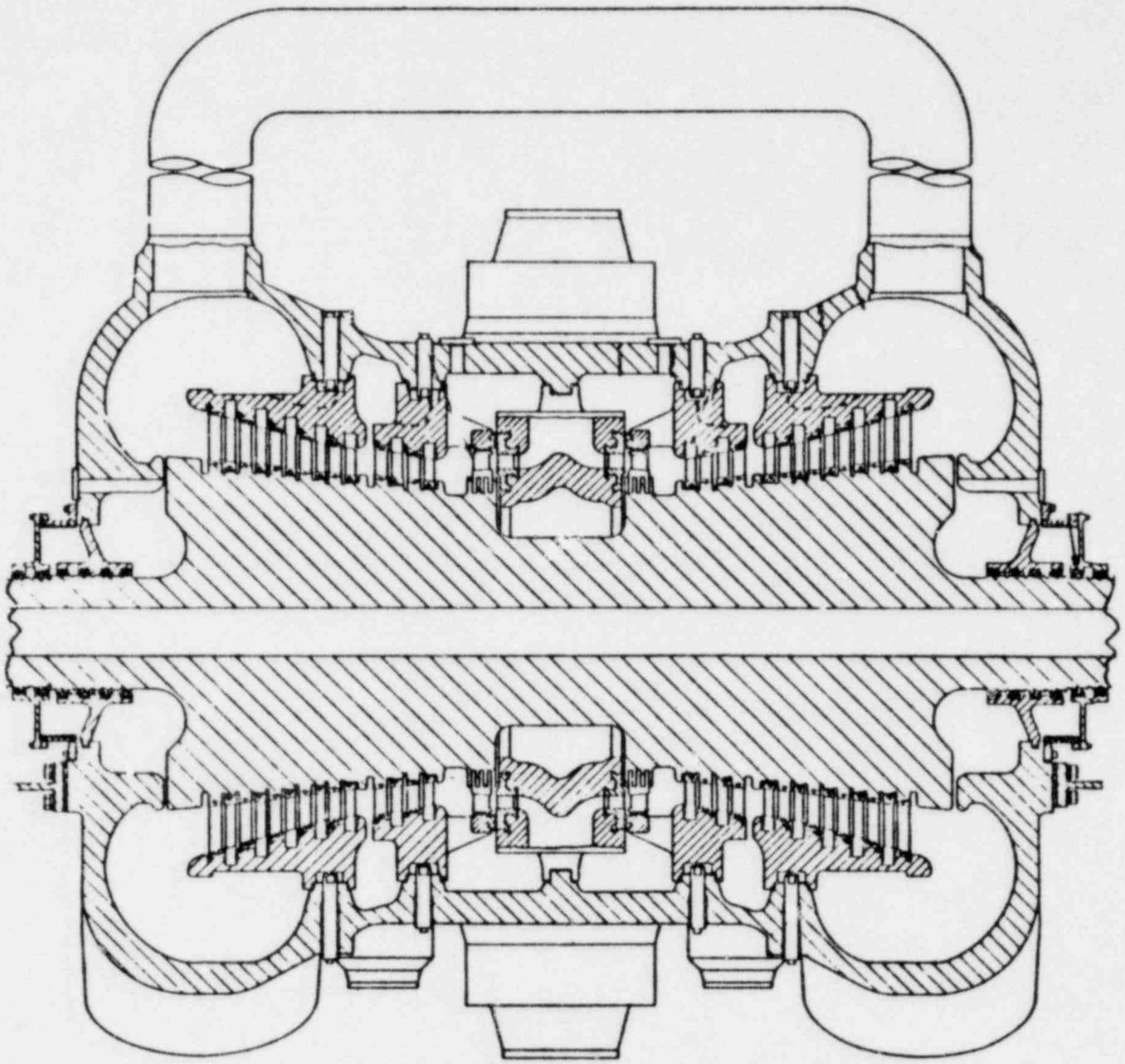

Figure 3.2
DETAILED SECTION HP TURBINE TYPE III A

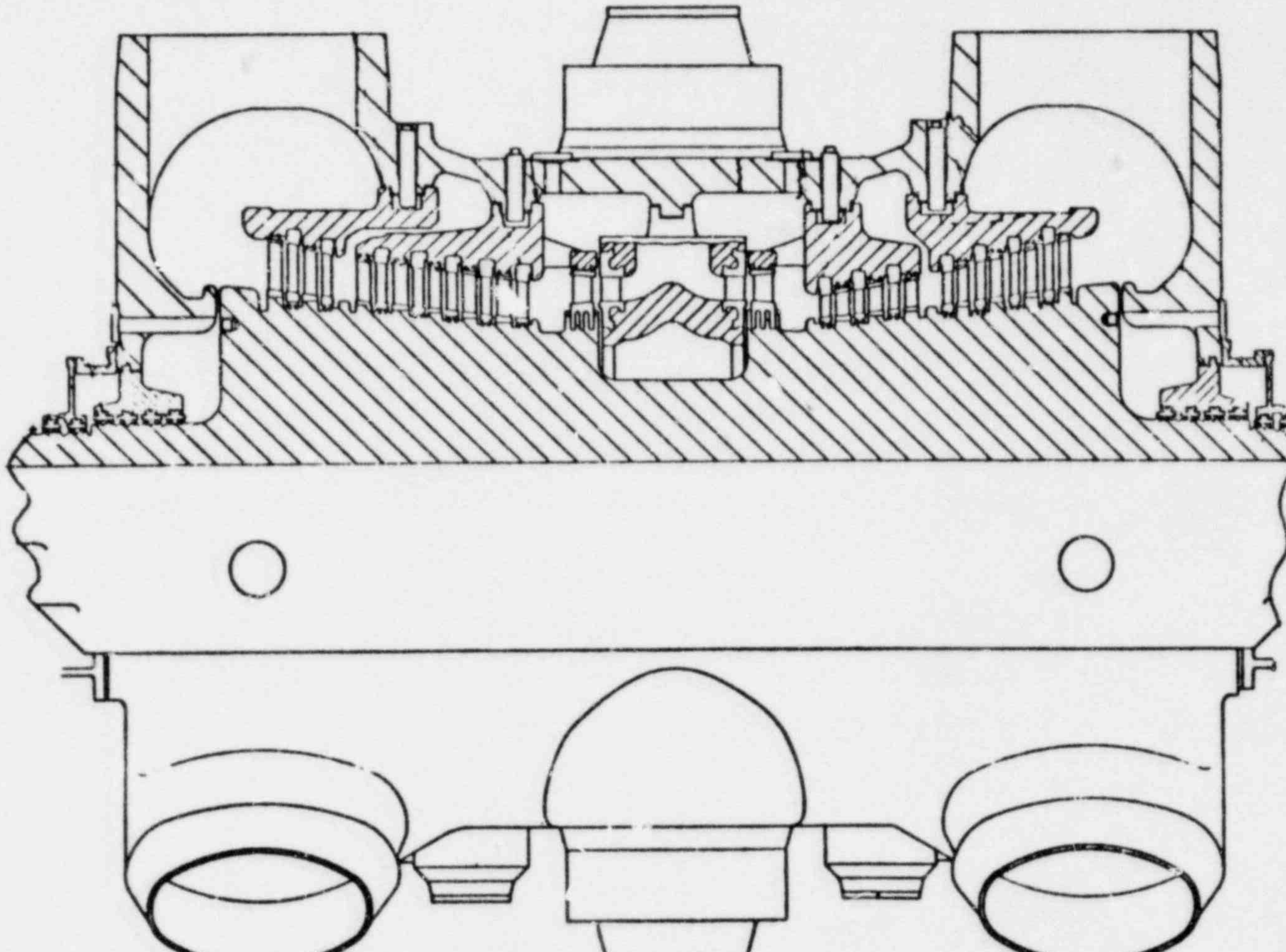

Figure 3.3
DETAILED SECTION HP TURBINE TYPE III B

4.0 HF ROTOR CONSIDERATIONS FOR MISSILE ANALYSIS

1. The rotor is assumed to fracture at the transverse centerline and at each end. The two sections of the rotor each break into four parts thus generating eight rotor fragments. The two end sections of the rotor do not become missiles, Figure 4.1.

2. Each rotor section fails in steps with the result that two fragments gain velocity and two lose velocity. The four rotor fragments per section are assumed to be at the higher level for all containment calculations.

3. In predicting the ability of the rotor fragment to penetrate the turbine casing, test results and analytical considerations indicate that the translational kinetic energy of a fragment is of much greater importance than the rotational kinetic energy. Rotational kinetic energy tends to be dissipated as a result of friction forces developed between the surface of the disc or rotor fragment and the stationary part. Therefore, rotational kinetic energy is not considered in the penetration calculations.

[

]b

Figure 4.1
HP ROTOR FRACTURE SEQUENCE

5.0 MATERIAL PROPERTIES

1. The nuclear HP cylinders and blade rings are made from [ ][b]. The dynamic strength of this material will be set at [ ][b] The ultimate strength of [ ][b] This value is based on the minimum purchase requirements. The ratio of the dynamic strength to the ultimate strength is 1.35*. Therefore, this ratio yields a dynamic strength for [ ][b]

2. Using the same method, the dynamic strengths for the horizontal joint bolting are:

Material	σ_{ult} (psi)	σ_d (psi)
[		][b]
[		][b]

3. The stationary blades are considered available material for compression energy. The stationary blades are made from material containing [ ][a], which has a higher dynamic strength than [ ][a] However, for simplification of the calculation procedure, the stationary blades are assumed to have the same dynamic strength as the carbon steel castings.

---

*Refers to Reference Numbers at the end of this part.

6.0 OUTER CYLINDER FOR HP MISSILE ANALYSIS - GENERAL DISCUSSION

1. The outer cylinder is divided into sections. The sections extend from the No. 1 blade ring fit to the No. 2 blade ring fit. The Figures 6.4, 6.6, 6.8 and 6.10 show the sections for the Nuclear Turbines.

2. The nominal thickness of the casting wall at the vertical centerline of the cylinder is selected as the thickness that represents the remainder of the cylinder wall. The wall thickness at all other locations is greater than the nominal thickness at the vertical centerline. This point is the result of casting feeds.

3. Another set of sections is established for the flange of the horizontal joint. The division of the flanges for the Nuclear Turbines is shown on Figures 6.5, 6.7, 6.9 and 6.11.

4. Detailed analyses for the calculation of the effective weights in the areas of inlet and exhaust connections are not performed. The nominal wall thickness of the casting is assumed to exist through the openings. Openings in castings have local reinforcement material that is added to the nominal wall thickness. The amount of added material is equal to the volume of material that is removed by the opening.

[

]a

Figure 6.4

VERTICAL CENTERLINE OF OUTER CYLINDER, TYPICAL HP TYPE II

[

C 18

][a]

Figure 6.5

HORIZONTAL JOINT OF OUTER CYLINDER, TYPICAL HP TYPE II

[

]a

Figure 6.6
VERTICAL CENTERLINE OF OUTER CYLINDER, TYPICAL SECTION - HP TYPE III A OR B

[

C 20

][a]

Figure 6.7

HORIZONTAL JOINT OF OUTER CYLINDER, TYPICAL HP TYPE III A OR B

[

][a]

Figure 6.8

VERTICAL CENTERLINE OF OUTER CYLINDER, TYPICAL SECTION - HP TYPE I A

C 22

[

][a]

Figure 6.9

HORIZONTAL JOINT OF OUTER CYLINDER, TYPICAL HP TYPE I A

[

C 23

]a

Figure 6.10

VERTICAL CENTERLINE OF OUTER CYLINDER, TYPICAL HP TYPE I B

[

C 24

][a]

Figure 6.11

HORIZONTAL JOINT OF OUTER CYLINDER, TYPICAL HP TYPE I B

7.0 OUTER CYLINDER BOLTING AND BLADE RING BOLTING AT THE HORIZONTAL JOINTS

1. The tension strength of the wall of a blade ring is stronger by a factor of 8 than the tension strength of the bolts that hold together the two halves of the blade ring, Figure 7.1.

2. The tension strength of the outer cylinder is stronger by a factor of 4 than the tension strength of the horizontal joint bolting. This situation does not indicate undersized bolts but rather the fact that there is a significant increase in wall thickness above the necessary amount for pressure and temperature considerations. This increase in thickness is primarily at the blade ring fits.

3. The difference in load carrying capacity of the walls and bolting results in modifying the available tension strain energy that can be removed from the system during a collision.

[

C 26

][a]

Figure 7.1

HORIZONTAL JOINT BOLTING DIAGRAM, TYPICAL

IMAGE EVALUATION
TEST TARGET (MT-3)

6″

IMAGE EVALUATION
TEST TARGET (MT-3)

6″

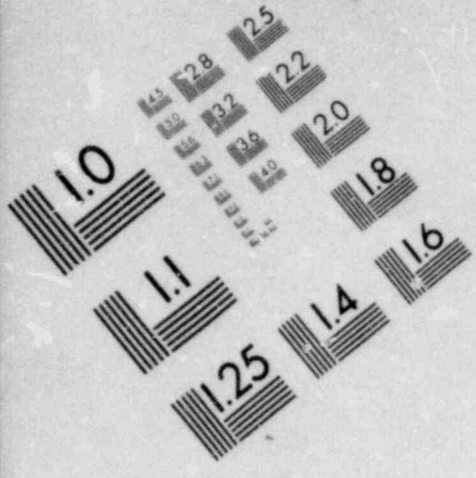

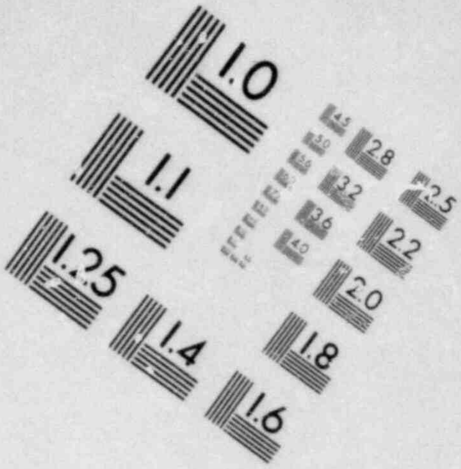

IMAGE EVALUATION
TEST TARGET (MT-3)

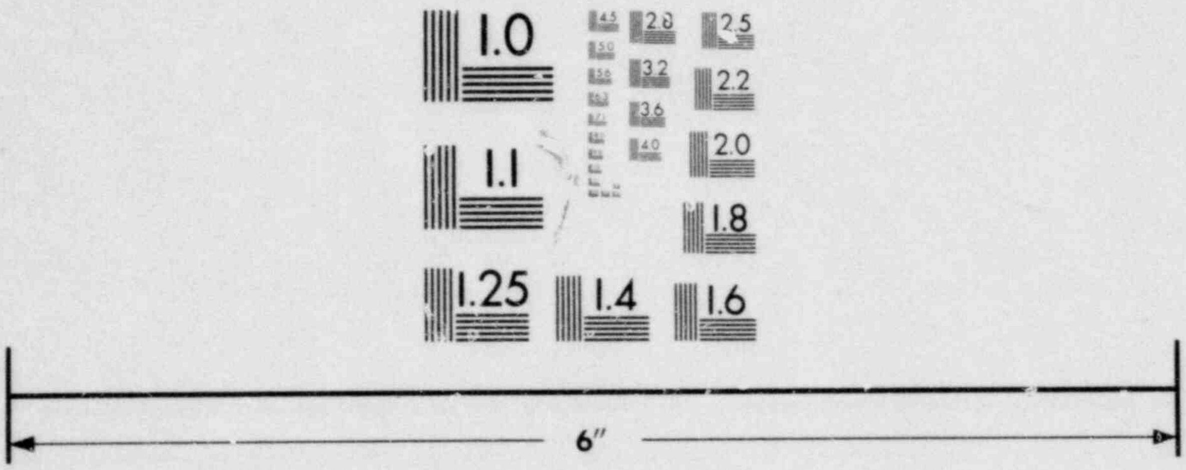

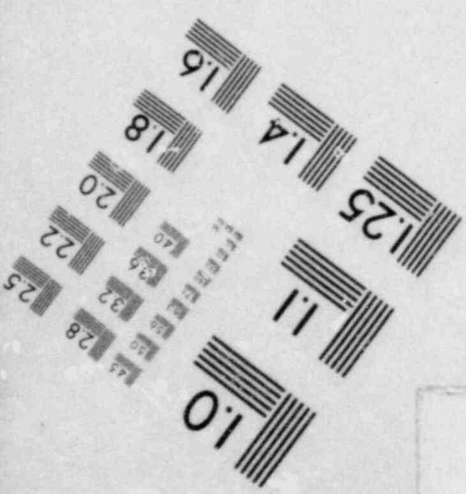

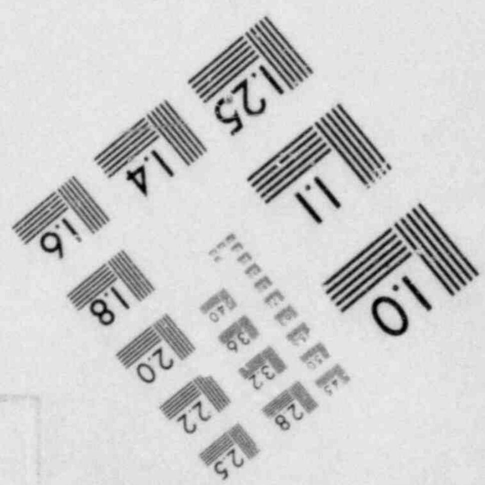

8.0 WEIGHT AND VOLUME DETERMINATION - GENERAL DISCUSSION

1. The material involved in the collision process will be determined by the establishment of radial lines. All material between the radial lines will be considered fully effective, [ ][a] All material outside of the radial lines will be considered partially effective, W_{22}.

2. Select a representative rotating row for each blade ring. Select a rotating row that is in line with the fit of the blade ring, Figures 3.1 and 3.2. Base the radius of the rotor on the base diameter of the selected rotating blade, R_D. Base the radius of the blade ring on the diameter above the rotating blade, R_i, Figure 9.1.

3. The included angle, θ_c, between the radial lines for each blade ring is:

$$\theta_c = \frac{\pi}{2} \quad \frac{R_D}{R_i}$$

This included angle will be used not only for the blade rings, but also for the outer cylinder.

4. Some turbine designs have the No. 1 blade ring extending underneath the No. 2 blade ring, Figure 3.3. For this configuration, the included angle, θ_c, for the No. 2 blade ring is established by selecting the first rotating row in the No. 2 blade ring.

9.0 HIT ABOVE FLANGE - WEIGHT AND VOLUME DETERMINATION FOR BLADE RINGS

1. Once the radial lines have been established, some physical properties of the blade rings have to be calculated. The cross-sectional area, A, weight, volume, wt^2 and center of gravity of the cross-section are required for each blade ring. An average cross-sectional area is selected for each blade ring. The effect of material removed by dowel pins, horizontal joint bolting and support keys is not included in the analysis.

2. The amount of weight and volume to be included in the energy calculations for the overhanging material is established by the following rules, Figure 9.1:

   A. Determine the center of gravity of the cross-section of the blade ring, R_m.

   B. Determine the equivalent thickness, t_{eq}, of the blade ring, according to $\frac{\Sigma wt^2}{\Sigma wt}$, Figure 9.6.

   C. Calculate the angle associated with the overhanging material, θ_{22}.

   The angle is the smaller of:

   a. $\theta_{22} = \frac{1}{2} \left(\frac{\pi}{2} - \theta_c\right)$

   or

   b. $\theta_{22} = \frac{3t_{eq}}{R_m}$

D. The effective weight and volume of the overhanging material is:

[ ]a

The efficiency factor, K_f, is determined from the curve, Figure 9.2, where:

$$\frac{L}{t} = \frac{R_m \theta_{22}}{t_{eq}}$$

For the case of $\theta_{22} = \frac{3t_{eq}}{R_m}$, set K_f to .34.

3. The selected amount of material in front of the rotor fragment is dependent upon the type of calculation to be performed. The weight of the material directly in front of the rotor fragment is established for all calculations by:

[ ]a

The volume of material to be selected is dependent upon the type of calculation. The volume of material for tension strain energy is:

$$V_T = V_{21} + V_{22}$$

$$= R_m \theta_C A + 2 R_m \theta_{22} A \quad (in^3)$$

The volume of material for compression is:

$$V_C' = R_m' \theta_C A_C.$$

For the majority of blade rings $V_C' = V_{21}$. However, some blade rings have shapes shown on Figure 9.3. For these cases the volume of compressed material is defined as the material immediately in front of the rotor fragment, but not including the material past undercuts. For Figure 9.3 only the shaded volume is considered in compression.

4. For turbine designs with the No. 1 blade ring extending underneath the No. 2 blade ring, [

]a

5. The No. 1 blade ring on HP Turbine Type III is composed of two rings connected by ribs. The center of gravity of the cross-section, equivalent thickness and assigned tension strain value is determined as though the rings were rigidly connected thus forming a single body, Figure 9.4.

6. The stationary blades are included in the analysis. The inner shroud, airfoil and outer shroud are considered added weight to W_{21}. The volume of the stationary blades can be included in the compression volume. However, the stationary blade volume cannot be included in the tension strain energy volume. In addition, only the stationary blades encompassed by θ_c are included in the analysis:

$V_{21b} = V_{360^0} (\theta_c/2\pi)$ (in^3) compression volume of blades

$W_{21b} = V_{21b} (.279)$ (lbf) weight of blades.

Therefore:

$$V_c = V_c' + V_{21b} \quad (in^3)$$

$$W_{21} = W_{21}' + W_{21b} \quad (lbf)$$

7. A tabulation form for blade ring properties is shown on Figure 9.5.

[

][a]

Figure 9.1

DETERMINATION OF θ_C AND θ_{22}

[

]^{ab}

Figure 9.2

EFFECTIVE MASS FACTOR, K_f

REF. "THE CONTAINMENT OF DISC BURST FRAGMENTS BY CYLINDRICAL SHELLS" - HAGG & SANKEY

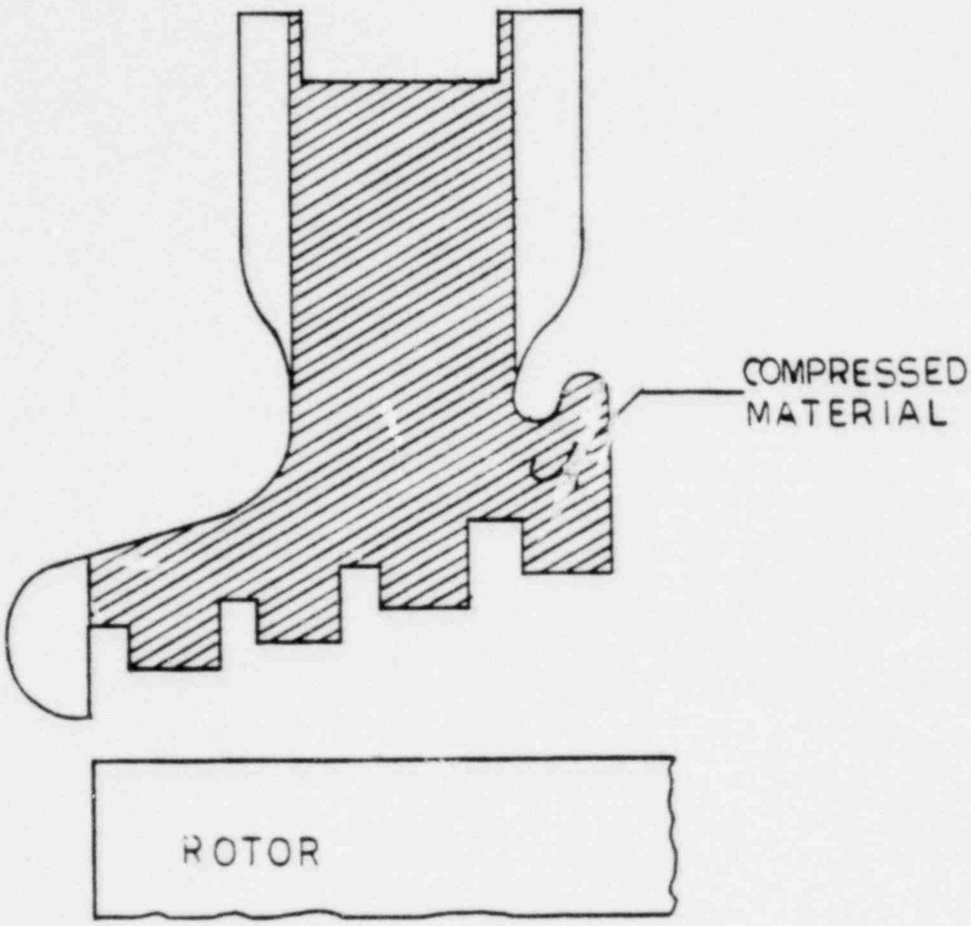

Figure 9.3
HIT ABOVE FLANGE - MATERIAL IN COMPRESSION

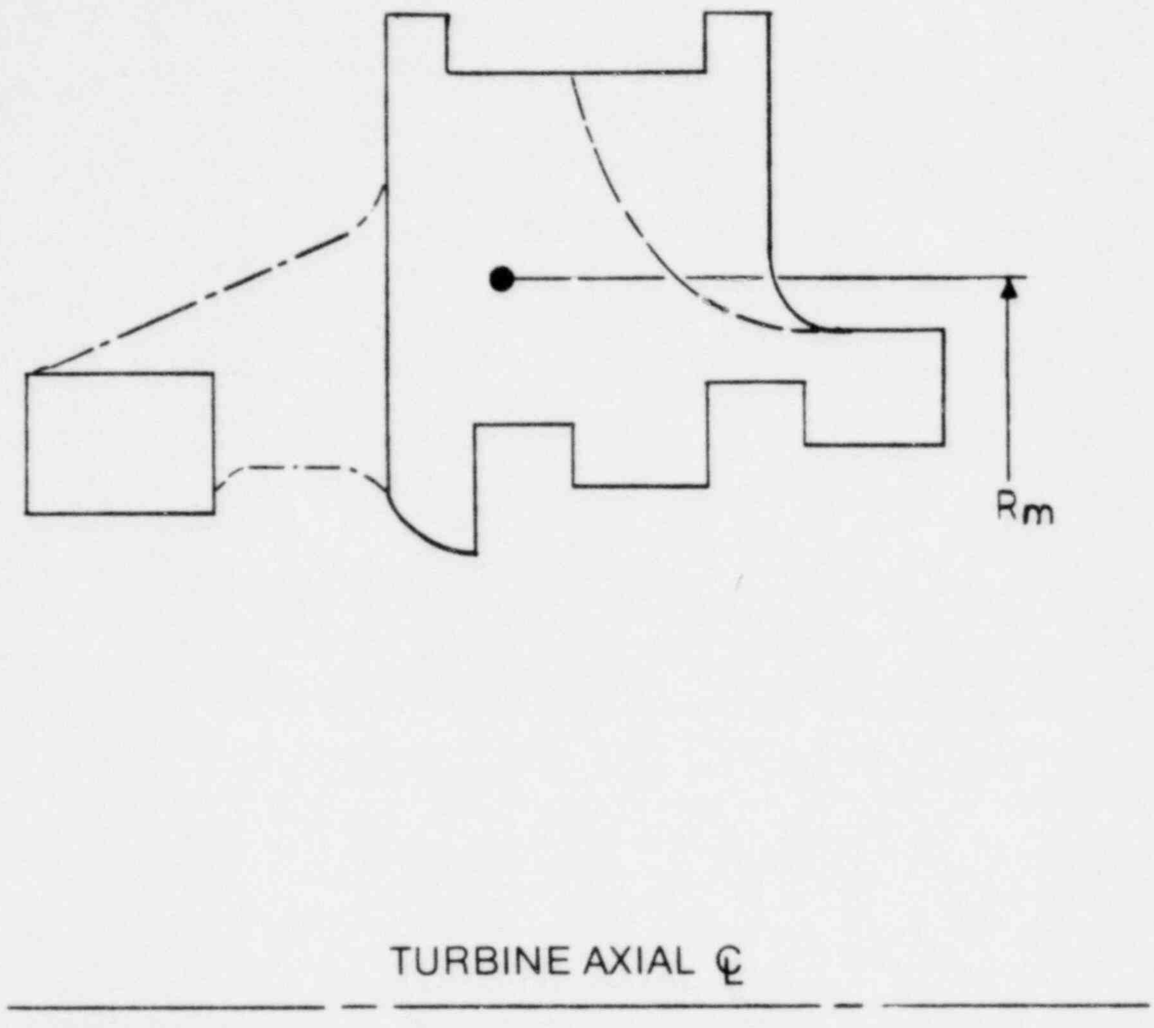

Figure 9.4
NO. 1 BLADE RING FOR HP TYPE III B

[

]ab

Figure 9.5
BLADE RING TABLE

[

]a

Figure 9.6
EQUIVALENT THICKNESS OF BLADE RING

10.0 HIT ABOVE FLANGE - WEIGHT AND VOLUME DETERMINATION FOR OUTER CYLINDER

1. The relationship of the four rotor fragments and the affected material on the outer cylinder for a hit above the flange is shown on Figures 10.3 and 10.4.

2. The radial lines established for the blade rings extend through the outer cylinder. The amount of material above each blade ring is governed by radial lines established by θ_c for that blade ring. The material between the blade rings on the outer cylinder, Section 5 of Figure 6.4, is controlled by an average of θ_c for the two blade rings.

3. Sections numbered 1 through 10 are considered material that is fully effective, W_{21}. Sections 0 and 11 form the material that is partially effective, W_{22c}, Figure 6.4. The axial length of the material for W_{22c} is set by [ ][a] An unwrapped section of an outer cylinder showing the relative proportions of W_{21} and W_{22} is shown on Figure 10.2.

4. There are many styles of blade rings. Some blade rings have only a partial fit, Figure 10.1. For these blade rings, Sections 1 through 10 are still considered to be fully effective, W_{21}. However, the volume of material for compression on the outer cylinder will be the volume of material that is in front of the partial blade ring fit.

5. The effective weight for Sections 0 and 11 is determined by using the standard Hagg and Sankey correction factor, Figure 9.2. [ ][a]

6. The volume and effective weight of the material between the rotor fragments, V_{22A} and W_{22A}, is established using a procedure similar to the procedure for the blade rings. However, a correction factor is applied to each section rather than to the total

cross-section as in the blade ring procedure. Therefore, calculate the angle associated with the overhanging material for each section.

The angle is the smaller of:

a. $\theta_{22} = \frac{1}{2} \left(\frac{\pi}{2} - \theta_c\right)$

or

b. [ ][a]

The effective weight and volume per end of the overhanging material for each section is:

[ ][a]

The efficiency factor, K_f, is determined from the curve on Figure 9.2 where:

$$\frac{L}{t} = \frac{R_c \, \theta_{22}}{t}$$

[ ][a]

7. A tabulation form for properties of the outer cylinder is shown on Figure 10.5.

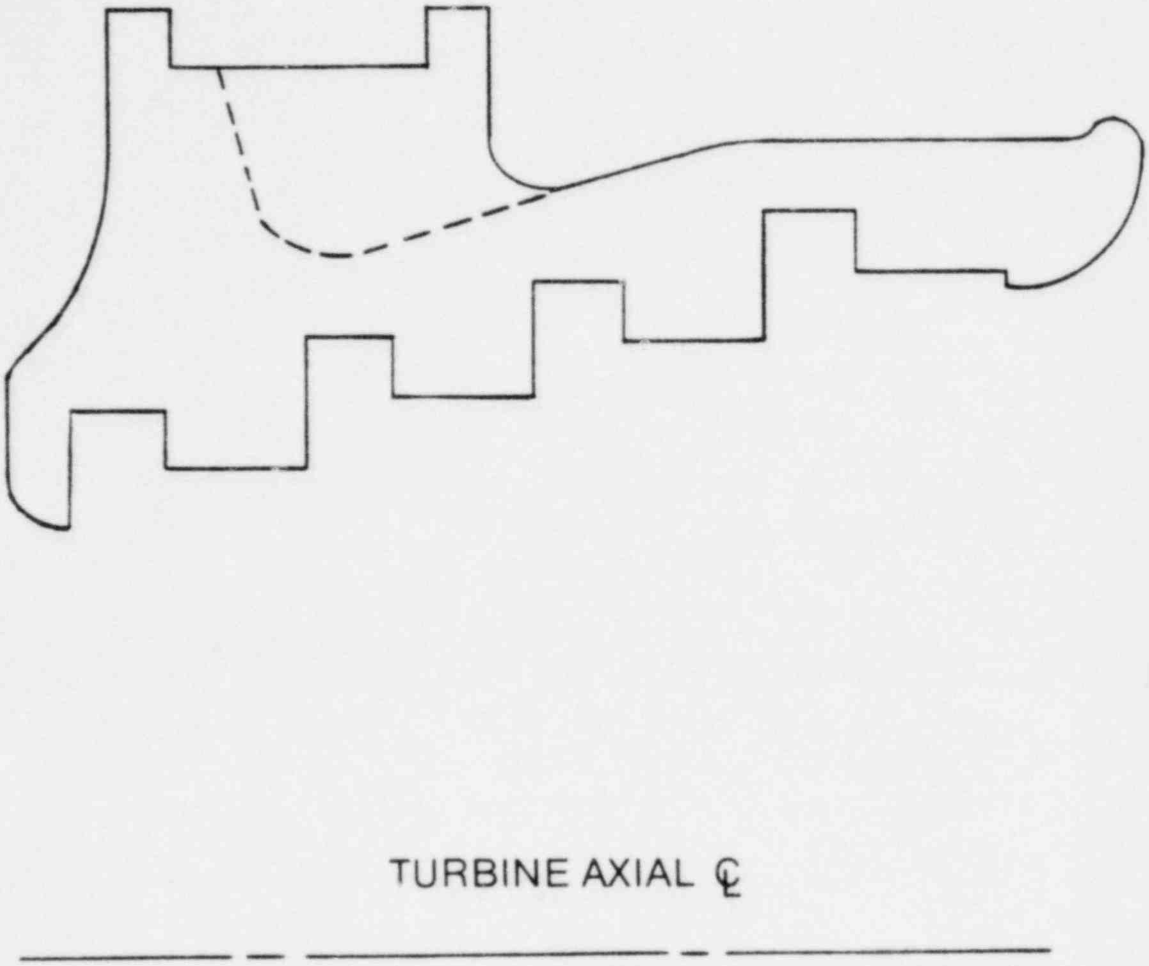

Figure 10.1
BLADE RING - PARTIAL FIT

[

Figure 10.2
HIT ABOVE FLANGE - PLAN VIEW][a]

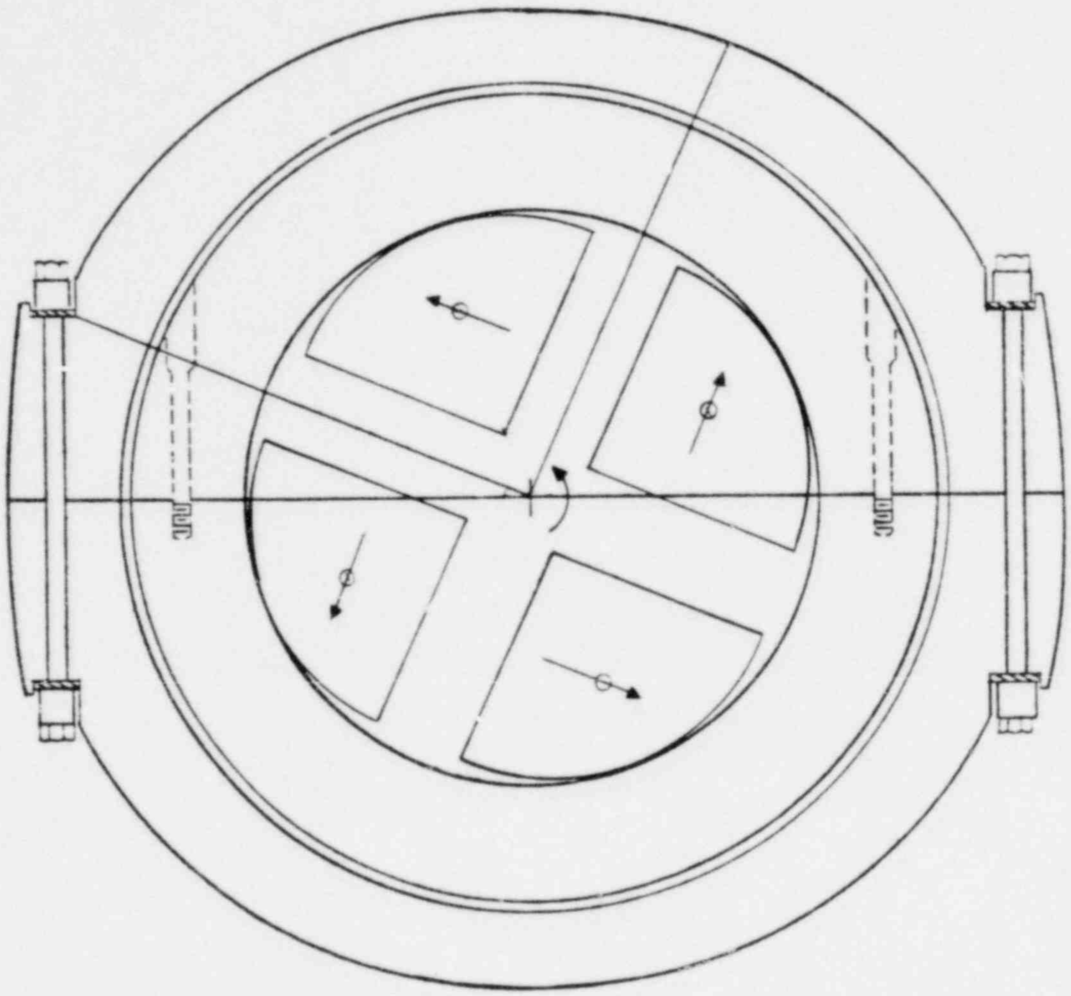

Figure 10.3
HIT ABOVE FLANGE

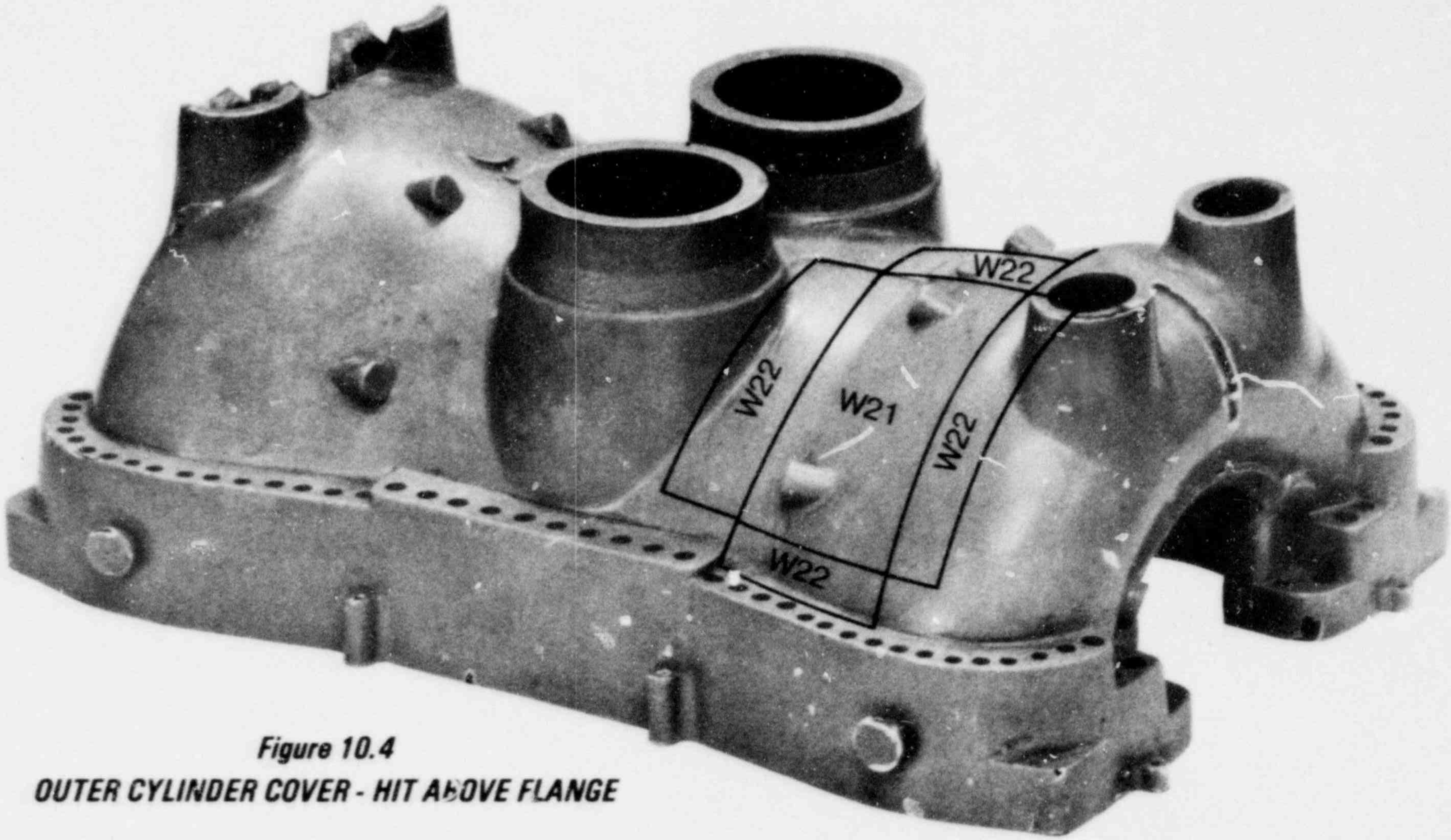

Figure 10.4
OUTER CYLINDER COVER - HIT ABOVE FLANGE

SECTION	w	t	A	R_i	R_c	θ_c	$R_c\theta_c$	$V_i = AR_c\theta_c$	$W_i = V_i(.283)$	$W_{22ci} = V_i(.283)(K_f)$
	(in.)	(in.)	(in.^{2})	(in.)	(in.)	(rad.)	(in.)	(in.^{3})	(lbf.)	(lbf.) [
0										
1										
2										
3										
4										
5										
6										
7										
8										
9										
10										
11										

AXIAL OVERHANG PER END [ ]ab

0	
1	
2	
3	
4	
5	
6	
7	
8	
9	
10	
11	]ab

Figure 10.5

OUTER CYLINDER - HIT ABOVE FLANGE TABLE

11.0 HIT ABOVE FLANGE - CALCULATION OF TENSION STRAIN VALUES AND TENSION ENERGY FOR BLADE RINGS

1. One rotor fragment is assumed to hit the blade rings and outer cylinder at a point above the flange of the outer cylinder. Since the location of the hit determines the strain values for the blade rings, the exact location of the hit has to be established.

2. The majority of the sections of the outer cylinder have the overhanging material controlled by $\theta_{22} = \frac{1}{2}(\frac{\pi}{2} - \theta_c)$. Therefore, set the angle of the rotor fragment such that the 90° line is above the flange, Figure 11.1.

3. The height of the flange as well as the distance of the flange from the center changes with each section of the flange. Also, θ_c and θ_{22} for the outer cylinder may not be the same for each section.

   The angle of the rotor fragment that is hitting above the flange is established by selecting the lowest angle above the horizontal joint.

   The lowest angle is established by inspection of the angles at Sections 2 and 8 of the outer cylinder, Figure 11.1.

   A. For Section 2 calculate:

   $$\theta_h = \frac{\theta_c}{2} + \theta_{22} + \theta_f$$

   B. For Section 8 calculate:

   $$\theta_h = \frac{\theta_c}{2} + \theta_{22} + \theta_f$$

   Select the lowest value of θ_h and set value to θ_H.

For the remainder of the calculations the overhanging material forming θ_{22} is considered to be part of the outer cylinder wall regardless of the flange angle θ_f.

4. Once the location of the rotor fragment is determined, the average tension strain, ϵ_T, for each blade ring can be established. The strain increases from

   [ ][a]

   This approach is conservative since there is a second rotor fragment that is hitting the lower part of the blade ring. This second fragment increases the strain in the blade rings to a value higher than zero.

5. The average tension strain and associated tension energy is calculated for each blade ring.

   For a typical blade ring, the strain value, ϵ', is determined by:

$$\epsilon' = \epsilon \frac{\theta_H - (\frac{\theta_C}{2} + \theta_{22})}{\theta_H}$$

   The tension strain energy for the material of the blade ring is:

   [ ][a]

   where $V_T = V_{21} + V_{22}$

$$\epsilon_T V_T = (\frac{\epsilon' + \epsilon}{2}) (\frac{V_T}{2}) + \epsilon \frac{V_T}{2}$$

$$= (\frac{\epsilon' + \epsilon}{2} + \epsilon) \frac{V_T}{2}$$

$$= (\frac{\epsilon'}{2} + 1.5\epsilon) \frac{V_T}{2}$$

$$\varepsilon_T V_1 = \left(\frac{\varepsilon}{4} + \frac{1.5\varepsilon}{2}\right) V_T$$

$$\varepsilon_T = \frac{\varepsilon}{4} + \frac{1.5\varepsilon}{2}$$

Repeat the calculation for each blade ring. The method for setting the maximum hoop tension strain, ε, is discussed in Section 13.0.

6. A second approach is to set the angle of the rotor fragment such that the [ ][a] the wall material of the outer cylinder.

   This approach yields rotor fragments after the collision with lower energy than the reported method. The reason is that the flange is a stronger member that is capable of absorbing more tension strain energy and shear energy than the wall of the outer cylinder.

[

]^{ab}

Figure 11.1

HIT ABOVE FLANGE - ESTABLISHING θ_H

[

]ab

Figure 11.2
BLADE RING STRAIN DIAGRAM - HIT ABOVE FLANGE

12.0 HIT ABOVE FLANGE -ESTABLISHING STRAIN LIMITS FOR OUTER CYLI 'ER

1. The wall of the outer cylinder is considered to be [
]a The wall of the outer cylinder is not a simple long shell or a simple short shell. Containment tests of long shells show that the maximum [
]b [ ]b
Containment tests of short shells show
[ ]b
[
]b

13.0 HIT ABOVE FLANGE - ESTABLISHING STRAIN LIMITS FOR BLADE RINGS

1. The maximum tension strain of each blade ring is a function of the tension strain in the outer cylinder and a function of the geometry of the outer cylinder and blade rings. There may be small gaps, [ ][a], between the outer cylinder and blade rings before the rotor fragment contacts the blade rings. Once the collision occurs the blade rings and outer cylinder remain in contact. The wall of the outer cylinder fails when the hoop tension strain reaches [ ][a]. Blade rings which are considered short shells would normally fail at a hoop tension strain of [ ][a]. The short shells are considered to be solid rings with no horizontal joint bolting. Since the blade rings are in contact with the outer cylinder, very high local strains will occur in the blade rings at the locations above which the outer cylinder fails. Therefore, the maximum hoop tension strain, ϵ, in the blade ring is greater than [ ][a]

2. Once the collision starts, the outer cylinder is strained in the hoop direction. The center of gravity of the cross-section of the outer cylinder moves outward a distance of ΔR_c at failure:

   [ ][a]

   Since the blade rings are in contact with the outer cylinder, the center of gravity of the blade ring cross-section is strained to a higher value than [ ][a] by the equation:

   [ ][a]

3. The maximum tension strain for each blade ring is calculated because the geometry of the outer cylinder and blade rings is different for each blade ring. In addition, base the radius of the outer cylinder for blade ring No. 1 on R_c for Section 2 and for blade ring No. 2 on R_c for Section 8, Figure 6.4. This convention is conservative since additional material on either side of these two sections will increase R_c and increase the failure strains of the blade rings.

4. A limit is placed on the tension strain of the blade rings. In no case is the tension strain in the blade rings to [ ][a]

14.0 HIT ABOVE FLANGE - STAGE 1 PROCESS

1. The primary failure of the nuclear HP turbine is a stage 2 or tension failure. However, the stationary parts have to be checked for a possible stage 1 failure. The general method for calculating a stage 1 process is discussed in Reference 1.

2. Since stage 1 occurs before stage 2, a stage 1 failure eliminates the possibility of taking credit for the tension strain energy in some or all of the stationary parts.

3. The collision process is assumed to be a [ ][a]. Therefore, the volume of compressed material includes not only the blade rings but also the outer cylinder. The rules for determining the compressed volume of the blade rings are discussed in Section 9.0.

4. The volume of material that is compressed on the outer cylinder is the material immediately in front of the blade ring fits. The volume of Sections 1, 2, 3, and 7, 8, 9 of Figure 6.4 is the material considered to be compressed by the rotor fragment hitting the blade ring which in turn hits the outer cylinder. The affected material is encompassed by θ_C. For a typical section, Figure 10.5:

$$V_i = (A\ R_C\ \theta_C)_i \quad (in^3).$$

Therefore, the total volume of material that is compressed on the outer cylinder is:

$$V_{c\text{-}cyl.} = \Sigma\ V_i\ (in^3).$$

5. Some blade rings for the HP Type III have partial contact with the fit on the outer cylinder. Therefore, include as material for compression on the outer cylinder only the material that the blade ring contacts, Figure 10.1.

6. The compression energy, E_c, is based on the compression volume and a compression [ ]^b. The [ ]^b is based on measurements of the change in thickness of a plate or ring after impact. The method assumes uniform strain through the thickness of the plate or ring. The actual strain through the plate is a maximum at the surface next to the impact. The strain quickly reduces as the distance from the contact face increases, Figure 14.1.

7. The tests did [ ]^b However, the effect can be estimated by inspection of the curve, Figure 14.1. Since the majority of the strain energy in compression is accounted for by the material near the contact surface, [ ]^b Therefore, [ ]^b in the blade rings is not included in the analysis. [ ]^b

8. The second source of energy for a stage 1 analysis is shear energy,

[ ]^b

where "A_s" is shear area and "t" is the thickness.

The [ ]^b is an experimentally determined constant that is made up of two effects. The dynamic shear strength, τ_d, is a function of the dynamic plastic flow strength, σ_d, according to:

[ ]^a

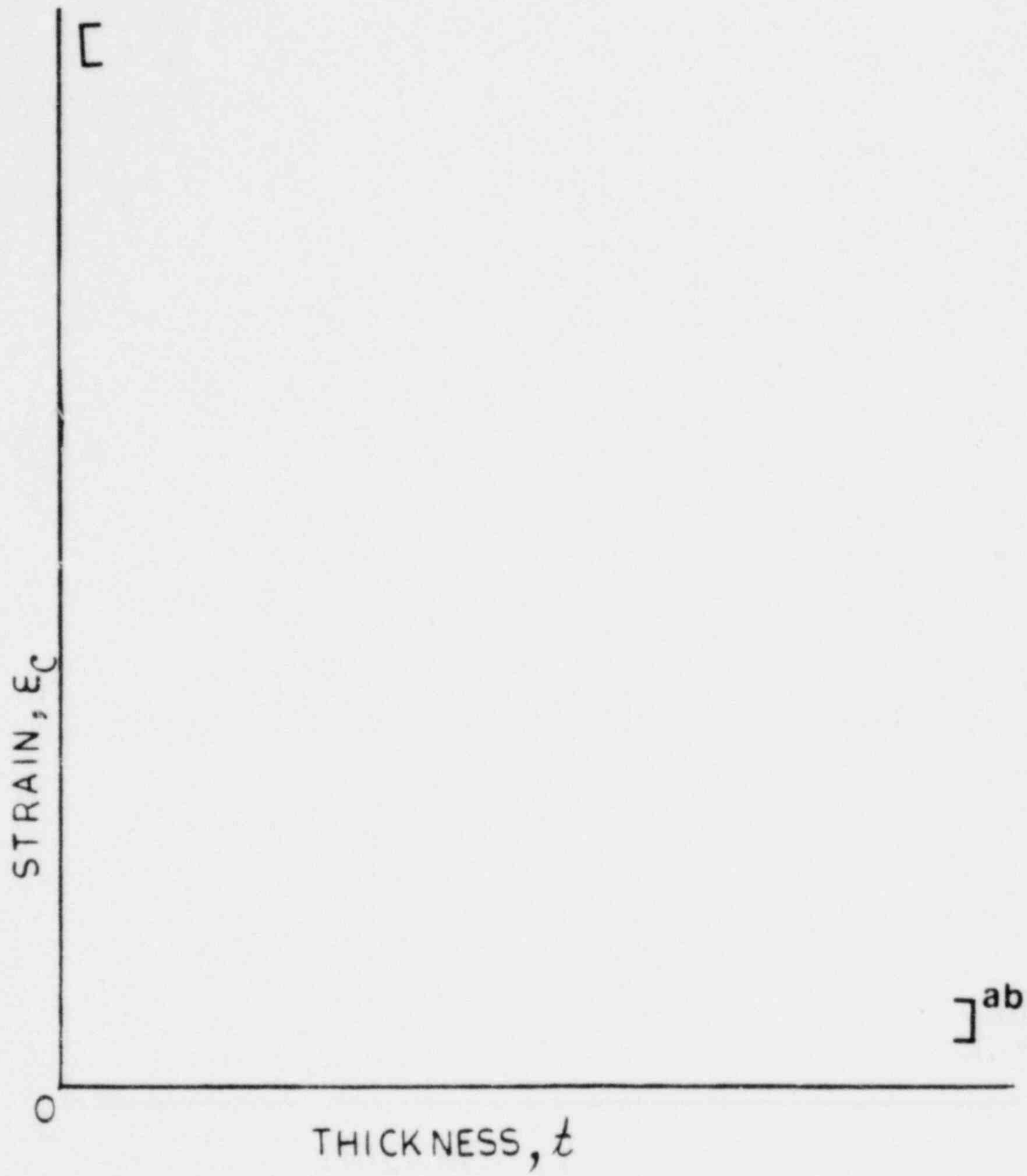

Figure 14.1
COMPRESSION STRAIN

The second effect relates to how parts shear. From tests one side of the shear plane can be moved [ ]b before the part fails in shear. Therefore, the two effects yield the shear energy:

[ ]b

9. The possible shear planes to be considered are dependent upon the circumferential distance between rotor fragments. The possible shear planes for both the blade rings and outer cylinder are established by the distance between rotor fragments, 2L, as expressed by a multiple of the thickness of the blade ring:

A. For the condition $2L < 2t_{eq}$ or $2R_m \theta_{22} < 2t_{eq}$, the rotor fragment cannot shear through the blade ring. The blade ring will not fail in stage 1. The only possible failure mode is a stage 2 failure of the blade ring. In addition, the outer cylinder can fail only along circumferential planes through Sections 0 and 11 of Figure 6.4. A stage 1 failure will cause a 360° ring to be punched out of the outer cylinder. To determine the failure mode calculate U_{pc}:

$$U_{pc} = E_{c\text{-cyl.}} + E_{c\text{-rings}} + E_{sc\text{-sect. 0}} + E_{sc\text{-sect. 11}}$$

where

[ ]b

$$E_{c\text{-cyl.}} = \frac{\sigma_d}{12} (.07) V_{c\text{-cyl.}}$$

$$E_{c\text{-rings}} = \frac{\sigma_d}{12} (.07) (V_{c\text{-ring 1}} + V_{c\text{-ring 2}})$$

Compare U_{pc} to ΔKE where ΔKE is:

[ ]^b

A.1. For $U_{pc} > \Delta KE$

Stage 1 is contained and the failure process enters stage 2.

A.2. For $U_{pc} < \Delta KE$

Stage 1 is not contained and the rotor fragment fails a 360° ring out of the outer cylinder.

B. For the condition $2L > 2t_{eq}$ or $2R_m \theta_{22} > 2t_{eq}$ the rotor fragment can shear across the face of a blade ring. For this condition the outer cylinder can be sheared not only along circumferential planes but also along axial planes, Sections 1 through 10 of Figure 6.4. To determine the failure mode, calculate U_{pcA}:

$$U_{pcA} = E_{c-cyl.} + E_{c-rings} + E_{scA-sect.\ 0} + E_{scA-sect.\ 11} + 2\ E_{sA-rings} + 2\ E_{sA-cyl.}$$

where:

[ ]^b

[ ]^b

[ ]^b

[ ]^b

B.1. For $U_{pcA} > \Delta KE$

Stage 1 is contained and the failure process enters stage 2.

B.2. For $U_{pcA} < \Delta KE$

Stage 1 is not contained and the rotor fragment fails a plug out of both the blade rings and outer cylinder.

The energy of the rotor fragment after the collision for condition B.2 is calculated according to Equations 12 through 15 of Reference 1.

The energy of the rotor fragment after the collision for condition A.2 is calculated following the rules for a hit above the flange Section 15.0. The outer cylinder will extend from Sections 1 through 10 of Figure 6.4. A stage 1 calculation is not repeated for this 360° ring.

The energy of the rotor fragment after conditions A.1 and B.1 is calculated following the rules for stage 2.

10. The failure mode for all nuclear HP turbines that have been calculated to date is a normal stage 2. All units show containment in stage 1.

A modification to the procedure which produces a conservative check for stage 1 is:

$$U_p = E_{c\text{-cyl.}} + E_{c\text{-rings}} + E_{s\text{-sect. }0} + E_{s\text{-sect. }11}$$

where

[ ]^b

[ ]^b

If $U_p > \Delta KE$ stage 1 is contained.

15.0 HIT ABOVE FLANGE - CALCULATION OF MISSILE ENERGY FOR STAGE 2

1. If the stage 1 process is contained, the residual energy if any, of the rotor fragment can be calculated for stage 2:

For the wall of the outer cylinder

[ ]^a

For the blade rings

$$E_{T\text{-ring }1} = \left[\frac{\sigma_d}{12}\, \varepsilon_T\, V_T\right]_{\text{ring }1} \quad \text{(ft-lbf)}$$

$$E_{T\text{-ring }2} = \left[\frac{\sigma_d}{12}\, \varepsilon_T\, V_T\right]_{\text{ring }2} \quad \text{(ft-lbf)}$$

where ε_T and V_T are the strain values and effective volumes of each part.

The kinetic energy of the rotor fragment after the collision is:

[ ]^a

where $E_T = E_{T\text{-cyl.}} + E_{T\text{-ring }1} + E_{T\text{-ring }2}$.

16.0 OUTER CYLINDER AND BLADE RINGS - HIT ABOVE JOINT

1. A rotor fragment oriented so that the edge of the fragment is near the horizontal joint results in straining the flange of the outer cylinder. The amount of material that is considered fully effective is established by radial lines extending through the blade rings and outer cylinder, Figures 16.1 and 16.2.

2. There are three included angles, one for each blade ring and an average of the two blade rings. The included angle for the average of the two blade rings, θ_{cav}, will control the orientation of the rotor fragment, Figures 16.1 and 16.2. The center of the rotor fragment will be set at an angle of $\theta_{cav}/2$ above the horizontal joint.

3. The small amount of material encompassed by θ_{22} that is below the horizontal joint will not be included in the analysis. The horizontal joint bolts are significantly weaker in shear energy than the wall of flange.

4. The weight and volume of material for the wall of the outer cylinder is composed of the material from the top of the flange to the center of the rotor fragment plus one-half of the material calculated for the hit above the flange, Figure 16.1.

5. The flange of the outer cylinder is considered to be a series of solid blocks for which the volume and weight of each section is calculated, Figure 6.5. Sections numbered 1 through 10 are considered to be material that is fully effective. Sections 0 and 11 form the material that is partially effective, W_{22c}. The axial length of the material forming Section 11 is [ ]^{a}. The axial length of the material forming Section 0 is [ ]^{d}. The axial length may be limited by the distance to the center of the turbine [ ]^{a}. The efficiency factor, K_f, is selected from Figure 9.2.

6. Except for the overhanging material associated with θ_{22}, the weight and volume of material for the blade rings will follow the calculation procedure for a hit above the flange. The overhanging material below the horizontal joint is not included in the analysis.

7. Tabulation forms for the properties of the flange and wall of the outer cylinder are shown on Figures 16.3 and 16.4.

[

]ab

Figure 16.1
HIT ABOVE JOINT

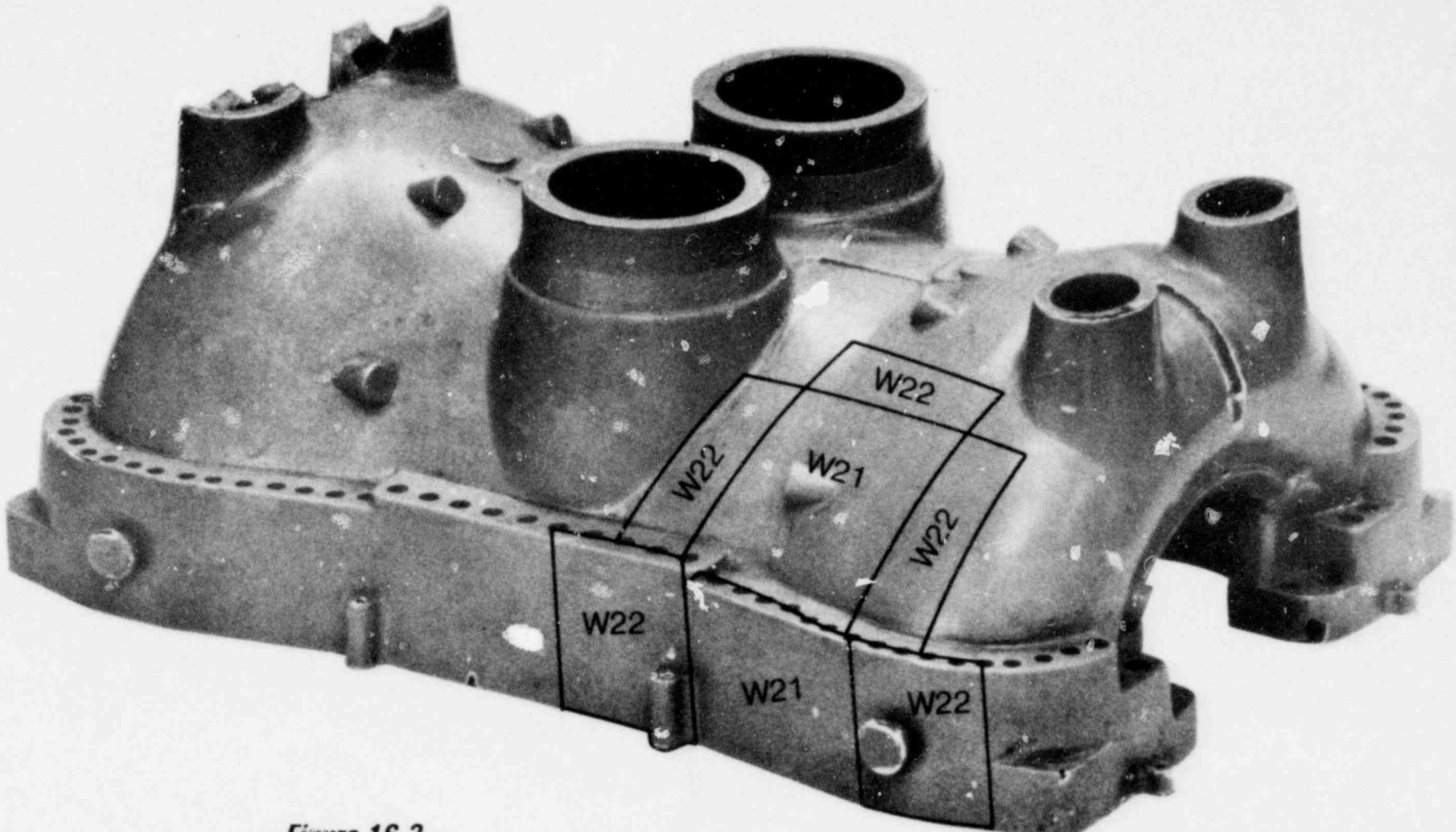

Figure 16.2
OUTER CYLINDER COVER - HIT ABOVE JOINT

SECTIONS	W	t	h	S [				]ab
	(in.)	(in.)	(in.)	(in.)	(in^2.)	($in.^3$)	(lbf.)	(lbf.)
0								
1								
2								[
3								
4								
5								
6								
7								
8								
9								
10								
11								

C 63

	R_c	h	<	θ_f
	(in.)	(in.)	(DEGREE)	(RAD.)
0				
1				
3				
4				
5				
6				
7				
8				
9				]ab
10				
11				

Figure 16.3

FLANGE PROPERTIES ON OUTER CYLINDER TABLE

SECTIONS	t (in.)	A (in.^{2})	R_c (in.)	θ_{cav} (rad.)	θ_f (rad.)	[(rad.)	(in.)	(in.^{3})	(lbf.)	(lbf.)]^{ab}	K_f
0											
1											
2											
3											
4											
5											
6											
7											
8											
9											
10											
11											

C 64

[ ]^{ab}

Figure 16.4

OUTER CYLINDER - HIT ABOVE JOINT TABLE

17.0 HIT ABOVE JOINT - CALCULATION OF STRAIN VALUES AND TENSION ENERGY FOR BLADE RINGS

1. The tension strain for the blade rings increases from 0% near the joint to a maximum of ε at the center of the rotor fragment. From the center of the rotor fragment to the next rotor fragment the tension strain is ε, Figure 17.1.

2. The tension strain energy for the material of a blade ring is:

$$E_{T\text{-ring}} = \frac{\sigma_d}{12} \varepsilon_T V_T \quad \text{(ft-lbf)}$$

$$= \frac{\sigma_d}{12} \left[\frac{\varepsilon}{2} \left(\frac{V_{21}}{2}\right) + \varepsilon \left(\frac{V_{21}}{2} + \frac{V_{22}}{2}\right)\right]$$

3. The maximum hoop tension strain, ε, in a blade ring is set by the radius ratio:

$$\varepsilon = \varepsilon_{cT} \frac{R_c}{R_m} = .035 \frac{R_c}{R_m} \quad \text{(in/in)}$$

The method is discussed in Section 13.0.

4. The calculation is repeated for each blade ring.

[

]ab

Figure 17.1
BLADE RING STRAIN DIAGRAM - HIT ABOVE JOINT

18.0 HIT ABOVE JOINT - CALCULATION OF STRAIN VALUES AND TENSION ENERGY FOR OUTER CYLINDER

1. The wall of the outer cylinder is considered to be strained to [ ][b]. The included volume of material is one-half the volume of material calculated for a hit above the flange plus the volume of material designated as V_{21w} and V_{22w}, Figures 16.1 and 16.4.

   The tension strain energy is:

   [ ][b]

   where

   $$\frac{V_2}{2} = \frac{V_{21}}{2} + \frac{V_{22c}}{2} + \frac{V_{22A}}{2} \quad (in^3)$$

2. The flange is considered as a beam with holes along the neutral axis, Figure 18.1. This beam is loaded by the rotor fragment and undergoes two types of deformation, bending and tension. The bending causes tension on the outer fibers away from the fragment and compression on the inner fibers nearer to the fragment. The tension loading causes deformation primarily at the holes and is greatest at the minimum section at the surface of the hole and diminishes away from the neutral axis, Figure 18.2. Therefore, the deformation of the beam is concentrated at the holes and at the ligaments equal to the hole diameter. The peak strain at fracture for the beam material is equal to the true strain at fracture which is the natural logarithm of A_0/A or $\ell n \left(\frac{1}{1 - RA}\right)$ where RA is the reduction in area and the true strain has a value of [ ][a]

   The peak strain of [ ][a] will be that at the hole surface at the minimum section and will decrease to near zero in the axial direction at the full section. For the outer ligament the strain at the minimum section is nearly constant from the peak strain at the surface of the hole to the maximum bending strain at the outer surface but the strain also decreases to near zero in the axial direction at the full section. The average strain at rupture for the outer ligament is [ ][a] For the inner ligament, the strain decreases from the peak strain at the surface of the hole to near zero at the inner surface and decreases to near zero in the axial direction. The average strain at rupture is thus only [ ][a] The average strain at rupture for the combined ligaments is thus [ ][a]. A conservative value of [ ][a] is recommended for the volume of material in the ligaments at the holes in the beam.

3. The calculation should include all flange bolt holes along the length of the flange, Sections 0 through 11 of Figure 6.5. However, the material at the blade ring fits should not be included. This material may not be in the plastic zone, because of the increased cross-sections relative to the cross-sections through the flange at other locations.

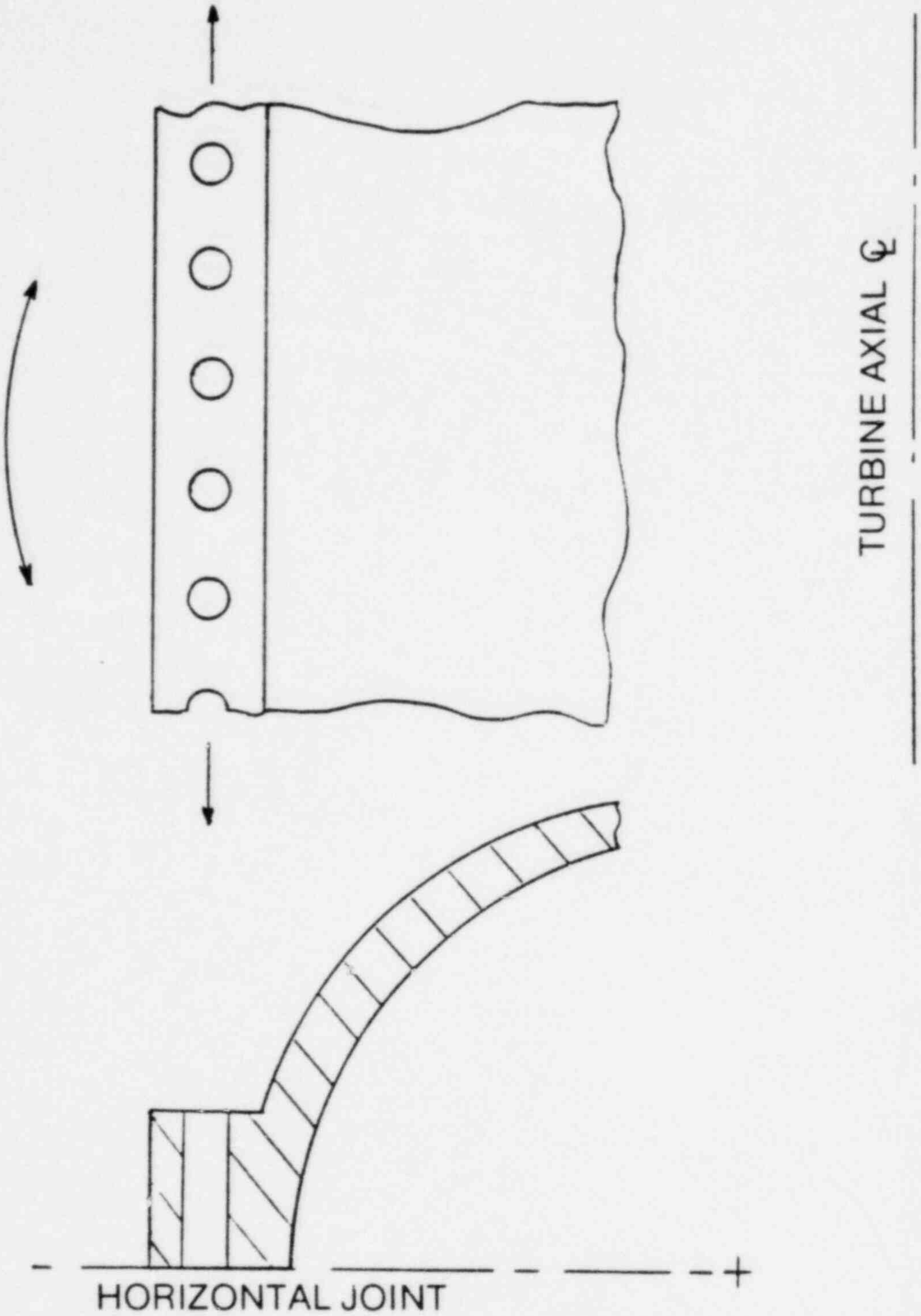

Figure 18.1
PRIMARY LOADS ON FLANGE OF OUTER CYLINDER

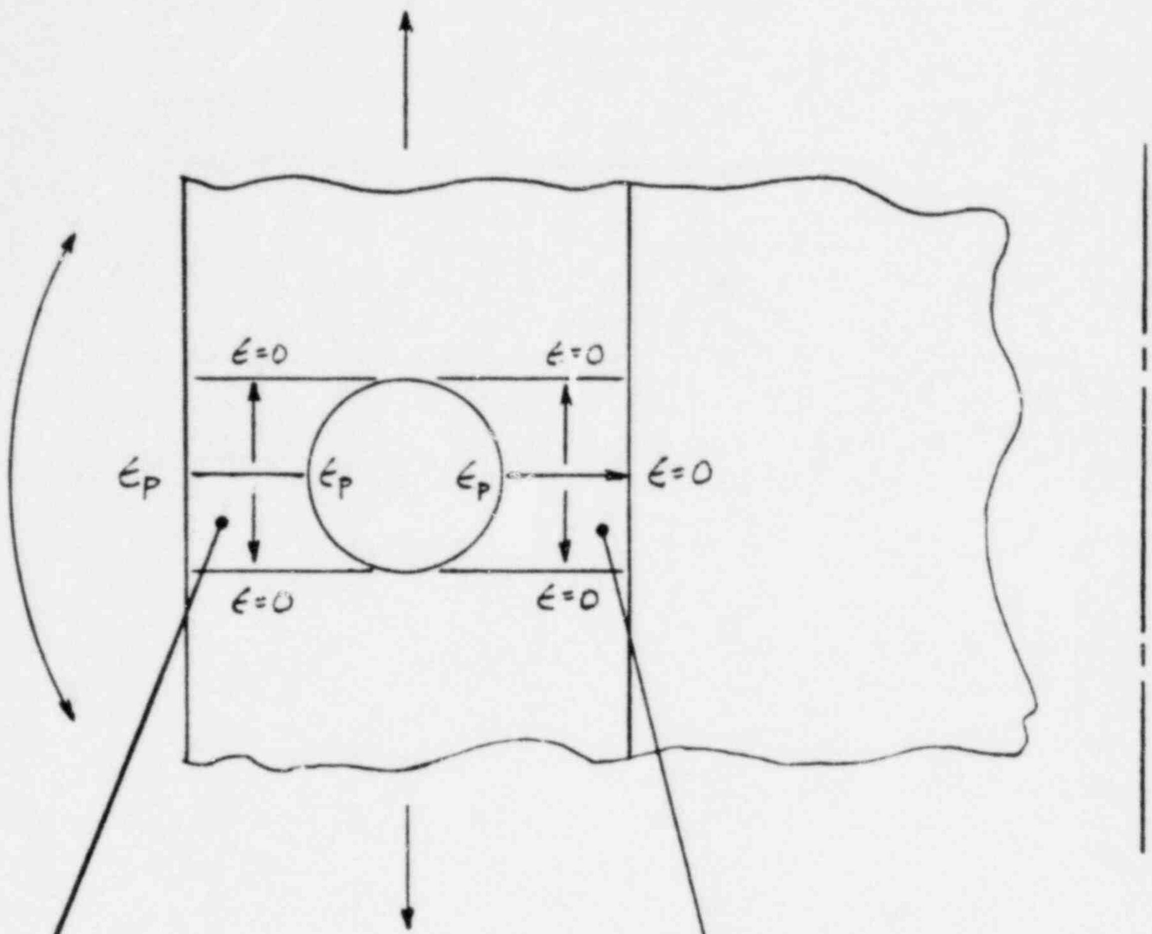

[ ]ab

[ ]ab

[ ]ab

Figure 18.2
LIGAMENT STRAIN VALUES

19.0 HIT ABOVE JOINT - STAGE 1 PROCESS

1. The calculation procedure for stage 1 with a hit above the joint follows the general concepts discussed in Section 14.0. However, a hit above the joint involves possible shearing of not only the cylinder wall but also the flange.

2. The derivation of the energy in shear is discussed in Section 14.0.

3. The flange is considered a solid block for calculation of the energy of compression. The method is conservative since the energy to shear through the longitudinal center plane of a bolt is greater than the compression energy of the volume of material removed by the bolt hole.

4. It is assumed that any shear plane through the flange occurs at a location where a bolt hole exists. Inspection of outer cylinder drawings shows that the shear planes through Sections 0 and 11 of the flange may not occur at a bolt hole, Figure 6.5. A conservative assumption is to assume shear through a section that contains a bolt hole.

5. Even though the flange material is not homogeneous through the cross-section, the total thickness, t, is used in determining the distance through which the shear force acts.

Therefore, the equation for shear energy, E_{sf}, for each plane through the flange is:

[ ]^b

[ ]^b

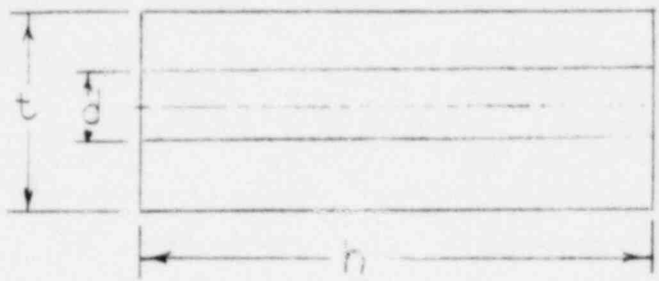

6. The calculation procedure with regard to compressed material follows the method in Section 14.0. The volume of material that is compressed on the flange is the material immediately in front of the blade ring fits. The volume of Sections 1, 2, 3 and 7, 8, 9 of Figure 6.5 is the flange material that is considered to be compressed. The remainder of the outer cylinder material that is encompassed by θ_c is the wall material of the outer cylinder, Sections 1, 2, 3 and 7, 8, 9 of Figure 6.4. The rules for volume of compressed material are discussed in Section 14.0.

7. The blade rings with partial contact with the outer cylinder will have for compressed material on the outer cylinder only the material of the flange and wall that the blade ring contacts.

20.0 HIT ABOVE JOINT - CALCULATION OF MISSILE ENERGY FOR STAGE 2

1. Since the collision involves flange material, wall material and blade ring material; a careful accounting of material and strain volumes should be followed. Assuming containment in stage 1, the stage 2 process follows:

Outer Cylinder Flange

$$W_{Tf} = W_{21f} + W_{22f} \quad \text{(lbf)}$$

$$V_{Tf} = \text{ligament material, Section 18.0} \quad (in^3)$$

Outer Cylinder Wall

$$W_{Tw} = W_{21w} + W_{22wc} + \frac{W_{21}}{2} + \frac{W_{22c}}{2} + \frac{W_{22A}}{2} \quad \text{(lbf)}$$

$$V_{Tw} = V_{21w} + V_{22wc} + \frac{V_{21}}{2} + \frac{V_{22c}}{2} + \frac{V_{22A}}{2} \quad (in^3)$$

Blade Rings

$$W_{ring\ 1} = (W_{21} + \frac{W_{22}}{2})_{ring\ 1}$$

$$V_{T\text{-}ring\ 1} = (V_{21} + \frac{V_{22}}{2})_{ring\ 1}$$

$$W_{ring\ 2} = (V_{21} + \frac{V_{22}}{2})_{ring\ 2}$$

$$V_{T\text{-}ring\ 2} = (V_{21} + \frac{V_{22}}{2})_{ring\ 2}$$

2. The tension strain energy for each of the components is:

Outer Cylinder Flange

[ ]b

Outer Cylinder Wall

[ ]b

Blade Rings

$$E_{T\text{-ring }1} = \frac{\sigma_d}{12}\left[\frac{\varepsilon}{2}\left(\frac{V_{21}}{2}\right) + \varepsilon\left(\frac{V_{21}}{2} + \frac{V_{22}}{2}\right)\right]_{\text{ring }1}$$

$$E_{T\text{-ring }2} = \frac{\sigma_d}{12}\left[\frac{\varepsilon}{2}\left(\frac{V_{21}}{2}\right) + \varepsilon\left(\frac{V_{21}}{2} + \frac{V_{22}}{2}\right)\right]_{\text{ring }2}$$

3. The kinetic energy of the rotor fragment after the collision is:

$$KE_R = KE_o\left(\frac{W_R}{W_R + W_{Tf} + W_{Tw} + W_{\text{ring }1} + W_{\text{ring }2}}\right)^2$$

$$- E_T\left(\frac{W_R}{W_R + W_{Tf} + W_{Tw} + W_{\text{ring }1} + W_{\text{ring }2}}\right) \quad \text{(ft-lbf)}$$

where

$$E_T = E_{Tf} + E_{Tw} + E_{T\text{-ring }1} + E_{T\text{-ring }2}$$

4. The decision process for containment in stage 1 follows the same rules in Section 14.0. However, if there is a stage 1 failure for a hit above the flange and containment in stage 1 for a hit above the joint, the outer cylinder wall and blade rings are assumed to support no tension energy. The only tension strain energy that can be considered in the

inelastic collision is the flange tension energy. The flange being treated like a beam is strained in the axial direction.

5. A stage 1 failure for a hit above the joint results in taking no credit for tension strain in the flange regardless of the distance between rotor fragments. The shearing of the flange results in the loss of tension capability of the flange.

21.0 HIT AT JOINT - OUTER CYLINDER AND BLADE RINGS

1. A rotor fragment that is oriented so that the center of the fragment hits the horizontal joint results in straining not only the wall of the outer cylinder but also the flanges of the cylinder cover and base, Figures 21.1 and 21.2.

2. The calculation procedure for determining the volume and weight of material is similar to the method for a hit above the joint. The primary difference is that the flange material composes the major resistance to the rotor fragment, Figure 21.3.

3. The weight and volume of material for the blade rings follows the calculation procedure for a hit above the flange.

4. A tabulation of the properties of the wall of the outer cylinder is shown on Figure 21.4.

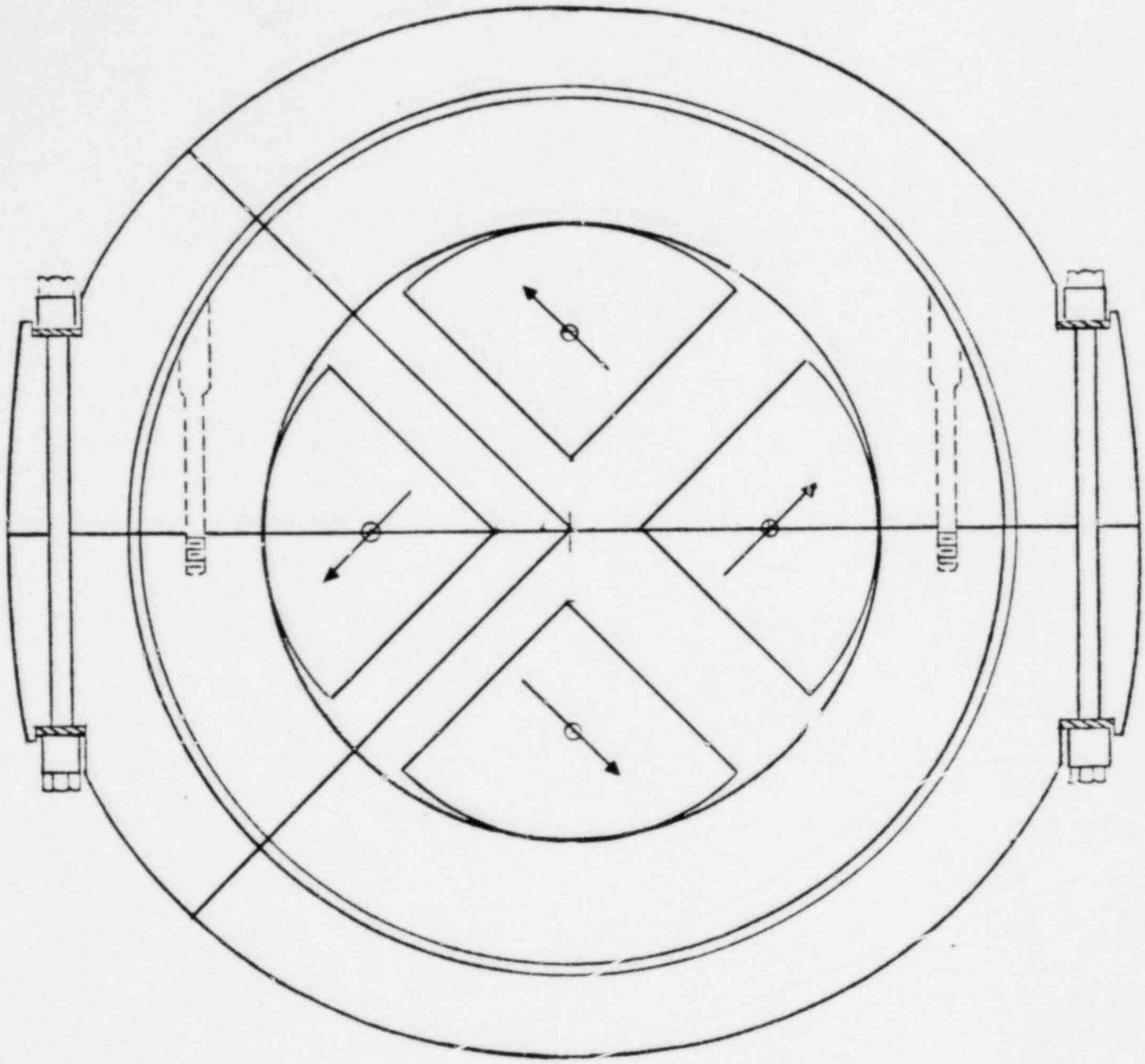

Figure 21.1
HIT AT JOINT

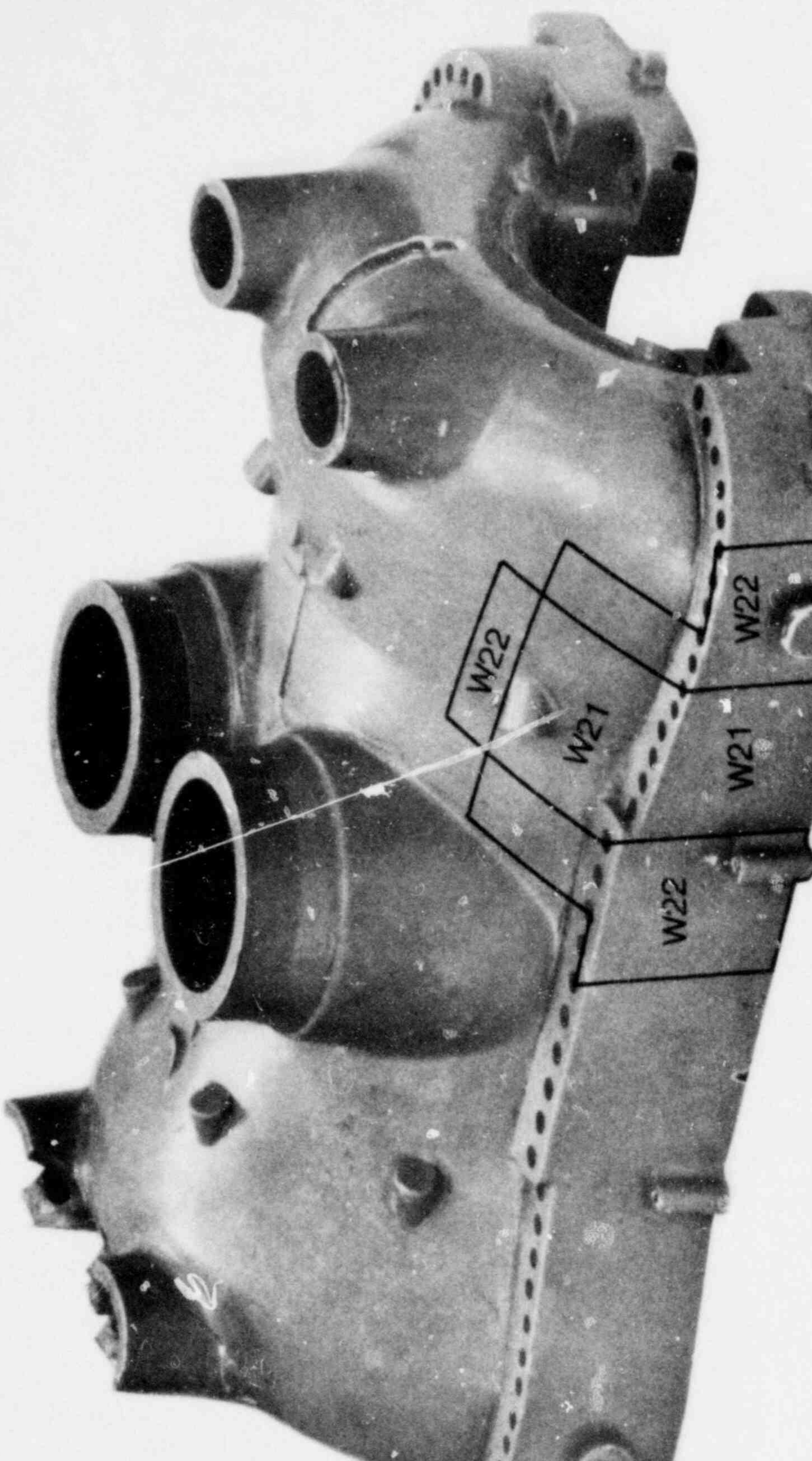

Figure 21.2

OUTER CYLINDER COVER - HIT AT JOINT

[

]ab

Figure 21.3
OUTER CYLINDER - HIT AT JOINT

OUTER CYLINDER-HIT AT JOINT

SECTIONS	t (in.)	A (in.^{2})	R_c (in.)	θ_c (rad.)	θ_f (rad.)	[(rad.)	(in.)	(in.^{3})	(lbf.)	(lbf.)]^{ab}
0										
1										
2										
3										
4										
5										
6										
7										
8										
9										
10									[	
11										

]^{ab}

Figure 21.4

OUTER CYLINDER - HIT AT JOINT TABLE

22.0 HIT AT JOINT - TENSION STRAIN VALUES AND ENERGY FOR OUTER CYLINDER

1. The wall of the outer cylinder is strained to a value of [ ]b. The volume of material is $V_{21e} + V_{22ec} + V_{22A}$, Figure 21.3 and 21.4. Therefore, the tension strain energy is:

   [ ]b

2. The calculation method for the tension strain energy of the flange is identical to the method discussed in Section 18.0. The only difference is that two flanges instead of one are involved. Therefore, the calculated strain energy for a hit above the joint is multiplied by two.

23.0 HIT AT JOINT - TENSION STRAIN VALUES AND STRAIN ENERGY FOR BLADE RINGS

1. The tension strain for the blade rings increases from [ ][a] near the edge of the rotor fragment, Figure 23.1. For simplification of the calculations the maximum strain for each blade ring will be considered to reach [.][a] The tension strain energy of the material for a blade ring is:

$$E_{T\text{-}ring} = \frac{\sigma_d}{12} \varepsilon_T V_T \quad \text{(ft-lbf)}$$

$$= \frac{\sigma_d}{12} \left(\frac{\varepsilon}{2}\right) V_T$$

2. Since the maximum strain and volume of material for each blade ring may be different, the calculation is repeated for each blade ring.

3. Because of the physical contact between the blade rings and outer cylinder, the maximum hoop tension strain, ε, in a blade ring is set by the radius ratio:

$$\varepsilon = \varepsilon_{cT} \frac{R_c}{R_m}$$

The method is discussed in Section 13.0. [ ][a]

[

]ab

Figure 23.1

HIT AT JOINT - BLADE RING STRAIN VALUES

24.0 HIT AT JOINT - STAGE 1 PROCESS

1. The calculation procedure for stage 1 with a hit at the joint follows the concepts discussed in Sections 14.0 and 19.0. The difference is that both the flanges of the cover and base of the outer cylinder are included in the analysis.

25.0 HIT AT JOINT - CALCULATION OF MISSILE ENERGY FOR STAGE 2

1. A hit at the joint involves a significant amount of flange material combined with wall material and blade ring material. The weight and volume of material involved in the collision for stage 2 is:

Outer Cylinder Flange

$$W_{Tf} = 2\,(W_{21f} + W_{22f}) \quad \text{(lbf)}$$

$$V_{Tf} = 2\ \text{(Ligament Material), Section 18.0} \quad (\text{in}^3)$$

Outer Cylinder Wall

$$W_{Te} = W_{21e} + W_{22ec} + W_{22A} \quad \text{(lbf)}$$

$$V_{Te} = V_{21e} + V_{22ec} + V_{22A} \quad (\text{in}^3)$$

Blade Rings

$$W_{ring\ 1} = (W_{21} + V_{22})_{ring\ 1}$$

$$V_{T\text{-}ring\ 1} = (V_{21} + V_{22})_{ring\ 1}$$

$$W_{ring\ 2} = (W_{21} + W_{22})_{ring\ 2}$$

$$V_{T\text{-}ring\ 2} = (V_{21} + V_{22})_{ring\ 2}$$

2. The tension strain energy for each of the components is:

Outer Cylinder Flange

[ ]b

Outer Cylinder Wall

[ ]b

Blade Rings

$$E_{T\text{-ring }1} = \left[\frac{\sigma_d}{12}\left(\frac{\varepsilon}{2}\right) V_T\right]_{\text{ring }1}$$

$$E_{T\text{-ring }2} = \left[\frac{\sigma_d}{12}\left(\frac{\varepsilon}{2}\right) V_T\right]_{\text{ring }2}$$

3. The kinetic energy of the rotor fragment after the collision is:

$$KE_R = KE_o \left[\frac{W_R}{W_R + W_{Tf} + W_{Te} + W_{\text{ring }1} + W_{\text{ring }2}}\right]^2$$

$$- E_T \left[\frac{W_R}{W_R + W_{Tf} + W_{Te} + W_{\text{ring }1} + W_{\text{ring }2}}\right] \qquad \text{(ft-lbf)}$$

where

$$E_T = E_{Tf} + E_{Tw} + E_{T\text{-ring }1} + E_{T\text{-ring }2}$$

26.0 HIT AT TOP

1. Figures 26.1 and 26.2 show the rotor fragment and the effective material for a hit at the top.

2. The weight and volume of material for the outer cylinder and blade rings follows the calculation procedure for a hit above the flange.

3. The calculation procedure for stage 1 with a hit at the top is the same as the procedure for a hit above the flange, Section 14.0.

4. For the stage 2 process, the wall of the outer cylinder is strained to [ ]b The tension strain energy is:

[ ]b

5. The entire tension volume, V_T, of a blade ring is strained to a value of ε. Therefore,

[ ]b

The tension energy for the blade rings is:

$$E_{T\text{-ring } 1} = \left(\frac{\sigma_d}{12} \varepsilon_T V_T\right)_{\text{ring } 1} = \left(\frac{\sigma_d}{12} \varepsilon V_T\right)_{\text{ring } 1} \quad \text{(ft-lbf)}$$

$$E_{T\text{-ring } 2} = \left(\frac{\sigma_d}{12} \varepsilon V_T\right)_{\text{ring } 2}$$

The kinetic energy of the rotor fragment after the collision is:

$$KE_R = KE_o \left(\frac{W_R}{W_R + W_{cyl.} + W_{ring\ 1} + W_{ring\ 2}}\right)^2$$

$$- E_T \left(\frac{W_R}{W_R + W_{cyl.} + W_{ring\ 1} + W_{ring\ 2}}\right) \quad \text{(ft-lbf)}$$

where

$$E_T = E_{T\text{-}cyl.} + E_{T\text{-}ring\ 1} + E_{T\text{-}ring\ 2}$$

6. Since the value of tension strain, ε, for each blade ring is a constant for the entire tension volume of that blade ring, any residual energy of the rotor fragment, KE_R, will be less than the residual energy of a rotor fragment that is hitting above the flange. Therefore, a hit at the top does not have to be calculated.

[

]ab

Figure 26.1
HIT AT TOP

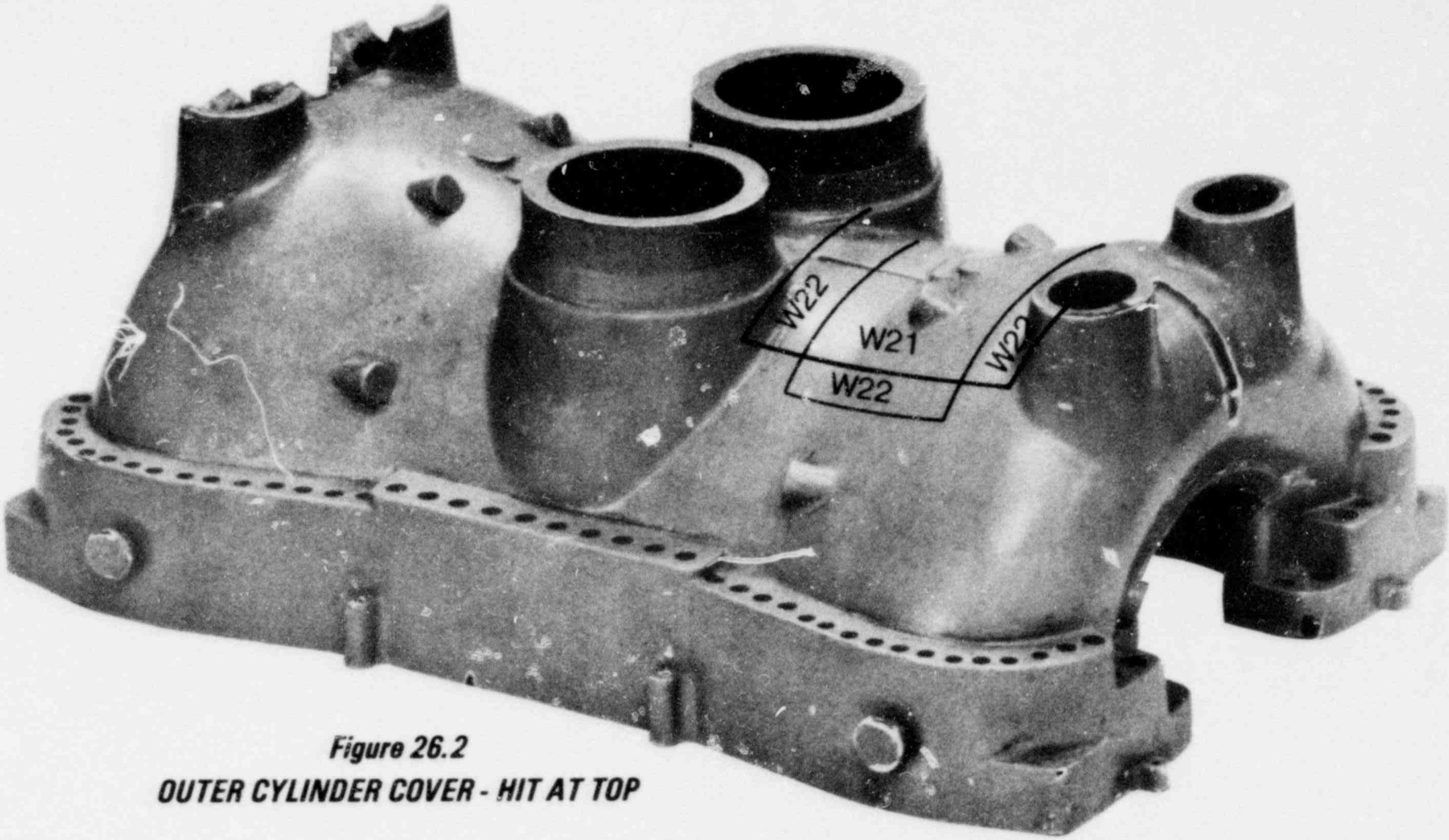

Figure 26.2
OUTER CYLINDER COVER - HIT AT TOP

27.0 FRAGMENT SIZES TO BE REPORTED TO CUSTOMER

1. The rotor fragment will be the same size and weight as used for the missile calculations. The fragment sizes and weights for the blade rings and outer cylinder will be based upon the material in front of the rotor fragment, W_{21}. For a stage 2 failure, there is more material than W_{21} involved in the collision process. However, the exact sizes of the pieces is not known. Tests show that the material composing W_{21} breaks into several pieces. However, the convention of using W_{21} for the reported fragments will be followed. For a stage 1 failure W_{21} is the exact amount of material for the blade rings and cylinder fragments.

2. The blade rings and cylinder fragments are represented as curved bars according to the following rules, shown on Figures 27.1, 27.2 and 27.3.

3. Since four hits per end with a total of eight hits per turbine are being considered, the hit that results in the highest rotor energy, KE_R, after the collision is the hit that is reported to the customer.

4. The energies of the blade rings and cylinder fragments after a stage 2 failure are:

$$V_R = \sqrt{\frac{2g\ KE_R}{W_R}} \qquad \text{(ft/sec)}$$

$$KE_{ring\ 1} = \left(\frac{1}{2}\ \frac{W_{21}}{g}\ V_R^2\right)_{ring\ 1}$$

$$KE_{ring\ 2} = \left(\frac{1}{2}\ \frac{W_{21}}{g}\ V_R^2\right)_{ring\ 1}$$

$$KE_{cyl.} = \left(\frac{1}{2}\ \frac{W_{21}}{g}\ V_R^2\right)_{cyl.}$$

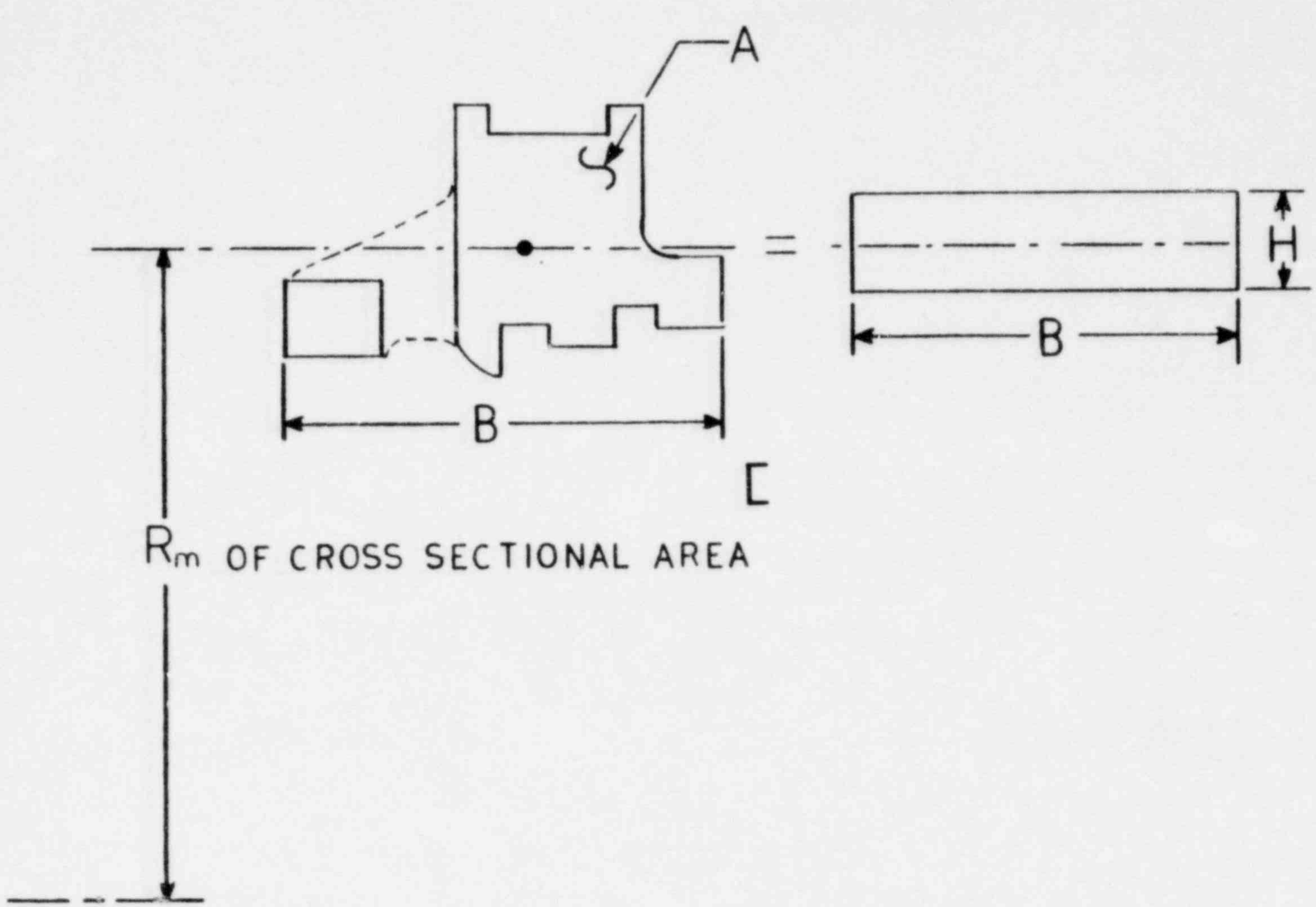

]ab

Figure 27.1
REPORTED BLADE RING FRAGMENTS - BLADE RING #1

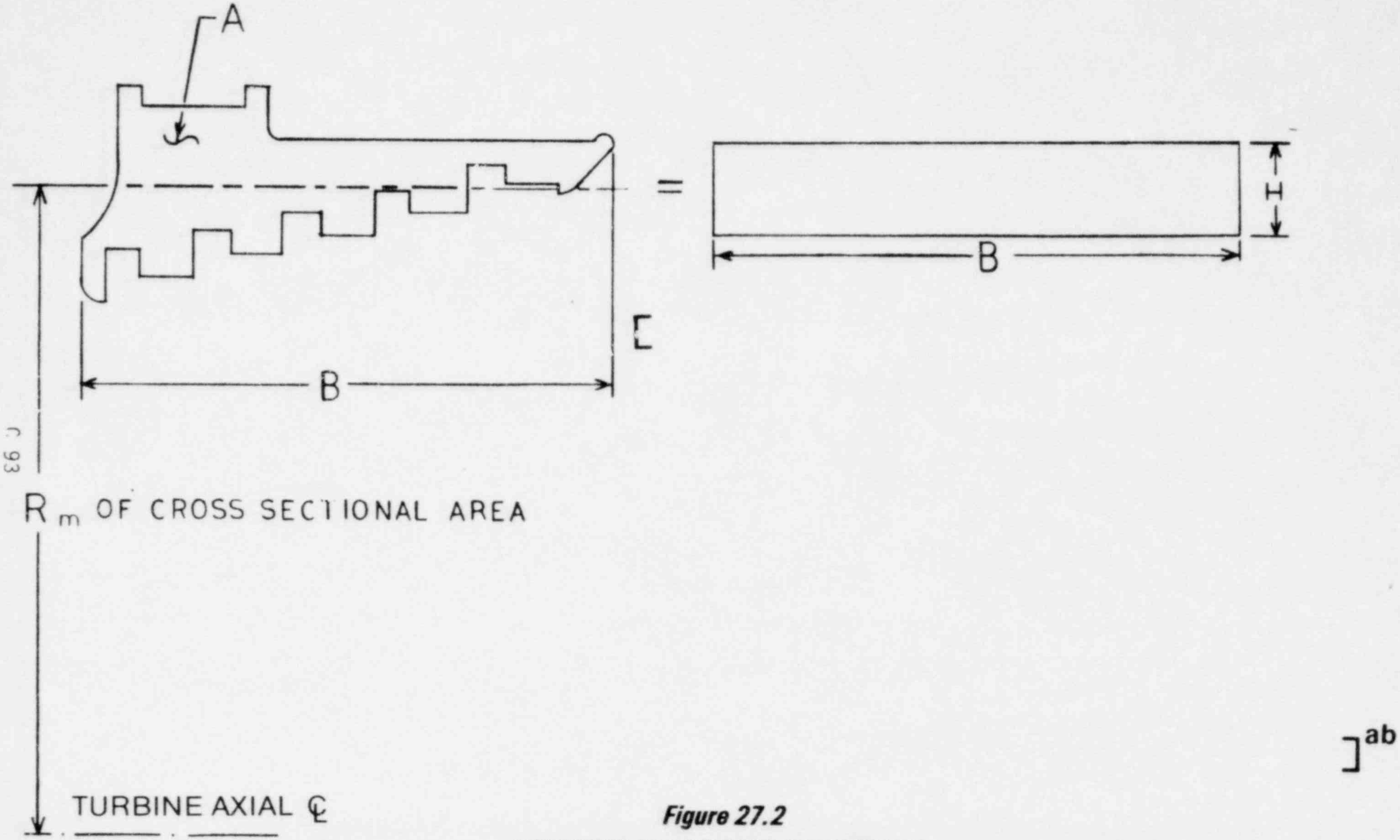

Figure 27.2

REPORTED BLADE RING FRAGMENTS - BLADE RING #2

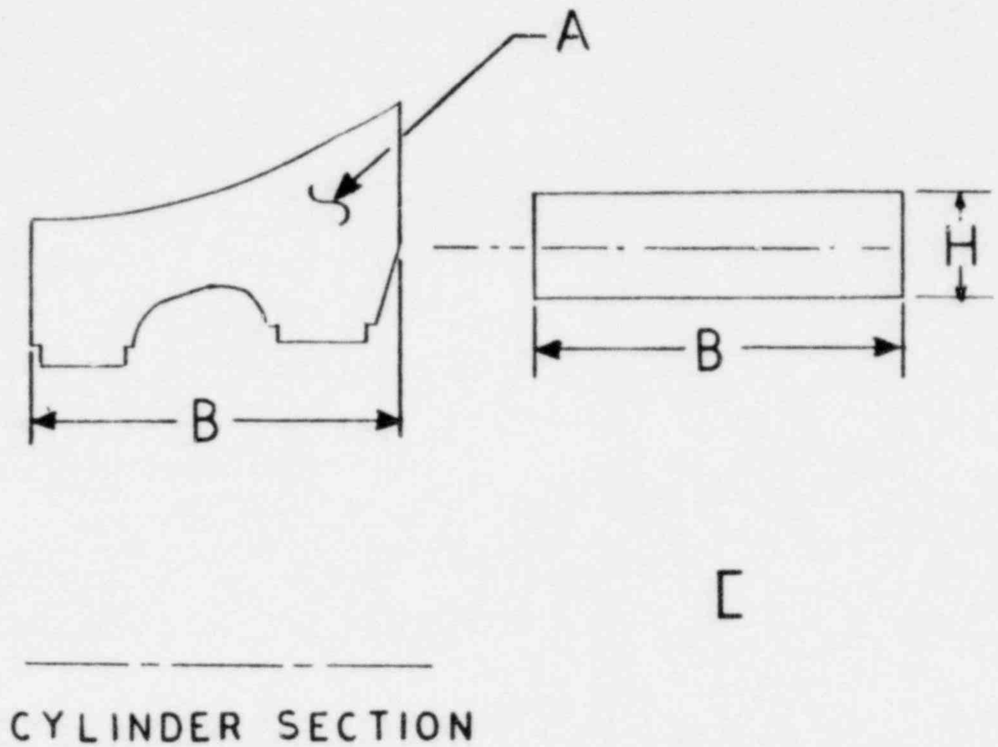

[

]ab

Figure 27.3
REPORTED OUTER CYLINDER FRAGMENTS

28.0 REFERENCES

1. "The Containment of Disk Burst Fragments by Cylindrical Shells", Hagg, A. C., Sankey, G.O., ASME Paper No-73-WA/PWR 2 August 1, 1973.